

**Full Scale Testing of Two Excavations in an Unsaturated Piedmont Residual Soil**

by

Richard E. Burrage Jr.

A dissertation submitted to the Graduate Faculty of  
Auburn University  
in partial fulfillment of the  
requirements for the Degree of  
Doctor of Philosophy

Auburn, Alabama  
December 12, 2015

Keywords: Residual Soil, Unsaturated Soil, Slope Stability,  
Stand-Up Time, Finite Element Modeling

Copyright 2015 by Richard E. Burrage Jr.

Approved by

J. Brian Anderson, Chair, Associate Professor of Civil Engineering  
Joel S. Hayworth, Associate Professor of Civil Engineering  
Wesley C. Zech, Associate Professor of Construction Engineering and Management  
David T. King Jr., Professor of Geology

## **ABSTRACT**

Residual soil behavior can be difficult to predict using current geotechnical formulas, because it exhibits properties that are not common to transported soils. These unique properties are mainly influenced by the fabric structure of the soil and cemented nature of weathered-in-place soil, which can result in increased amounts of strength when compared to transported soils. Proper characterization and modeling is further complicated due to the fact that residual soils often contain a high percentage of silt and clay sized particles which can introduce large amounts of apparent cohesion when the soil is unsaturated. This apparent cohesion can be detected by common insitu tests, but is often times incorrectly identified as being a result of cementation or fabric structure. Such classification can be dangerous for use in designs, because the apparent cohesion of the soil is reduced as the water content of the soil increases. Conversely, it is also common practice to ignore the cohesive component of the soil completely, which can lead to designs that are inefficient.

In this research, two excavations were instrumented at the Auburn National Geotechnical Experimentation Site (NGES) in Opelika, AL. Preliminary modeling was used to determine the depth of excavation that would remain stable when unsaturated, but would become unstable as the surrounding soil neared saturation. The excavations were constructed approximately 6m deep x 30m long with a vertical face. The primary goal of this experiment was to determine the boundary conditions that resulted in failure of the excavation, and compare the results to a finite element model with the same boundary conditions. In doing so, conclusions could be drawn

regarding the accuracy of common laboratory test methods for estimating the strength properties of residual soil.

The instrumentation plan was designed to monitor real-time pore water pressures (positive and negative) surrounding the excavation, as well as the deflection throughout the course of each 1-year test period. Time-lapse cameras were used to identify when failures had occurred, and the approximate geometry of the failure planes. Although the Auburn NGES is a highly characterized site, undisturbed soil samples were taken and used in conjunction with previous soil test results to accurately define the material properties and layering based on common laboratory test methods. In addition to common laboratory tests, unsaturated triaxial tests were also conducted, and soil-water characteristic curves were measured to further define the unsaturated properties of the soil.

In both excavations, failure was observed along a similar plane, which began at the bottom of the excavation, and propagated to the surface (approximately 2m behind the face of the excavation) along existing tension cracks that were developed during the construction of the excavation. The boundary conditions and the laboratory soil properties were input into a finite element model, and the model predicted a factor of safety of approximately one at the critical state, with the factor of safety being significantly higher when dry conditions were simulated. Based on these results, recommendations were made regarding the most appropriate test methods for determining the strength properties of residual soil for use in geotechnical design.

## ACKNOWLEDGEMENTS

First, I would like to express my gratitude to the Federal Highway Administration Dwight David Eisenhower Transportation Fellowship Program for the financial support throughout my graduate studies. Without their support, my graduate studies would have not been possible.

I would like to acknowledge my committee members, Dr. J. Brian Anderson, Dr. Wesley Zech, and Dr. Joel Hayworth for their valuable guidance throughout this research.

I would like to express my deepest gratitude to Dr. J. Brian Anderson for his mentorship and friendship over the past decade. Dr. Anderson has gone above and beyond what anyone could expect for a graduate advisor. Because of this, I have not only obtained my degree, but I have also been able to obtain professional engineering licensure, and most importantly, I have gained a lifelong friend. I would also like to thank Elizabeth Anderson, and the entire Anderson family for opening their home to me, and providing me a place to stay during my visits to Auburn, as well as all of the wonderful meals they have provided.

I would like to acknowledge the Alabama Department of Transportation, and Lankelma, Inc, for their kind support, and providing insitu testing for this project. I would also like to thank Dr. Vinson Ogunro, Dr. Miguel Pando, and Dr. Allen Cottingham for their support.

Finally, I would like to thank my family for their support and encouragement. I would like to thank my parents for pushing me to strive for excellence, and providing the support for me to do so. I would like to especially thank my wife and children, for their love, support and understanding during the many hours that were spent working on this project.

## TABLE OF CONTENTS

Abstract .....	ii
Acknowledgements .....	iv
Table of Contents .....	v
List of Tables .....	xii
List of Figures .....	xiv
List of Abbreviations .....	xix
Chapter 1: Introduction .....	1
1.1 Purpose.....	2
1.2 Scope.....	2
1.3 Project Summary.....	3
1.4 Research Outline .....	4
Chapter 2: Literature Review .....	4
2.1 Residual Soil .....	4
2.1.1 Properties and Behavior.....	4
2.1.2 Shear Strength.....	6
2.1.3 Insitu Testing .....	8
2.1.4 Laboratory Testing.....	9
2.2 Unsaturated Soil.....	10
2.2.1 State of Stress.....	11

2.2.2 Shear Strength .....	12
2.2.3 Characterization and Testing .....	14
2.2.4 Laboratory Testing.....	15
2.2.5 Matric Suction.....	15
2.2.6 Shear Strength.....	17
2.2.7 Insitu Testing .....	17
2.2.8 Full Scale Field Testing .....	19
2.3 Lateral Earth Pressure Theory .....	19
2.3.1 Rankine Lateral Earth Pressure Model .....	21
2.3.2 Coulomb Lateral Earth Pressure Model.....	22
2.3.3 Logarithmic Spiral Lateral Earth Pressure Model .....	25
2.3.4 Soil Structure Interaction Approach .....	26
2.3.5 Finite Element Method .....	29
2.3.6 Case Studies .....	29
2.4 Slope Stability Analysis.....	30
2.4.1 Limit Equilibrium Analysis .....	31
2.4.2 Finite Element Analysis.....	34
2.4.3 Case Studies .....	34
2.5 Other Relevant Research.....	35
2.5.1 Stand Up Time and Excavation Failure .....	35
2.5.2 Trenching and Excavation Safety .....	35
Chapter 3: Background .....	37
Chapter 4: Site Information .....	38

4.1 Site Schematic Plans .....	40
4.1.1 Excavation #1 (2011).....	40
4.1.2 Excavation #2 (2012).....	41
Chapter 5: Instrumentation .....	43
5.1 Overview / Objectives.....	43
5.2 Instrumentation Equipment.....	43
5.2.1 Suction Sensors.....	44
5.2.2 Piezometers .....	46
5.2.3 Tensiometers .....	46
5.2.4 Water Content Reflectometers .....	47
5.2.5 Soil Temperature Sensors .....	47
5.2.6 Slope Inclinerometer .....	48
5.2.7 Data Acquisition System.....	48
5.2.8 Time-lapse Cameras.....	49
5.3 Instrumentation Installation .....	50
5.3.1 Borehole Sensor Installation .....	50
5.3.2 Insitu SWCC Installation .....	51
5.3.3 Inclinerometer Casing Installation .....	53
5.3.4 Water Level Piezometer Installation.....	53
5.4 Instrumentation Plans.....	54
5.4.1 Excavation #1 (2011).....	54
5.4.2 Excavation #2 (2012).....	56
Chapter 6: Site Characterization .....	61

6.1 Site Geology.....	61
6.2 Previous Auburn NGES Characterization .....	63
6.2.1 Previous Index Tests .....	64
6.2.2 Previous Triaxial Tests .....	67
6.2.3 Previous Insitu Test Results.....	68
6.3 Insitu Testing .....	68
6.3.1 Standard Penetration Test .....	68
6.3.2 Cone Penetration Test .....	69
6.4 Laboratory Testing.....	69
6.4.1 Shear Strength Testing.....	69
6.4.2 Pressure Plate Test .....	72
6.4.3 Permeability Test .....	72
Chapter 7: Unsaturated Triaxial Method .....	74
7.1 Modifications to the Standard Triaxial Apparatus.....	74
7.1.1 Triaxial Cell Modification .....	75
7.1.2 Modification to Apply Matric Suction.....	77
7.1.3 Volume Change Measurement.....	78
7.2 Test Procedure .....	81
7.2.1 Sample Preparation / Mounting.....	81
7.2.2 Matric Suction Application.....	82
7.2.3 Suction Equalization .....	82
7.2.4 Flushing the HAE Disk.....	84
7.2.5 Consolidation.....	85

7.2.6 Shear .....	85
7.3 Unsaturated Triaxial Test Results .....	86
7.4 Method Comparison.....	90
7.5 Limitations .....	91
Chapter 8: Insitu SWCC Method.....	94
8.1 Data Analysis .....	96
8.1.1 Unresponsive Data.....	97
8.1.2 Sensor Lag .....	97
8.2 Results.....	100
8.2.1 Primary Curve Approximation .....	101
8.3 Limitations .....	103
8.3.1 Sensor Limitations .....	103
8.4 Recommendations.....	104
Chapter 9: Data Analysis .....	106
9.1 Site Specific Sensor Calibrations.....	106
9.1.1 Watermark Sensor Calibration.....	106
9.1.2 CS-616 Dielectric WCR Calibration .....	109
9.2 Sensor Data Reduction.....	111
9.2.1 Geokon Suction Sensor Data Reduction.....	111
9.2.2 Excavation Water Level Data Reduction.....	112
9.2.3 Slope Inclinator Data Reduction .....	112
Chapter 10: Results .....	114
10.1 Observational Results .....	114

10.2 Matric Suction Data .....	123
10.3 Site Conditions / Weather Data.....	126
10.4 Inclinometer Data.....	127
Chapter 11: Finite Element Modeling.....	130
11.1 Sigma/W Analysis (Before Excavation).....	132
11.2 Seep/W Analysis.....	135
11.3 Sigma/W Analysis #2 .....	138
11.4 Slope/W Analysis.....	140
Chapter 12: Conclusions.....	144
12.1 Validity of Experiment .....	144
12.2 Residual Soil Properties .....	144
12.3 Unsaturated Behavior.....	145
12.4 Mode of Failure.....	146
Chapter 13: Recommendations.....	147
13.1 Residual Soil Characterization.....	147
13.2 Retaining Structures and Slope Stability .....	148
13.3 Unsaturated Soil Strength in Design.....	148
References.....	149
Appendix A - Datalogger Wiring Diagrams.....	163
Excavation #1 Wiring Diagram .....	163
Excavation #2 Wiring Diagram .....	164
Appendix B - Datalogger Programs.....	165
Excavation #1 Datalogger Program.....	165

Excavation #2 Datalogger Program .....	167
Appendix C - Insitu Soil Test Data.....	171

## LIST OF TABLES

Table 1 - Remolding effects on Atterberg limits for lateritic residual soil (Townsend, 1985).....	6
Table 2 - Summary of techniques for measuring soil suction (Lu and Likos, 2004). .....	16
Table 3 – Limit equilibrium procedures and assumptions (Duncan and Wright, 2005).....	33
Table 4 - Instrumentation location and details (Excavation #1). .....	56
Table 5 - Instrumentation location and details (Excavation #2). .....	60
Table 6 - Testing Summary (Vinson and Brown, 1997).....	63
Table 7 - Summary of index testing (Vinson and Brown, 1997).....	65
Table 8 - Specific gravity (Vinson and Brown, 1997).....	65
Table 9 - Triaxial results (Vinson and Brown, 1997). .....	67
Table 10 - Triaxial results with depth (Vinson and Brown, 1997). .....	67
Table 11 - PMT modulus results (Vinson and Brown, 1997).....	68
Table 12 - Triaxial test conditions at failure. ....	71
Table 13 - Shear strength with depth based on triaxial test results.....	71
Table 14 – Permeability results.....	73
Table 15 - Initial sample conditions for triaxial tests. ....	86
Table 16 - Saturated triaxial test conditions at failure. ....	87
Table 17 - Unsaturated triaxial test conditions at failure. ....	87
Table 18 - Shear strength parameters for relevant unsaturated soils. ....	91
Table 19 - Temperature compensating calibration coefficients.....	110

Table 21 - Finite element analysis steps. ....	131
Table 22 - Material properties for initial Sigma/W analysis.....	132
Table 23 – Boundary conditions for transient seepage model.....	135
Table 24 - Slope stability analysis results for various methods.....	141
Table 25 - Calculated factors of safety for various water levels in tension crack. ....	142
Table 26 - Calculated factors of safety for various pore pressure conditions.....	142

## LIST OF FIGURES

Figure 1 – Research steps and obstacles to overcome. ....	4
Figure 2 - Mohr-Coulomb failure criterion (Coulomb, 1776). ....	12
Figure 3 - Extended Mohr-Coulomb failure criterion for unsaturated soil (Lu and Likos, 2004). ....	13
Figure 4 – Rankine earth pressure theory (Rankine, 1857). ....	22
Figure 5 – Coulomb earth pressure theory (Coulomb, 1776). ....	24
Figure 6 – Logarithmic spiral theory. ....	26
Figure 7 – Simple p-y relationship. ....	28
Figure 8 – Experimental p-y curves from literature. ....	28
Figure 9 – Method of slices illustration (Duncan and Wright, 2005). ....	32
Figure 10 - Vicinity map (Google Maps, 2012). ....	38
Figure 11 - (a) Map of Piedmont province (USGS, 2001); (b) Alabama soil map (University of Alabama, 2012). ....	39
Figure 12 - NGES aerial with approximate excavation locations overlaid (Pictometry, 2012). ..	40
Figure 13 - Excavation #1 schematic. ....	41
Figure 14 - Excavation #2 schematic. ....	42
Figure 15 - Sensors. ....	44
Figure 16 - Data acquisition system. ....	49
Figure 17 - Time-lapse camera. ....	50
Figure 18 - Instrumentation installation. ....	51

Figure 19 - Sensor installation schematic for insitu SWCC. ....	52
Figure 20 - Excavation #1 instrumentation plan.....	54
Figure 21 - Excavation #1 instrumentation / construction details. ....	55
Figure 22 - Excavation #2 instrumentation plan.....	58
Figure 23 - Excavation #2 instrumentation / excavation details.....	59
Figure 24 – Geologic map of the Parkers Crossroads quadrangle (Carter and Steltenpohl, 2002). .....	62
Figure 25 - Vinson and Brown (1997) test locations (Pictometry, 2012).....	64
Figure 26 - Grain size distribution summary (Vinson and Brown, 1997). ....	66
Figure 27 - Atterberg limits summary (Vinson and Brown, 1997).....	66
Figure 28 - Triaxial summary (Vinson and Brown, 1997). ....	67
Figure 30 - Failure criterion for consolidated drained triaxial tests at 2.4m-4.6m depth. ....	70
Figure 31 - Failure criterion for consolidated drained triaxial tests at 4.6m-6.1m depth. ....	70
Figure 32 - Failure criterion for consolidated drained triaxial tests at 6.1m-7.8m depth. ....	70
Figure 34 - Schematic diagram of the modified triaxial apparatus.....	75
Figure 35 - Modified triaxial cell base (a) side view, (b) top view showing groove pattern.....	77
Figure 36 - Volume change method comparison #1 (a) volume change vs. strain (b) difference in volume methods.....	80
Figure 37 - Volume change method comparison #2 (a) volume change vs. strain (b) difference in volume methods.....	80
Figure 38 - Sample equalization time based on Seep/W modeling software. ....	84
Figure 39 - (a) Deviatoric stress vs. axial strain (b) volumetric strain versus axial strain.....	88
Figure 40 - Failure criterion for (a) saturated samples and (b) unsaturated samples.....	89

Figure 41 - (a) Volumetric water content and soil temperature vs. time, (b) Suction, precipitation and soil temperature vs. time. ....	96
Figure 42 - (a) Measured equalization curves. (b) calculated instantaneous equalization rate (first order derivative of equalization curves). ....	98
Figure 43 - Equalization rate versus sensor lag (error). ....	99
Figure 44 - Instantaneous equalization rate throughout duration of SWCC measurement. ....	100
Figure 45 - Drying curves recorded during insitu SWCC test (0.3m depth). ....	101
Figure 46 - Bounding and scanning curves. ....	102
Figure 47 - Approximate location of primary drying curve based on insitu data. ....	102
Figure 48 - Alternate sensor configuration ....	104
Figure 49 - (a) Site specific calibration data, (b) calibration curve comparison. ....	108
Figure 50 - Comparison of Watermark linear calibration curve (site specific) with Geokon piezometer data. ....	109
Figure 51 - (a) Measured period vs. temperature for 4 different volumetric water contents, (b) Calibration parameters $\alpha$ and $\beta$ versus volumetric water content. ....	111
Figure 52 - Thin layers present in undisturbed soil samples. ....	115
Figure 53 - Undermining from water in bottom of trench. ....	115
Figure 54 – Excavation construction. ....	116
Figure 55 - Excavation #1 before and after failure (South facing). ....	117
Figure 56 - Excavation #1 before and after failure (North facing). ....	117
Figure 57 – Material being removed from non-instrumented side of Excavation #2. ....	118
Figure 58 - Excavation #2 time-lapse photos. ....	119
Figure 59 – Excavation #2 after initial failure on 9/21/11. ....	120

Figure 60 – Tension cracks developed during Excavation #1. ....	121
Figure 61 – Tension cracks developed during Excavation #2. ....	121
Figure 62 - Tension crack progression over time (Excavation #1).....	122
Figure 63 – Tension crack progression over time (Excavation #2).....	122
Figure 64 - Geokon piezometer matric suction data (Excavation #2). ....	123
Figure 65 - Matric suction and precipitation vs. time (Excavation #1). ....	124
Figure 66 - Matric suction and precipitation vs. time 4.6m offset (Excavation #2). ....	125
Figure 67 - Daily precipitation (Excavation #1). ....	126
Figure 68 - Daily precipitation (Excavation #2). ....	127
Figure 69 - Water level in bottom of Excavation #2. ....	127
Figure 70 - Inclinator data (Excavation #1). ....	128
Figure 71 - Inclinator casings after failure (Excavation #1). ....	128
Figure 72 - Inclinator data (Excavation #2). ....	129
Figure 73 – Inclinator casing after failure (Excavation #2). ....	129
Figure 74 – Finite element model flow chart. ....	132
Figure 75 – Key in materials dialogue for initial Sigma/W analysis. ....	133
Figure 76 - Volumetric water content function.....	134
Figure 77 - Input parameters for Fredlund and Xing hydraulic conductivity function approximation. ....	134
Figure 78 - Permeability function. ....	135
Figure 79 - Initial boundary conditions for Seep/w analysis. ....	136
Figure 80 - Seepage model initial boundary conditions profile view. ....	136
Figure 81 - Transient seepage model results (profile view). ....	137

Figure 82 – Model predicted pore pressures vs. depth. .... 138

Figure 83 - Results of Sigma/W analysis at critical state (15x exaggeration). .... 139

Figure 84 - Predicted lateral displacement at time of failure. .... 140

Figure 85 - Slope stability analysis critical slip surface. .... 141

## **LIST OF ABBREVIATIONS**

AASHTO - American Association of State Highway and Transportation Officials

ANSI - American National Standards Institute

ASTM - American Society for Testing and Materials

BST - Borehole Shear Test

CD - Consolidated Drained

CHT - Crosshole Seismic Test

CPMT - Cone Pressuremeter Test

CPT - Cone Penetration Test

CU - Consolidated Undrained

DAQ - Data Acquisition

DMT - Dilatometer Test

FDM - Finite Difference Model

FEM - Finite Element Model

GSD - Grain Size Distribution

HAE - High Air Entry

LL - Liquid Limit

M-C - Mohr-Coulomb

NGES - National Geotechnical Experimentation Site

NIOSH - National Institute for Occupational Safety and Health

OSHA - Occupational Safety and Health Administration

PCPT - Piezocone Penetration Test

PDEs - Partial Differential Equations

PI - Plasticity Index

PL - Plastic limit

PMT - Pressuremeter Test

PRS - Piedmont Residual Soil

PVC - Polyvinyl Chloride

SCPT - Seismic Cone Penetration Test

SDMT - Seismic Dilatometer Test

SMP - Soil Matric Potential

SPT - Standard Penetration Test

SSI - Soil Structure Interaction

SWCC - Soil Water Characteristic Curve

Typ. - Typical

UC - Unconfined Compression

US - United States

USCS - Unified Soils Classification System

USGS - United States Geological Survey

UU - Unconsolidated Undrained

WC - Water Content

WCR - Water Content Reflectometer

## CHAPTER 1: INTRODUCTION

Residual soil behavior can be difficult to predict using existing geotechnical formulas, because it exhibits properties that are not common to transported soils. These unique properties are mainly influenced by the fabric structure of the soil, and the cohesive nature of undisturbed residual soils that remains from the weathering process of the parent rock. Because of these unique properties, residual soils do not fit in the typical categories of "sand" or "clay" when used in geotechnical design, but exhibit behaviors of both, along with some unique behavior not seen in most design methods. Classical engineering design methods usually assume that soil will behave as either sand ( $c=0$ ), or clay ( $\phi=0$ ). However because of its unique properties, residual soil is often considered to be a  $c-\phi$  soil, having both frictional and cohesive properties. Several obstacles exist that need to be overcome before residual soil mechanics can be implemented into routine engineering practice:

- Residual soil strength properties can easily be mistaken for unsaturated strength properties.
- Unsaturated properties are volatile in nature and can change over time as the soil moisture conditions change which could result in failure.
- Most common characterization methods are unable to differentiate residual soil strength from unsaturated strength.

## **1.1 Purpose**

The main goal of this project was to learn more about the behavior of unsaturated residual soils, and to be able to apply this knowledge to classical engineering design methods to both promote efficiency, and safety in design. Although substantial research has supported the theory that residual soil behaves as a  $c-\phi$  soil (having both frictional and cohesive properties), there have been other case studies of residual soil slopes that have failed after being seemingly stable for long periods of time, causing researchers and practitioners to question whether or not the  $c-\phi$  nature should be considered in designs that may need to withstand decades or even centuries. Furthermore, determining the strength parameters for design can be challenging, because many characterization methods are not able to differentiate the cohesion created by negative pore pressures from the cohesion that is caused by cementation, making it difficult to determine the strength parameters for use in long term designs. For these reasons, further research is needed to better understand the behavior of residual soil to enable the engineering community to take advantage of its strength properties without sacrificing safety.

## **1.2 Scope**

In this project, two excavations were proposed in which the factor of safety would be close to one so that failure could be observed and monitored. Two test methods were also developed to aid in the determination of unsaturated residual soil properties. The primary objectives were as follows:

- Evaluate the cause(s) of failure in residual soil slopes.
- Determine the most effective characterization methods for estimating residual soil properties.

- Develop a method to differentiate the cohesion caused by negative pore pressures, and the cohesion that is caused by cementation and fabric structure of residual soil.
- Use the information obtained by the experiment to make recommendations regarding the implementation of residual soil mechanics into engineering practice.

### **1.3 Project Summary**

This project consisted of constructing two excavations in residual soil, and observing them for a period of 1 year. The excavations were instrumented to measure the pore pressures, and the lateral movement over the duration of the experiment. Before the excavations were constructed, undisturbed soil samples were taken from each of the excavation areas and were used to characterize the soil in close proximity to the excavations. Two new soil test methods were also developed to further characterize the unsaturated residual soil properties. The soil properties and boundary conditions collected from the instrumentation and characterization were then input into a finite element model to determine if the failures observed in the field matched those predicted by the model. From this analysis, conclusions were drawn with respect to the effectiveness of the characterization methods for determining the properties of residual soil, and recommendations were made for determining the strength properties of residual soil for use in design. Figure 1 summarizes the steps involved in this research, and illustrates the obstacles that each of these steps were to overcome.

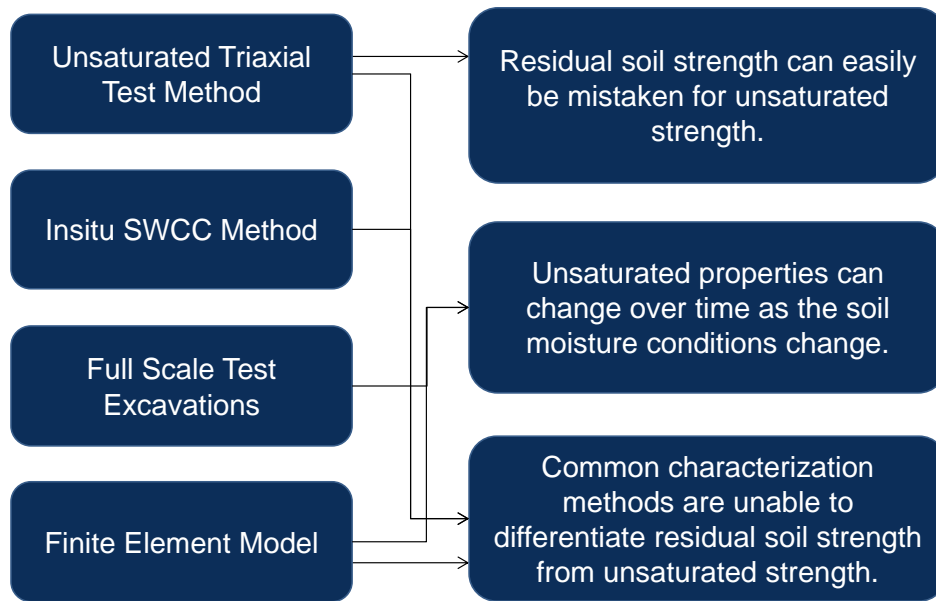


**Figure 1 – Research steps and obstacles to overcome.**

#### **1.4 Research Outline**

The following outline will be used to present the research herein:

- Review of relevant literature
- Project background
- Excavation specifications and site information
- Instrumentation specifications
- Site characterization plan and results
- Unsaturated triaxial test method and results
- Insitu SWCC method and results
- Excavation data analysis
- Excavation results
- Finite element model description and results
- Conclusions and recommendations

## CHAPTER 2: LITERATURE REVIEW

### 2.1 Residual Soil

Residual soils are formed by a natural process of chemical weathering insitu. They are unique in that they have not been transported at any time since formation. Their characteristics can vary depending on the type of parent material, and environmental factors such as the climate and physical features of the land (topography, drainage, etc.).

The determination of residual soil properties for use in geotechnical design is a topic that has proven to be full of challenges, due to unique nature of residual soil. Residual soils tend to be anisotropic and heterogeneous in nature and their properties can vary greatly from one location to the next. The majority of the existing published literature focuses on determination of material properties of these soils, and there are limited amounts of research that regard specific designs in residual soil.

#### *2.1.1 Properties and Behavior*

Although many types of residual soils exist, three classifications that are commonly used for engineering purposes include: lateritic soils, allophanic soils, and black soils. Townsend (1985) describes these soils as follows:

- Lateritic soils are highly weathered reddish tropical soils that have concentrated oxides of iron and aluminum with kaolin as the predominant clay mineral. In these soils, gravel nodules or a cemented cuirasse may be present, and upper layers exist as microclusters cemented by the iron and aluminum sesquioxides.

- Allophanic soils are derived from volcanic ash and extrusive rocks under conditions similar to lateritic soil, but they contain allophane (amorphous silica) and halloysite, as well as the sesquioxides of iron and alumina. Montmorillonites may exist in early weathering stages, while kaolin and gibbsite form as end products.
- Black soils are dark clays which contain appreciable amounts of montmorillonite, and shrink and swell considerably with changes in moisture content.

Properties of residual soils can vary as a function of the degree of weathering that has taken place in the soil (Rahardjo et al., 2004). The degree of weathering generally decreases with depth, but can be higher around joint surfaces and percolation paths (Blight, 1997).

Understanding the degree of weathering is further complicated by the existence of fault zones or inter-bedded lithologies that can weather preferentially (Brand, 1985).

Reproducible results of geotechnical tests have proven to be difficult to obtain in residual soils, because of their sensitivity to drying and remolding prior to, and during testing. Buchanan gave the term lateritic to the soil based on the Latin word "later" which means "brick" to describe a soil soft enough to be cut by a knife, but hardens irreversibly upon exposure (Townsend, 1985). This irreversible effect of drying has been attributed to the increased cementation due to the oxidation of iron and aluminum sesquioxides, however, these drying effects would be seen in soil which are from depths greater than the normal oxidation levels, whereas the near-surface lateritic soils will be more susceptible to remolding effects (Townsend, 1985). Remolding effects are caused by the breakdown of friable aluminum and iron cementing bonds between clay clusters which result in a change in the physical properties of the soil. Previous research has showed that these changes can be quite substantial. Table 1 shows the effects of remolding on Atterberg limits.

**Table 1 - Remolding effects on Atterberg limits for lateritic residual soil (Townsend, 1985).**

Soil type and Location (1)	Liquid Limit		Plasticity Index		Source (6)
	Natural (2)	Remolded (3)	Natural (4)	Remolded (5)	
Red clay, Kenya	74	84	36	45	Newill, 1961
Red clay, Kenya	77	91	16	32	Newill, 1961
Lateritic Cuba	46	53	15	22	Winterkorn and Chandrasekharan, 1951
Lateritic, Panama	60	70	21	30	Townsend et al., 1969

Research concerning general classification of residual soil has been performed by many researchers, including: Sowers and Richardson (1983), Sowers (1994), Townsend (1985), Viana de Fonseca et al. (1994), Failmezger et al. (1999), Lutenegeger et al. (2003), Waisnor et al. (2001), Mayne et al. (2000, 2003), Lunne et al. (1997), and Petersen et al. (1999).

In addition to these, more specific studies of residual soil behavior have been completed by Wang and Borden (1996), who studied deformation characteristics, and Hertz (1986) who studied various engineering properties of residual soil. Willmer et al. (1982), Wesley (1994), and Barksdale et al. (1982, 1986) researched settlement from various insitu test methods. Strength and stiffness were studied by Vinson and Brown (1997) and Brown and Vinson (1998). Piezocone tests have been performed by Finke and Mayne (1999), Finke (1998), and Finke et al. (1999). Dynamic testing has been completed by Hoyos and Macari (1999), and seismic effects have been examined by Martin and Mayne (1998).

### *2.1.2 Shear Strength*

Shear strength of residual soil was investigated comprehensively by Brenner et al. (1997). These researchers identify six special features encountered with residual soils which are mainly responsible for the difference in stress-strain and strength behavior in comparison with transported soils:

- Stress history – residual soils are formed by weathering history and the particles evolve as a result of chemical processes. Weathering is a weakening process and may cause some vertical and lateral unloading due to the loss of mineral matter in the altering rock. This implies a progressive modification of the insitu stresses which modifies the effect of previous stresses on the structure of the weathering material. It is therefore reasonable to consider the current structure of residual soils to be in equilibrium with and associated with their current state of stress. The effect of past stresses to which they have been subjected during their formation will be small (Vaughan, 1988).
- Grain/particle strength – weathering produces soil particles with variable degrees of weakening. The particles will, therefore, display a much wider variability in crushing strength than usually encountered with transported soils.
- Bonding – the bonds between residual soil particles represent a component of strength and stiffness that is independent of effective stress and void ratio/density.
- Relict structure and discontinuities – the parent rock of a residual soil deposit may contain discontinuities of low shear strength, which can develop surfaces with low residual strength. After decomposition of rock, these surfaces will also exist in the residual soil.
- Anisotropy – as a result of stress anisotropy in a soil, the response to a shear stress application depends on the direction of the stress. With residual soils, the anisotropic behavior has usually mainly been inherited from the fabric structure of the parent rock.

- Void ratio/density – the void ratio in a residual soil is a function of the stage that the weathering process has reached and is usually not directly related to stress history.

Because of the effects of remolding, the strength characteristics of the soils are greatly affected, as well as the hydraulic properties. Researchers such as Vargas (1973), Foss (1973), and Prusza et al., (1983) have all observed a collapse in the soil structure in lateritic soils upon saturation. Typical consolidation curves for these soils show an apparent preconsolidation pressure due to the cementation of the clays, and possibly soil suction, but upon saturation the preconsolidation pressure decreases, and large settlements occur (Townsend, 1985).

### *2.1.3 Insitu Testing*

A summary of insitu testing methods used for characterizing soils is presented by Failmezger et al. (1999), in which a number of specific problems are identified with the standard penetration test (SPT), the most routinely used of all insitu tests. The appropriateness of the SPT for use in residual soils has long been questioned. Blight (1985) stated that the test may at most give a rough index to soil strength or compressibility. A survey by Brand and Phillipson (1985) showed that the cone penetration test (CPT) is fairly widely used in residual soils, mainly for shallow foundation and pile design. Detailed examination, however, by researchers such as Frank (1990) show that relationships exist among various insitu test methods, including the SPT, flat plate dilatometer test (DMT), and CPT, based on trends in penetration resistance and layer boundary recognition.

Cruz et al. (2004) presents research on residual soils from northern Portugal that suggest structural cementation inherited from the original weathered rock mass is responsible for the existence of an effective cohesive strength, among other things. DMT, CPT, and laboratory

triaxial tests were used to establish correlations for deriving shear strength parameters due to cemented structure by the Mohr-Coulomb criterion.

#### *2.1.4 Laboratory Testing*

Extensive laboratory testing has been performed by a number of researchers. One issue that is of constant concern is the quality of samples retrieved from field exploration. Mayne et al. (2000) presents brief summaries of selected test results from the Opelika National Geotechnical Experimentation Site near Spring Villa, Alabama. Specifically, index parameters, consolidation characteristics, and triaxial test behavior are discussed. Other types of laboratory tests on undisturbed samples of Piedmont residuum are said to have been reported but are not included within this report; permeability testing (Finke et al., 1999), direct shear testing (Vinson and Brown, 1997), and resonant column (Borden et al., 1996, Hoyos and Macari, 1999, Schneider et al., 1999).

Consolidation testing is one of the highly debated and unresolved issues of residual soil. Weathering and de-bonding from parent rock are a likely cause of the fact that the residual soils of the Piedmont typically show no specific preconsolidation stress. Inadequate sampling techniques are also believed to complicate the issue. Nevertheless, a quasi-preconsolidation effect is often seen from consolidation testing (Mayne et al., 2000). Mitchell and Sitar (1982) attributed the apparent preconsolidation pressure in residual soil to the presence of cementation, while Sowers and Richardson (1983) reasoned that it is the reflection of residual mineral bonds and unrelieved tectonic stresses. It could also, however, be attributed to desiccation (Wang and Borden, 1996).

Although the properties of residual soil have been somewhat thoroughly researched, limited research exists on the application of these properties in geotechnical design.

Conventional techniques of geotechnical design have inherent problems when applied to residual soil. According to Blight (1997b), even the conventional concept of a soil grain is inapplicable to many residual soils because the residuals often consist of aggregates of crystals that can break down and become progressively finer as the soil is manipulated. Therefore, what appears to be coarse, sandy gravel in the insitu state may deteriorate to a fine, sandy silt during the process of excavation, mixing, and compaction. Furthermore, Fourie (1997) discussed classification and index testing of residual soils and identified many problems. Some examples of these problems include false measurement of water content due to loss of water in crystallization (moisture within the structure of the minerals present in the solid particle) and decrease in liquid limit and plasticity index because of air-drying samples prior to testing—the latter of which was previously studied by researchers such as Terzaghi (1958), Rouse et al. (1986), and Townsend (1985).

## **2.2 Unsaturated Soil**

The study of unsaturated soil mechanics is a relatively new topic to geotechnical engineering. Although it has been a topic of interest for the past 50 years, the amount of research performed is not as exhaustive as other topics in geotechnical engineering. In fact, until recently, unsaturated soils were studied more heavily in agricultural and soil science disciplines. Nonetheless, unsaturated soils are encountered in almost every geotechnical design, and knowledge of the physical properties of these soils is necessary. In addition, when characterizing the strength of residual soil, a good knowledge of the unsaturated properties is necessary to delineate between the strength provided by negative pore water pressures versus the strength provided by the residual properties such as cementation and fabric structure.

### 2.2.1 State of Stress

Effective stress was defined by Terzaghi (1943) as the difference between the total stress and pore pressure (Equation 1). This has been widely accepted throughout the field of geotechnics.

$$\sigma' = \sigma - u \quad (1)$$

Bishop (1959) expanded on this theory by making provisions for stresses acting in the air phase of the soil, and the matric suction in the soil, suggesting that the effective stress in unsaturated soils should be represented as:

$$\sigma' = (\sigma - u_a) + \chi(u_a - u_w) \quad (2)$$

In this equation,  $u_a$  is the pore air pressure  $u_w$  is the pore water pressure, and  $\chi$  is the effective stress parameter which is generally a value between 0 and 1 (0 corresponding to completely dry soil, and 1 corresponding to saturated soil);  $(\sigma - u_a)$  is referred to as the net normal stress, and  $(u_a - u_w)$  as the matric suction.

Bishop's original treatment of effective stress for unsaturated soil has been challenged by several researchers (Lu and Likos, 2004). Jennings and Burland (1962) explored the limitations of Bishop's theory, suggesting that it may not be adequate for certain deformation phenomena, such as collapse. However, Khalili et al. (2004) opposed Jennings and Burland, stating that those deformations could indeed be described within Bishop's effective stress framework. The effective stress approach for unsaturated soil mechanics continues to be a subject of debate (Lu and Likos, 2004).

Coleman (1962) suggested the use of the net normal stress  $(\sigma - u_a)$  and the matric suction  $(u_a - u_w)$  as stress variables. This has been supported by Bishop in his subsequent research (Bishop and Blight, 1963), and by Fredlund (1973) and Fredlund and Morgenstern (1977).

### 2.2.2 Shear Strength

When excavations are made in unsaturated soil, apparent cohesion can exist due to the negative pressures (matric suction) in the soil. The shear strength of a saturated soil is defined by the Mohr-Coulomb failure criterion, and Terzaghi's effective stress concept (Terzaghi, 1936).

This is shown as:

$$\tau = c' + \sigma' \tan \phi' \quad (3)$$

Where  $\tau$  is the shear stress on the failure plane at failure,  $c'$  is the effective cohesion,  $\sigma'$  is the effective normal stress ( $\sigma - u_w$ ), and  $\phi'$  is the effective angle of shearing resistance. Figure 2 illustrates the Mohr-Coulomb failure criterion for saturated soils.

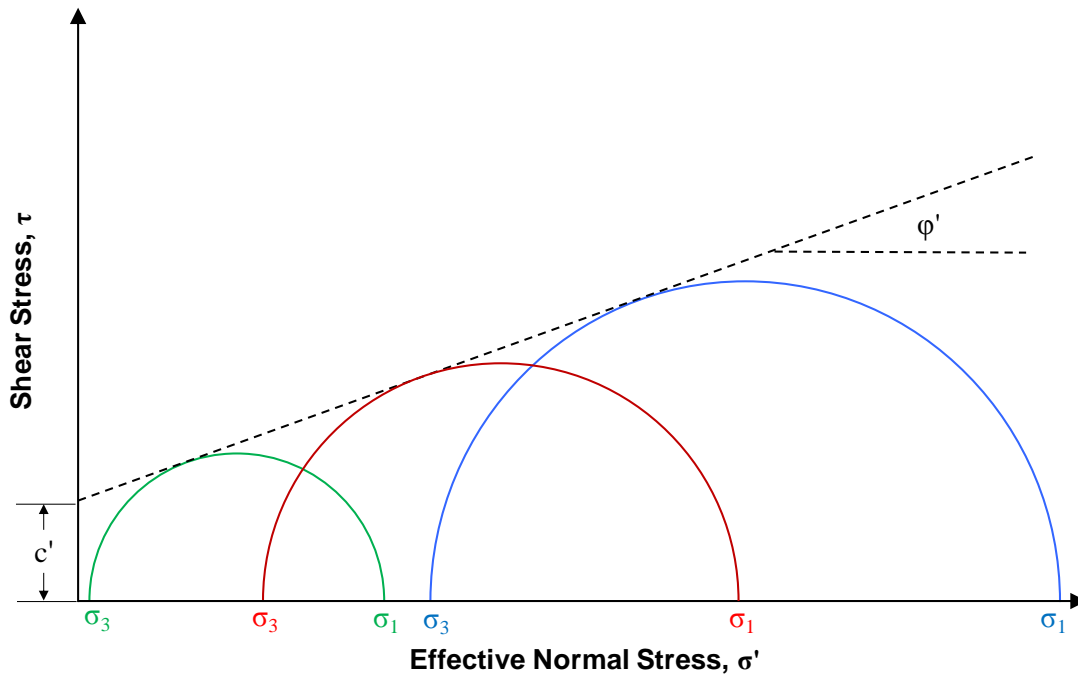
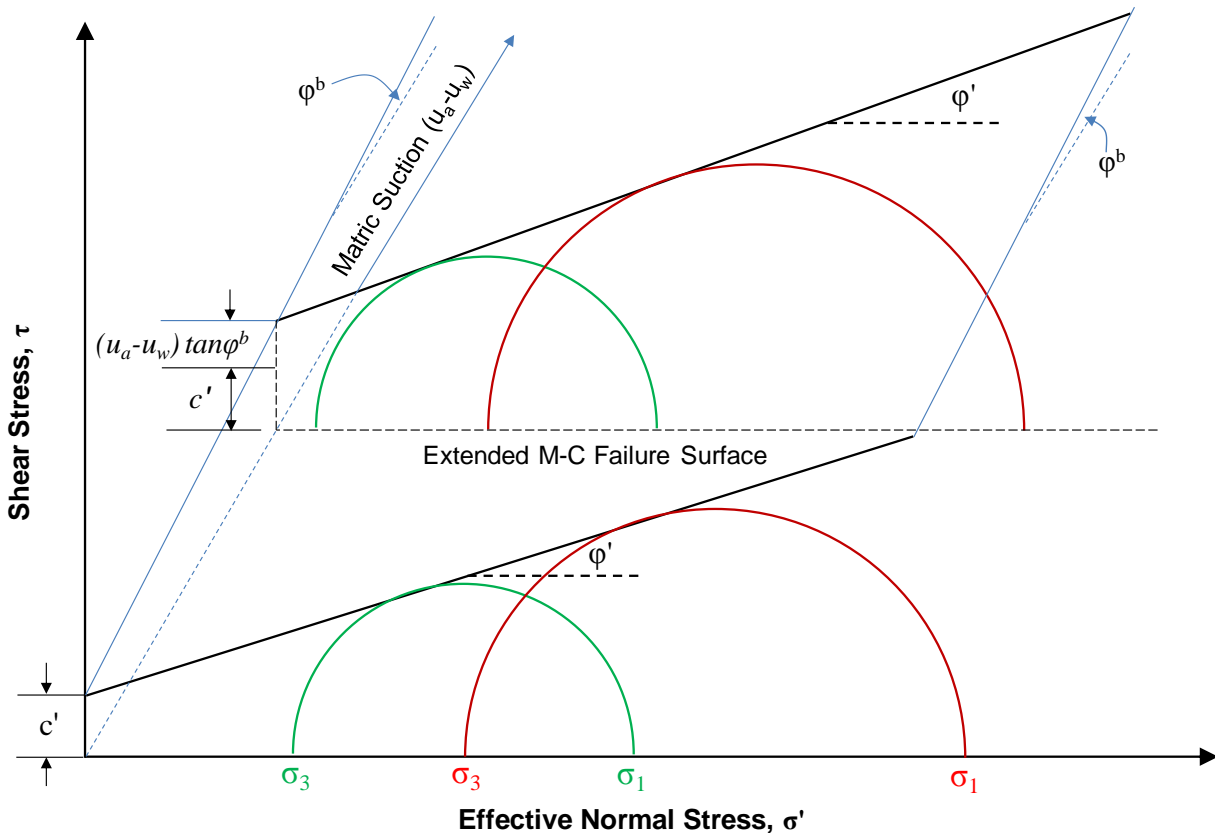


Figure 2 - Mohr-Coulomb failure criterion (Coulomb, 1776).

Fredlund et al. (1978) concluded that the shear strength of an unsaturated soil could be formulated in terms of independent stress state variables. This led to the development of the following equation for calculating the shear strength of unsaturated soils:

$$\tau = c' + (\sigma - u_a) \cdot \tan \phi' + (u_a - u_w) \cdot \tan \phi^b \quad (4)$$

Where:  $c'$  is the effective cohesion at zero matric suction and zero net stress,  $\phi'$  is the effective internal friction angle with respect to changes in  $(\sigma - u_a)$  when  $(u_a - u_w)$  is kept constant, and  $\phi^b$  is an angle that can be regarded as controlling an apparent cohesion which is related to levels of matric suction  $(u_a - u_w)$  in the sample. Further research by Lu and Likos (2006) has shown however that this approach is not valid over a wide range of saturations, because the increase in apparent cohesion with matric suction does not behave linearly as suggested by Fredlund et al. (1978), therefore this method is only valid for suction levels near saturation.



**Figure 3 - Extended Mohr-Coulomb failure criterion for unsaturated soil (Lu and Likos, 2004).**

Research conducted by Vaunat et al. (2006) supports the fact that the existence of negative pore pressure will result in higher strength properties of the soil. Although the increased strength is present, it is often not the practice of engineers to design using the

unsaturated shear strength. Fredlund and Rahardjo (1993) attribute this to the possibility of environmental changes that might cause a change in the matric suction of an unsaturated soil mass. In other words, a soil mass appears to be stronger initially, but over time the apparent cohesion (matric suction) may dissipate, causing a reduction in the strength of the soil mass.

This decrease in strength was seen in an investigation of a soil nail wall in Singapore. Research conducted by Wong et al. (1997) showed that over time, displacements in the nail wall increased due to seepage from rainwater into the soil causing the negative pore pressure to dissipate. Although this investigation proves this phenomenon, the properties of the soil itself are difficult to determine from this study alone, because the study was conducted on an earth retaining structure.

### *2.2.3 Characterization and Testing*

In order to test unsaturated soils using traditional laboratory methods, one of the most difficult tasks is to impose a known matric suction on the sample. Matric suction is defined as the difference between pore air pressure,  $u_a$ , and pore water pressure,  $u_w$ . Matric suction can be applied to a soil sample by applying a negative water pressure to the sample, but this approach of applying negative water pressure is limited by water cavitation to a maximum matric suction of 1 bar. Hilf (1956) introduced the axis translation technique to overcome this limitation. The axis translation technique has been widely used to control matric suction in unsaturated soil testing (e.g., SWCC determination using the pressure plate device). The axis translation technique consists of applying a positive air pressure ( $u_a$ ) and a less-positive or zero water pressure ( $u_w$ ), such that the sample is subjected to the desired matric suction ( $u_a - u_w$ ). Matric suction can be applied to a soil sample by imposing these air and water pressures at the boundaries of the sample, and allowing time for the pressures to equalize throughout the sample. The axis

translation technique assumes the shear strength of unsaturated soils is a function of two independent stress variables: net stress ( $\sigma - u_a$ ) and matric suction ( $u_a - u_w$ ) (Fredlund and Morgenstern, 1977). For these state variables, the shear strength of unsaturated soil is commonly represented by the extended Mohr-Coulomb shear strength envelope Shown in Equation 4 (Fredlund et al., 1978).

Several triaxial testing devices have been proposed and developed for unsaturated soils including Padilla et al. (2006), Wulfsohn et al. (1998), Thom et al. (2008), Cabarkapa and Cuccovillo (2006), Jotisankasa et al. (2007), Cui et al. (2007), and Sivakumar et al. (2006).

#### *2.2.4 Laboratory Testing*

Numerous methods have been developed to determine properties of unsaturated soils in the laboratory. However, the properties of unsaturated soils are more difficult to obtain than saturated soils. Fredlund (2006) stated that "one of the 'roadblocks' standing in the way of implementation of unsaturated soil mechanics has been the excessive cost and demanding laboratory testing techniques associated with the direct experimental assessment of unsaturated soil properties."

#### *2.2.5 Matric Suction*

Several methods have been devised to quantify negative pore pressures in the laboratory. Table 2 summarizes the various methods used to determine soil suction.

**Table 2 - Summary of techniques for measuring soil suction (Lu and Likos, 2004).**

Suction Component	Technique / Sensor	Practical Suction Range (kPa)	Laboratory / Field	References
Matric Suction	Tensiometers	0-100	Laboratory and field	Cassel and Klute (1986); Stannard (1992)
	Axis translation techniques	0-1.500	Laboratory	Hilf (1956); Bocking and Fredlund (1980)
	Electrical /thermal conductivity sensors	0-400	Laboratory and field	Phene et al. (1971a, 1971b); Fredlund and Wong (1989)
	Contact filter paper method	Entire Range	Laboratory and field	Houston et al. (1994)
Total Suction	Thermocouple psychrometers	100-8,000	Laboratory and field	Spanner (1951)
	Chilled-mirror hygrometers	1,000-450,000	Laboratory	Gee et al. (1992); Wiederhold (1997)
	Resistance capacitance sensors	Entire Range	Laboratory	Wiederhold (1997); Albrecht et al. (2003)
	Isopiestic humidity control	4,000-400,000	Laboratory	Young (1967)
	Two-pressure humidity control	10,000-600,000	Laboratory	Likos and Lu (2001, 2003b)
	Noncontact filter paper method	1,000-500,000	Laboratory and field	Fawcett and Collis-George (1967); McQueen and Miller (1968); Houston et al. (1994) Likos and Lu (2002)

One of the easiest and most inexpensive methods used is the filter paper method. Both the contact and the non-contact filter paper methods are described by ASTM Standard D5298. In this method, the total suction can be estimated by measuring the amount of moisture that is transferred from the soil to the filter paper.

A more accurate device for determining soil suction is the pressure plate device (ASTM D6836). The device consists of a steel pressure vessel with a high air entry ceramic plate inside, or a cellulose membrane. In this method, negative pressure can be measured for samples that are in contact with a HAE disk. Since the matric suction is the difference between the pore air, and the pore water pressure for a sample, the HAE disk allows the measurement of the pore water pressure of the sample by not allowing air to pass through the disk. The pore air pressure can be regulated, and is equal to the pressure in the chamber.

### *2.2.6 Shear Strength*

Shear strength testing of unsaturated soil is most commonly performed in the laboratory using an unsaturated triaxial testing device. An unsaturated triaxial testing device is similar to a traditional triaxial testing apparatus, with the addition of a HAE disk which allows a matric suction to be imposed on the specimen, and some type of device to measure the volume change of the specimen during testing. Several devices for measuring the volume change of the specimen include dual cell systems where the cell fluid is used to determine volume change, mechanical belts that are placed on the specimen to determine the diameter while testing, and digital imaging techniques.

Triaxial procedures and apparatuses for unsaturated soils have been devised by Padilla, et al. (2006), Wulfsohn et al. (1998), and Cabarkapa and Cuccovillo (2006). In addition to these, Leong, et al. (2003), Macari et al. (1997), and Gachet et al. (2007) all performed research on methods to determine volume change during a triaxial test. Cyclic loading, and multistage testing procedures have been researched by Ho and Fredlund (1982), and Sivakumar et al. (2006).

Currently one of the most widely accepted methods for unsaturated triaxial testing is a method developed by Cabarkapa and Cuccovillo (2006), where internal LVDTs and a radial strain belt are used to determine the volume change of the specimen. This method has proven to be accurate, but the greatest hindrance is the initial cost of the equipment.

### *2.2.7 Insitu Testing*

Few insitu soil tests have been devised specifically for unsaturated soils. However, unsaturated soil behavior can have an impact on insitu tests that are conducted in the vadose zone. Negative pore pressure in soil affects the strength, deformation, and flow properties of the

soil, which will in-turn affect the data collected from an insitu soil test. For example, an SPT test is likely to have higher blow counts in an area where there is a large amount of negative pore pressure in comparison to a similar soil that is fully saturated. In order to accurately assess the results of such tests, a knowledge of unsaturated soil behavior is necessary.

Several methods have been used to quantify negative pore pressure insitu. Gasmol et al. (1999) measured the negative pore pressure using tensiometers which comprised of a water filled plastic tube with a high air entry ceramic cup sealed at one end and a vacuum pressure gage and a jet-filled cup sealed at the other end (Cassel and Klute, 1986). Thermal conductivity sensors have also proven to be useful in determining the matric suction of soil (Fredlund et al., 2000). Zahn et al. (2006) used both methods to determine negative pore pressure in an unsaturated expansive soil slope in China.

Previous attempts at defining soil-water characteristic curves (SWCC) in residual soil have proven to be cumbersome and time consuming due to the heterogeneous nature of residual soil and its high susceptibility to disturbance. For this reason, Agus et al. (2001) suggested empirical parameters that could be used to estimate SWCC. Agus et al. (2001) and Aung et al. (2001) also evaluated the impact of weathering and porosimetry on the SWCC in residual soils.

Insitu measurements of soil-water relationships have been conducted by numerous researchers in the past including Nielsen et al. (1973), Dane and Hruska (1983), Greminger et al. (1985), and Paquet et al. (1993). One of the benefits of insitu SWCC determination is that soil water relationships can be measured with minimal sample disturbance. Various researchers such as Box and Taylor (1962), Campbell and Gardner (1971), Miller et al. (2002), Zhou and Yu (2005), and Ng and Pang (2000), concluded that the SWCC can be affected by numerous parameters including the bulk density, void ratio, initial moisture content, and stress state,

indicating that traditional laboratory test methods may introduce significant error due to the disturbance involved with sampling and preparing laboratory samples. Because of these findings, laboratory devices have been developed that allow the SWCC to be measured at various stress states. Malicki et al. (1992) developed a method of determining the soil-water characteristics within a core sample tube. Devices were also developed by Ng and Pang (2000), and Padilla and Perera (2005) which allow the simulation of confining pressure while determining the SWCC. Although substantial research has been performed on determining the SWCC of soil insitu, it is still an area full of challenge and worth studying further as changes in technology lead to the enhancement of equipment and sensors.

#### *2.2.8 Full Scale Field Testing*

Although many full-scale field tests have been conducted in unsaturated soils, few have had an objective of developing a relationship between the unsaturated properties of the soil, and the physical characteristics of the soil (strength, flow, and deformation properties). Gasmol et al. (1999) conducted full scale field tests while measuring unsaturated behavior by instrumenting an unsaturated residual soil slope in Singapore. Zahn, et al. (2006) instrumented an unsaturated expansive soil slope in Zaoyang China to determine the effect of negative pore pressure on slope stability. Similarly, Mariappan (2010) studied the unsaturated behavior of a residual soil slope in Malaysia where landslides are common. Wong et al. (1997) also monitored an instrumented soil nail wall in Singapore and related a decrease in soil strength to the dissipation of negative pore pressure.

### **2.3 Lateral Earth Pressure Theory**

Historically, the magnitude and effect of lateral forces on structures and components of structures, whose major design function is to resist lateral forces, represents one of the earliest

structural problems to be studied analytically by engineers. The magnitude of lateral earth pressure that can exist or develop in a soil mass is related to the strength and stress-strain properties of the material and the deformations that occur within the mass as a result of lateral movement (McCarthy, 2002).

There are three categories of lateral earth pressure—*earth pressure at rest*, *active earth pressure*, and *passive earth pressure*. Earth pressure at rest ( $P_0$ ) refers to lateral earth pressure caused by an unyielding retaining structure that does not experience any lateral movement. If a wall is permitted to move away from the retained soil mass a slight distance, the soil will expand laterally following the wall. Shearing resistance developed within the soil mass acts opposite to the direction of the expansion, resulting in a *decrease* in lateral earth pressure. The minimum lateral earth pressure is the active pressure ( $P_a$ ). Conversely, if a wall moves into the retained soil mass, the soil will be compressed laterally with the soil shearing resistance acting to oppose the lateral compression. The maximum lateral earth pressure condition is the passive pressure ( $P_p$ ).

The ratio of horizontal stress to vertical stress in a soil mass is referred to as the coefficient of lateral earth pressure,  $K$ . For the *at rest* condition in which no lateral deformation is allowed, the earth pressure coefficient is designated  $K_0$ . For the *active* pressure condition in which the retaining wall moves away from the backfill, the earth pressure coefficient is designated  $K_a$ . For the *passive* pressure condition in which the retaining wall is moved into the backfill, the earth pressure coefficient is designated  $K_p$ . Therefore, the lateral stress acting on an earth retaining structure can be calculated using the following equation, where  $K$  is the appropriate earth pressure coefficient depending on field conditions:

$$\sigma_h = K\sigma_v \quad (5)$$

Classically, the values of earth pressure that control the design of retaining structures are determined based on Rankine (Rankine, 1857), Coulomb (Coulomb, 1776), or logarithmic-spiral (Coulomb, 1776) theory. Each method uses certain assumptions, and some methods have limitations. When designing earth retaining structures, it is important to use the earth pressure model that best suits the application in the field.

### 2.3.1 Rankine Lateral Earth Pressure Model

The Rankine theory (Rankine, 1857) for determining lateral earth pressure is based on several assumptions, the most important being that there is no adhesion or friction between wall and soil. Pressures computed from Rankine theory are limited to vertical walls and failure is said to occur in the form of a sliding wedge along an assumed failure plane which is a function of the friction angle of the soil. The equations derived from these assumptions are widely used for the design of earth retaining structures; however, the results may differ appreciably from other more fundamentally accurate analyses. Results obtained from the Rankine method generally are slightly more conservative, resulting in an additional factor of safety.

The Rankine earth pressure model is illustrated in Figure 4. The equation for the magnitude of the resultant lateral force,  $P_a$ , in the active pressure case is given as:

$$P_a = \frac{1}{2}(H - z_c)(\gamma H K_a - 2c\sqrt{K_a}) \quad (6)$$

Where:

$$K_a = \tan^2\left(45 - \frac{\phi'}{2}\right) \quad (7)$$

$$z_c = \frac{2c}{\gamma\sqrt{K_a}} \quad (8)$$

The resultant force is said to act at  $H/3$  from the base of the wall. The value for  $K_a$  is derived based on assumptions made by the Rankine theory.

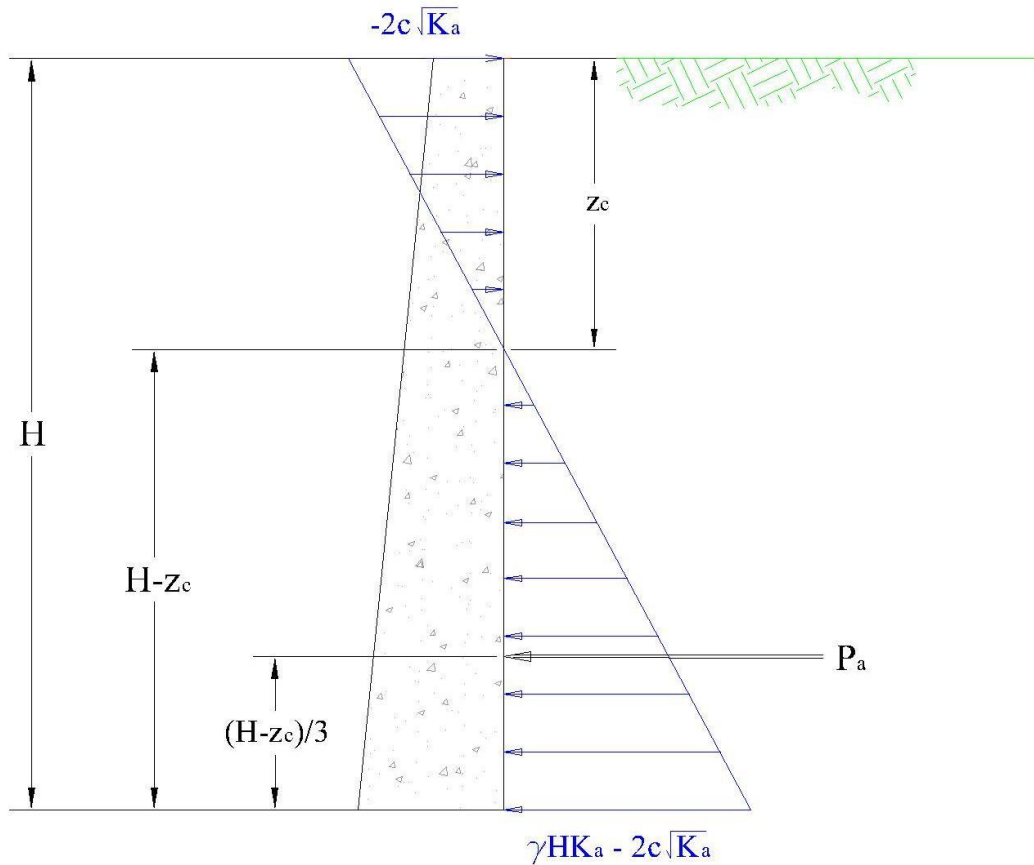


Figure 4 – Rankine earth pressure theory (Rankine, 1857).

### 2.3.2 Coulomb Lateral Earth Pressure Model

Coulomb's theory (Coulomb, 1776) for lateral earth pressure resulting from a retained mass of cohesionless soil considers that a failure wedge forms behind the wall by sliding along a plane. As the retaining structure moves away from the soil mass, lateral expansion is permitted and results in a relative movement between the wall and soil causing friction to develop on the back face of the wall (McCarthy, 2002). And so Coulomb, like Rankine, assumed that the failure surface due to lateral earth pressure would be a plane. The key difference in these two theories, however, is that Coulomb took into account friction between the backface of the wall and retained soil. For Coulomb's method, the resultant of this friction and lateral pressure,  $P_A$ , acts at

an angle,  $\psi$ , measured normal to the backface of the wall. When the failure wedge is satisfactorily retained by the wall, the forces acting on the wedge are in equilibrium. Therefore, when the unit weight,  $\gamma_t$ , and friction angle,  $\phi$ , for a retained soil are known, the force imposed on the wall as a result of the active pressure wedge,  $P_A$ , can be determined by vector addition, as shown in Figure 5. This force can also be calculated using the following equation:

$$P_A = \frac{1}{2}\gamma_t H^2 K_A = \frac{1}{2}\gamma_t H^2 \left[ \frac{\cos^2(\phi - \theta)}{\cos^2 \theta \cos(\delta + \theta) \left[ 1 + \sqrt{\frac{\sin(\delta + \phi)\sin(\phi - \alpha)}{\cos(\delta + \theta)\cos(\theta - \alpha)}} \right]^2} \right] \quad (9)$$

Similarly, the force imposed by the passive earth pressure wedge,  $P_p$ , can be calculated for the Coulomb case using the following equation:

$$P_p = \frac{1}{2}\gamma_t H^2 K_p = \frac{1}{2}\gamma_t H^2 \left[ \frac{\cos^2(\phi + \theta)}{\cos^2 \theta \cos(\delta - \theta) \left[ 1 - \sqrt{\frac{\sin(\delta - \phi)\sin(\phi + \alpha)}{\cos(\delta - \theta)\cos(\theta - \alpha)}} \right]^2} \right] \quad (10)$$

The actual active pressure condition for a given wall results from a unique failure wedge that provides the largest numerical value for the force  $P_A$ . But the above equation is only true for a uniform slope of soil backfill and where the back of the retaining wall is a plane surface. If this is not true, the proper  $P_A$ -value can be determined by trial-and-error procedure of analyzing a series of different sized failure wedges (McCarthy, 2002).

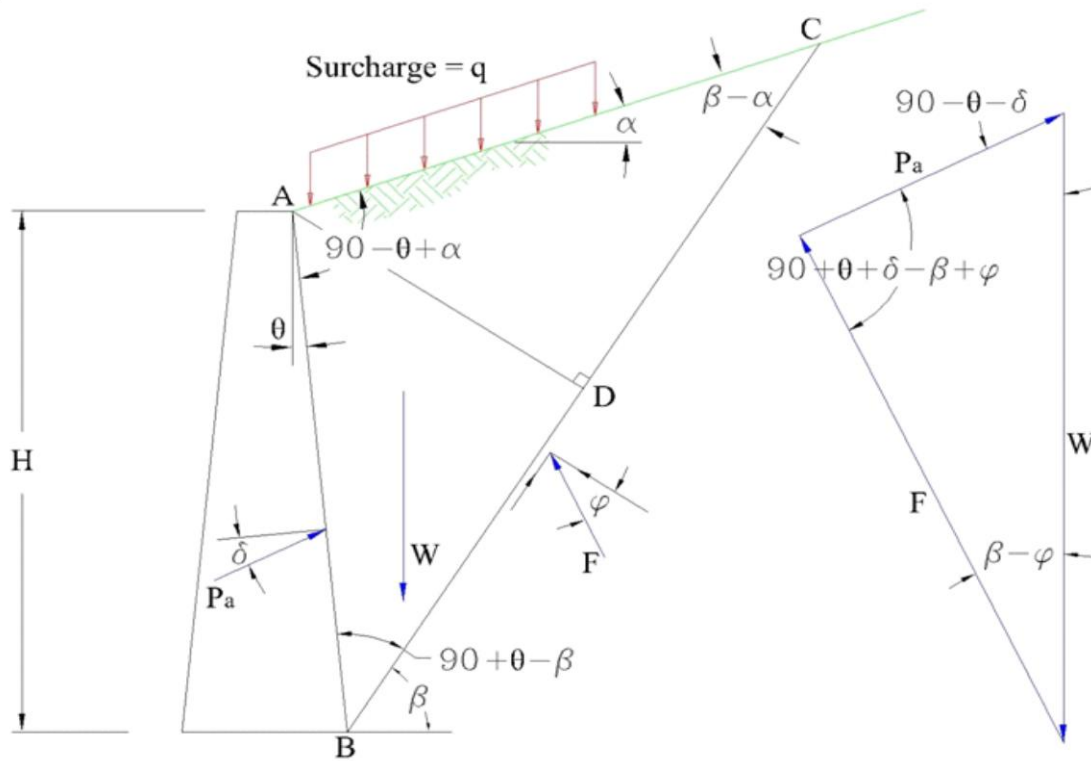


Figure 5 – Coulomb earth pressure theory (Coulomb, 1776).

When the retained soil mass has both cohesion and friction, the vector addition representing equilibrium forces acting on the failure wedge must include the total cohesive resistance,  $cL$ , acting on the failure plane.

Because the Coulomb theory assumes a planar failure, whereas the actual failure surface is typically curved, the lateral force calculated is slightly low. This discrepancy is typically minor, and so the Coulomb procedure for active pressure determination provides a practical accuracy. The value of  $P_A$  computed from the Coulomb method will be slightly larger than that of the Rankine method, but due to the difference in direction that these forces act, the Rankine method typically creates the more severe condition and results in a slightly more conservative value (McCarthy, 2002).

### 2.3.3 Logarithmic Spiral Lateral Earth Pressure Model

The logarithmic spiral method for calculating earth pressure assumes a failure surface that is a logarithmic spiral curve and becomes tangent to a vertical line at the backfill surface. The earth pressure on the wall, per unit of length, is designated by  $P_a$  to distinguish it from the active earth pressure  $P_A$  exerted by a similar mass against a retaining wall of height  $H$ . The upper part of the sliding wedge cannot move laterally, and therefore must intersect the ground surface at a right angle. The corresponding curve of sliding can be closely approximated by a logarithmic spiral having the following equation:

$$r = r_0 e^{\theta \tan \phi} \quad (11)$$

The center of the spiral is located on a straight line that passes through  $d$  and makes an angle  $\phi$  with the horizontal. The resultant earth pressure acts at an angle  $\delta$  to the horizontal because of the downward movement of the failure wedge. Theoretical investigations have shown the point of application of the earth pressure is determined by the shape of the sliding surface. For a curve similar to that seen in Figure 6(B), theory indicates that the pressure distribution is roughly parabolic and the elevation of the point of application,  $n_a H$ , lies between  $0.45H$  and  $0.55H$ . This theoretical conclusion has been confirmed by pressure measurements in full-sized tests (Terzaghi and Peck, 1948).

The position of the sliding surface may be determined by first selecting an arbitrary point,  $d_1$ , along the horizontal upper edge of the cut. A logarithmic spiral is then traced through the bottom of the cut,  $b$ , with its center on line  $d_1 D_1$ . The reaction  $F_1$  on the sliding surface passes through the center  $O_1$ . Taking moments about  $O_1$  we obtain

$$P_1 = \frac{W_1 l_w}{l_a} \quad (12)$$

A similar computation is made for  $d_2, d_3 \dots$  and by plotting the corresponding values  $P_1, P_2 \dots$ , etc., as ordinates above  $d_1, d_2 \dots$ , the curve  $P$  is obtained (Figure 6 – Logarithmic spiral theory). The active earth pressure  $P_a$  is equal to the maximum ordinate,  $C$ . For a preliminary estimate of  $P_a$  it is sufficiently accurate to assume (Terzaghi and Peck, 1948)

$$P_a = 1.1P_A \tag{13}$$

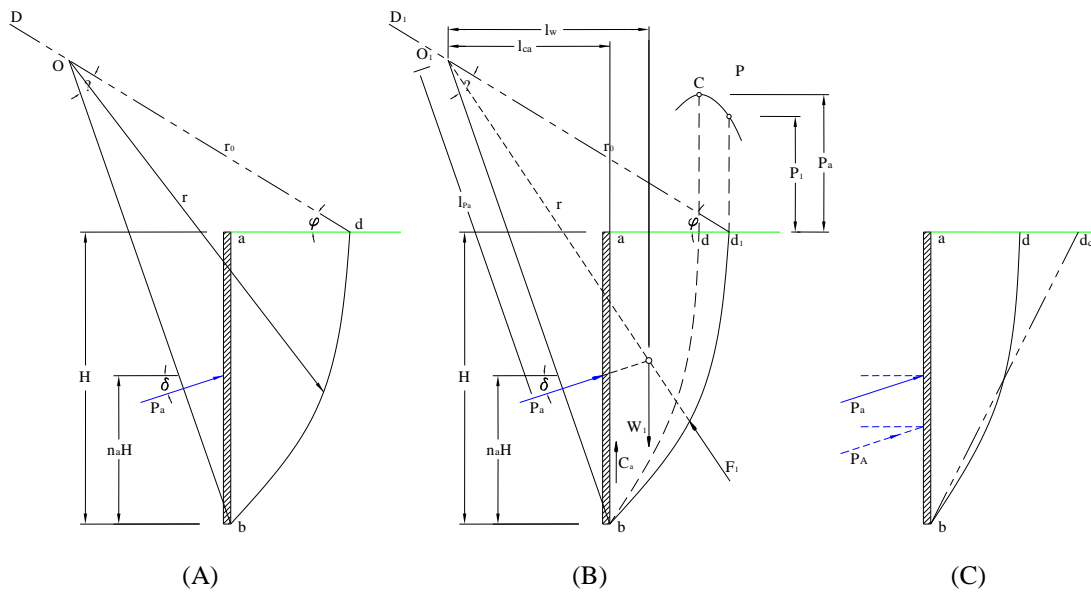


Figure 6 – Logarithmic spiral theory.

### 2.3.4 Soil Structure Interaction Approach

Given that Rankine and others have provided a convenient method for determining the lateral earth pressure, in any case, the soil mass must translate to achieve the minimum active pressure. If the soil mass does not translate one of two cases develop: either the at-rest pressure dominates or there is no lateral earth pressure on the structure. The soil structure interaction approach (SSI) can take this effect into account. Furthermore, this method allows for the beam behavior of the wall element to be included.

The most popular application of the SSI approach is for laterally loaded piles. Lymon Reese (Wang and Reese, 1993) popularized the solution of the differential equation governing the response of a pile under lateral load in the software, COM624. The soil in this case was reduced into a set of nonlinear slip springs connected to nodes on the pile. The pile was treated as a bending element. The response curves (p-y curves) represent a combination of active, passive, and shearing stresses on a single pile.

In the simplest case, a p-y curve can be a bilinear function with the slope  $k$  and a limiting value of lateral resistance  $P_u$ . The  $P_u$  in this case would be the sum of the components mentioned previously. The rate at which the resistance builds with deflection would be represented by the horizontal subgrade modulus  $k$ . Figure 7 shows a simple p-y relationship. In addition to using such a simple model, experimental studies by Wang and Reese (1993), O'Neill and Murchison (1983), and O'Neill and Gazioglu (1984) have yielded experimental p-y curves for traditional soils. Comparative curves by Reese et al. (1974) and O'Neill and Gazioglu (1984) for the same soil are shown in Figure 8. In addition, work by Robertson et al. (1985) and Robertson et al. (1989) resulted in additional p-y curves based on insitu tests.

The SSI method has been incorporated into two computer programs for the analysis of flexible retaining structures. CWALSSI, produced by the Computer Aided Structural Engineering group of the United States Army Corps of Engineers, uses the simpler model with  $k$  and  $P_u$ . Ensoft has adapted their LPILE software, the commercial version of COM624 to retaining structures in a program called PYWALL. This program uses the more advanced experimental p-y curves.

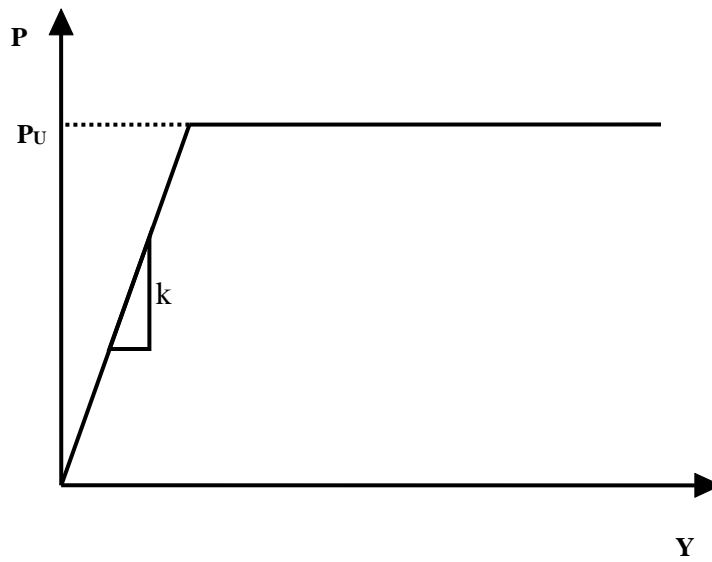


Figure 7 – Simple p-y relationship.

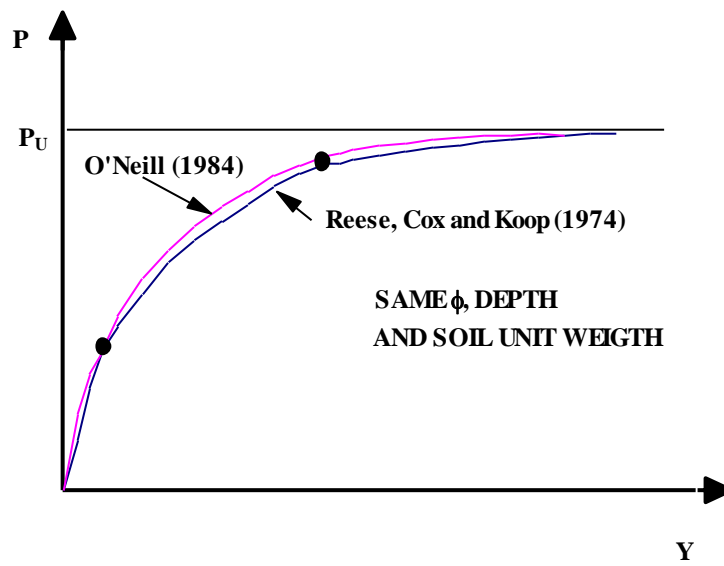


Figure 8 – Experimental p-y curves from literature.

### *2.3.5 Finite Element Method*

The finite element method (FEM) is often used in the analysis of complicated geotechnical problems where deformations related to applied stresses and vice versa are important. In addition, it provides a rational method of attacking problems that were solved classically by rote assumption of elastic conditions or infinite half spaces.

The FEM is a way to solve partial differential equations (PDEs) numerically. Extended to civil-structural-geotechnical problems, the PDEs arise from complex elemental shape functions, the determination of strain from stress, and constitutive models that incorporate viscosity, plasticity, and pore fluid dynamics.

A simpler perspective is that the finite element method is essentially a complicated way of expressing Hooke's Law. A model is developed where either forces or displacements are imposed on boundaries. The resulting displacements and stresses are determined based on the shape functions and constitutive models selected.

Traditionally, FEM codes are complicated and usually require extensive training and years of practice to develop a level of utility. In terms of retaining structures, a major benefit of an FEM analysis is the simulation of staged construction. Since the wall will not be magically placed into the ground as the entire soil mass is excavated, the transient stress and displacements of the wall during installation may be important or critical. The elemental division of the soil mass enables a more realistic stratification of soil layers while the physical wall structure and any inclusion can be simulated within the plane strain framework.

### *2.3.6 Case Studies*

Although the Rankine and Coulomb theories have resulted in successful earth retaining structure design, the calculated earth pressures can be quite different from the actual earth

pressure depending on the soil fabric structure and layered system. In many cases, these theories over-predict the values for earth pressure, leading to designs that are over-conservative.

Researchers such as Peck (1969) and Clough and O'Rourke (1990) have investigated retaining wall pressure and earth movements created by excavations. Other case studies of worldwide experience are also presented by Long (2001).

In addition, studies seeking to determine lateral earth pressures have been presented by researchers like Fang et al. (1994) who utilized a movable model retaining wall to study passive pressures. The same moveable retaining wall was presented by Fang et al. (1997) to study the effect of sloping backfill on earth pressures. Similarly, Georgiadis and Anagnostopoulos (1998) used a model cantilever sheet pile wall to study surcharge effects. Both studies dealt with carefully placed sand backfill in a controlled environment, but there are no known models in existence using residual soils as backfill. This is probably due to the fact that it is difficult to obtain and use residual soil samples without disturbing the fabric and particle bonds.

Full scale tests of earth retaining structures have been rare. Kort (2002) presents a study carried out on an anchored sheet pile wall in Rotterdam, Holland, where instrumented sheet piles were used to support an excavation in a full scale test. The soils were predominantly weak clay and peat, and the study was concerned with oblique bending and plastic hinging of sheet piles.

## **2.4 Slope Stability Analysis**

Evaluating the stability of slopes is a challenging aspect of civil engineering. According to Duncan and Wright (2005), the study of slope stability has driven some of the most important advances in our understanding of the complex behavior of soils, as well as the changes in soil properties that can occur over time, and the limitations of laboratory and insitu testing for evaluating soil strengths. In many cases, these advances in our understanding of soil properties

and behavior were derived from the evaluation of slope and embankment failures throughout history.

In addition to slopes, slope stability analysis also contributes to the safe design of excavations, embankments, earth dams, landfills and stockpiles (Abramson et al., 2002). Numerous methods have been developed for the analyses of slope stability, each having their own set of capabilities and limitations.

#### *2.4.1 Limit Equilibrium Analysis*

Limit-equilibrium analysis is the study of the point at which a material has reached the limit of its stability using the concept of yield criteria and the associated flow rule in the stress strain relationship (Allaby and Allaby, 1999). This analysis is commonly used in geotechnical engineering to assess the stability of slopes and embankments by analyzing sections in plain strain conditions. Numerous methods exist for the limit equilibrium analysis of slopes. Some of the first methods to be developed include the Swedish Circle Method (Fellenius, 1922), and The Ordinary Method of Slices developed by Fellenius (1927). Many of the methods are modeled after the Fellenius (1927) method and usually involve breaking the soil mass down into individual slices for evaluation. Figure 9 illustrates the general procedure for the method of slices approach.

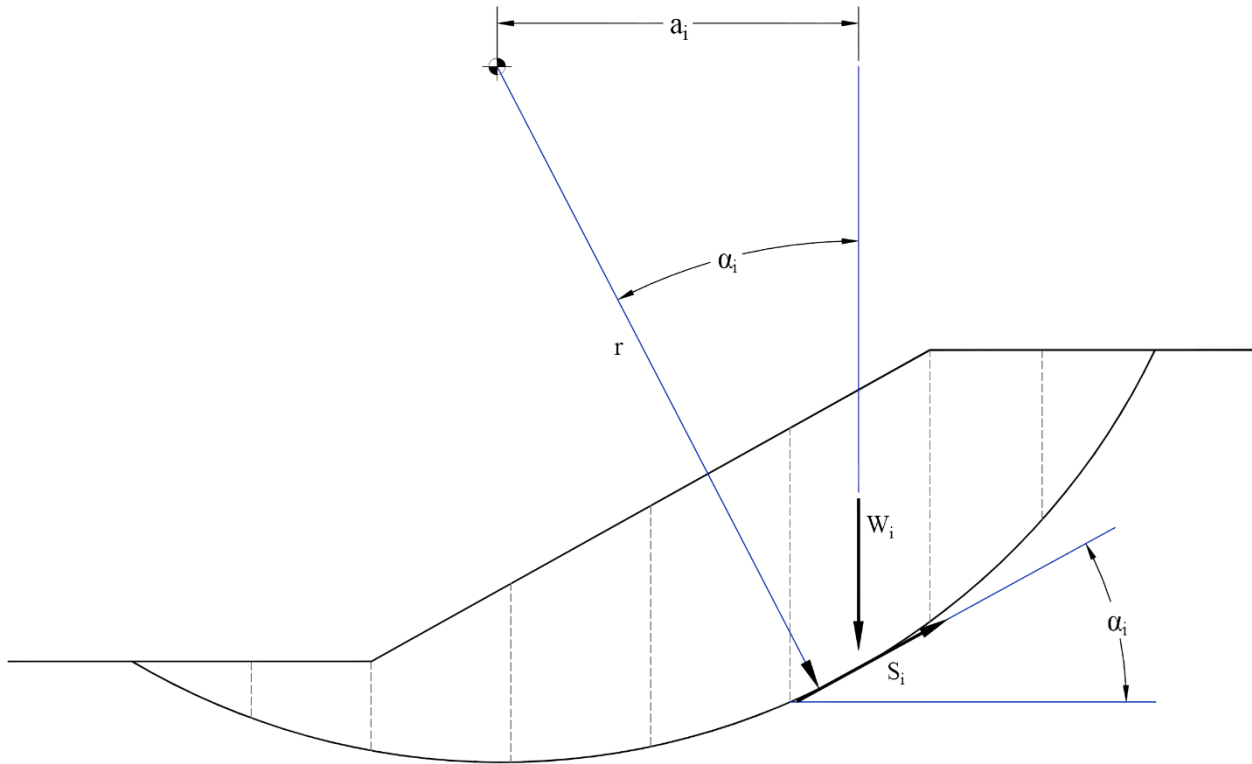


**Figure 9 – Method of slices illustration (Duncan and Wright, 2005).**

Each method has a specific set of assumptions, and they therefore vary in the complexity and accuracy of the calculation. Many of the simplified methods ignore side friction and other forces on the slices therefore resulting in a more conservative result. Table 3 lists some of the most popular limit equilibrium analysis methods, and states the assumptions for each.

**Table 3 – Limit equilibrium procedures and assumptions (Duncan and Wright, 2005).**

Procedure	Assumptions
Infinite Slope	A slope of infinite extent; slip surface parallel to slope face.
Logarithmic Spiral	The slip surface is a logarithmic spiral.
Swedish Circle ( $\varphi = 0$ )	The slip surface is circular; the friction angle is zero.
Ordinary Method of Slices	The slip surface is circular; the forces on the sides of the slices are neglected.
Simplified Bishop	The slip surface is circular; the forces on the sides of the slices are horizontal (i.e. there is no shear force between slices)
Spencer	Interslice forces are parallel; (i.e. all have the same inclination). The normal force ( $N$ ) acts at the center of the base of the slice (typically)
Morgenstern and Price	Interslice shear force is related to interslice normal force by $X = \lambda f(x) E$ ; the normal force ( $N$ ) acts at the center of the base of the slice (typically).
Chen and Morgenstern	Interslice shear force is related to interslice normal force by $X = [\lambda f(x) + f_o(x)]E$ ; the normal force acts at the center of the base of the slice (typically).
Sarma	Interslice shear force is related to the interslice shear strength ( $S_u$ ) by $X = \lambda f(x) S_u$ ; interslice shear strength depends on shear strength parameters, pore water pressures, and the horizontal component of interslice force;
Force Equilibrium (Lowe and Karafiath, Simplified Janbu, Corps of Engineer's Modified Sweedish, Janbu's GPS procedure)	The inclinations of the interslice forces are assumed; assumptions vary with procedure.

Numerous computerized programs have been developed to aid in such analyses, because although the methods are possible to be solved by hand, thorough analyses can take a considerable amount of time. This is because often, large numbers of faces need to be evaluated to locate the critical slip surface. Also, complex geometries could result in an analysis with large numbers of slices to be calculated for each slip surface. In this study, the software program Slope/W by Geo-Slope (2012) was used. This software is capable of performing all of the common limit equilibrium methods as well as finite element analysis for slopes.

#### *2.4.2 Finite Element Analysis*

The finite element method (FEM) is often used to analyze complex problems and find approximate solutions of partial differential equations and integrations that cannot be solved analytically. In order to apply a FEM, the soil mass is broken down into elements, and properties at each node (point between the elements) are determined by solving a governing equation for the soil properties, and applying boundary conditions (Fredlund and Rahardjo, 1993).

The finite difference method (FDM) is a discretization method of approximating the solution of ordinary and partial differential equations by replacing derivative expressions with equivalent difference quotients (Daintith, 2004). The FDM is similar to the FEM but can have more limitations with respect to the boundary conditions that can be applied in a model. Because of these limitations the FDM is more commonly used in unsaturated soils for one dimensional problems.

#### *2.4.3 Case Studies*

There has been substantial research published on case studies of slope failures in various soil types throughout the world. Some of those most relevant to the research presented in this paper include Jiru (2002), who used finite element modeling to simulate a failure of a slope excavation in clay soil. This model focused on deformation behaviors, and the formation and evolution of the failure surface. Gasmo et al. (1999) instrumented an unsaturated residual soil slope in Singapore, and Zahn, et al. (2006) instrumented an unsaturated expansive soil slope in Zaoyang China, both with the goal of determining the effects of negative pore pressure on slope stability. Additionally, Lim et al. (1996), Gasmo et al. (2000), Chen and Chen (2001), Cho and Lee (2001), Tsaparas et al. (2003), Rahardjo et al. (2005), Huat et al. (2006), Trandafir et al. (2007), and Mariappan (2010) all studied the effects of rain fall on matric suction in residual soil

slopes, and Ng et al. (2003) used artificial rainfall infiltration to test the performance of an unsaturated expansive soil slope. El-Ramly et al. (2005) performed an analysis of a failure that occurred in a residual soil cut slope (Shek Kip Mei cut) in Hong Kong. In this study, a probabilistic analysis methodology was developed in attempt to quantify uncertainties in shear strength of granitic soils.

## **2.5 Other Relevant Research**

### *2.5.1 Stand Up Time and Excavation Failure*

Kovacevic et al. (2007) used finite element analysis to predict the stand-up time of temporary clay slopes in London. Dunlop and Duncan (1970), and Burland et al. (1977) have studied the development process for failure in excavations of various depths in clay soils. More recent research by Leroueil (2001) has shown the importance of water on the failure of natural slopes and cuts of various soil types. Atkinson and Mair (1981), and Eisenstein and Samarasekera (1992) have performed research with similar goals pertaining to tunneling in soft ground. Additionally, DiBiagio and Myrvoll (1972), Aas (1976), and Tsai and Chang (1996) have studied the stability of slurry trench excavations in various types of soil, and Tsai et al. (2000) performed a full scale experiment on a diaphragm wall trench in sandy soil. A finite element simulation and stability assessment was performed by Jiru (2002) on slope excavations in clay, and Harp et al. (1990) studied pore pressure responses during pore water pressure induced failures of natural slopes.

### *2.5.2 Trenching and Excavation Safety*

In addition to civil engineering publications, various documents exist pertaining to trench and excavation failures in the construction industry. The U.S. Department of Labor, Occupational Safety and Health Administration (OSHA) 29 CFR Part 1926 Subpart P specifies

the requirements for safety precautions needed while performing trenching and excavation activities. Other standards for trenching and excavation safety include the Army Corp of Engineers, EM 385, the American National Standards Institute (ANSI) ASSE A10.12-11998 (R2010), and the National Institute for Occupational Safety and Health (NIOSH) DHHS Publication Number 2006-133D. These documents provide minimal standards in which a trench or excavation may be considered safe for entry. Although specific references are not listed for the means of determining the minimal standards for excavation safety in these documents, it is understood that some of the information is derived from private research performed by shoring manufacturers, as well as historical data from accident investigations in which fatalities occurred as a result of trench failure. Stanevich and Middleton (1988), and Toyosawa et al. (1993) are examples of publications that were made as a result of fatal accidents caused by trench failure. In addition, Cheng et al. (2002) developed an automated instrumentation system to assess the safety of excavations on construction sites in real time, which would help identify potential unsafe conditions before injury or death occur.

### **CHAPTER 3: BACKGROUND**

The origin of this project was directly influenced by a similar project, where instrumented sheet pile walls were used in attempt to measure the lateral earth pressure induced by residual soil (Anderson et al., 2004, Anderson and Ogunro, 2004, and Burrage, 2007). In this experiment, the final analysis determined that very little earth pressure (if any) was transferred to the sheet pile walls, and that a six meter tall soil embankment would have stood vertical without any shoring. However, due to the schedule for the property use, as well as safety, the excavation was only able to remain open for several days, which led to questionable results as far as the strength that might have been developed by negative pore pressures during excavation. As a result, it was decided that a similar excavation should be made (without shoring) in such a manner that it could remain open for as long as necessary to determine that the observed behavior was a result of the strength of the residual soil itself, and not a result of temporary pore pressures that were induced by the excavation process.

The goals of this experiment remained the same as Anderson et al. (2004), which was to (1) determine the impact that unique residual soil properties (i.e. fabric structure and cementation) have on the behavior of the soil, and (2) determine if these properties can be detected in common laboratory test methods (specifically the CD triaxial test), and implemented into a design method. In doing so, the overall goal was to maximize efficiency and safety of geotechnical designs in residual soil.

## CHAPTER 4: SITE INFORMATION

Due to the nature of the project and the concern for safety, the Auburn National Geotechnical Experimentation Site (NGES) located in Opelika, Alabama was selected to construct the test excavations and perform the in depth investigation. Figure 10 shows a vicinity map of the Auburn NGES. This site provided several benefits that made it ideal for this type of study. The main benefit is that the site has restricted access, with security fencing and surveillance to minimize the chance for disturbance and / or safety hazards. Another benefit was that since the site has been used for multiple research projects in the past, the Auburn NGES is a highly characterized site with multiple references for soil properties and characterization data.

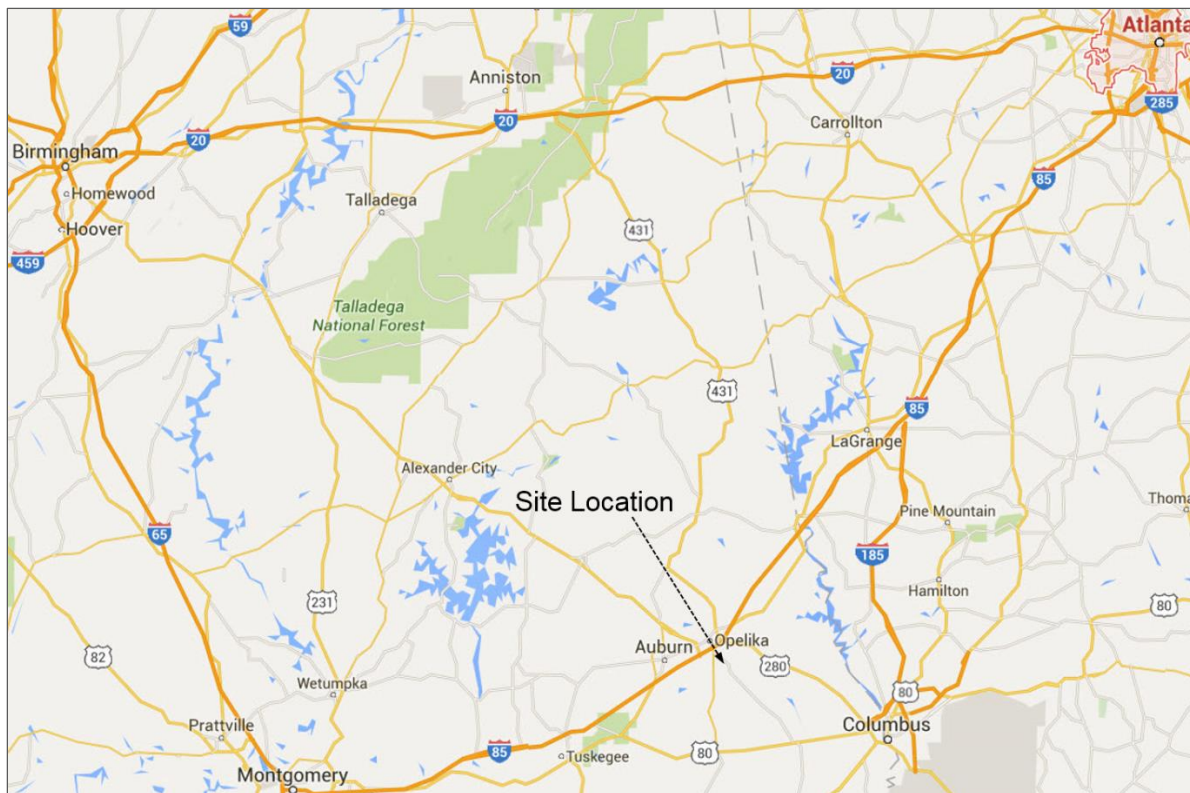


Figure 10 - Vicinity map (Google Maps, 2012).

The Auburn NGES is located in Lee County, Alabama which is at the south end of the Piedmont region of the US (32°35'39" N, 85°17'50" W). Figure 11 shows a map of the Piedmont region of the US (USGS, 2001), along with a soil map of the state of Alabama (University of Alabama, 2012). The Piedmont region of the US is predominately underlain by residual soil. This makes the study of residual soil a topic of high importance since it includes several major cities, including Atlanta, Charlotte, Baltimore, as well as Washington DC. Furthermore, any increases in the efficiency of designs in Piedmont residual soils (PRS) could lead to large cost savings, since so much of the nation's infrastructure is underlain by this region.

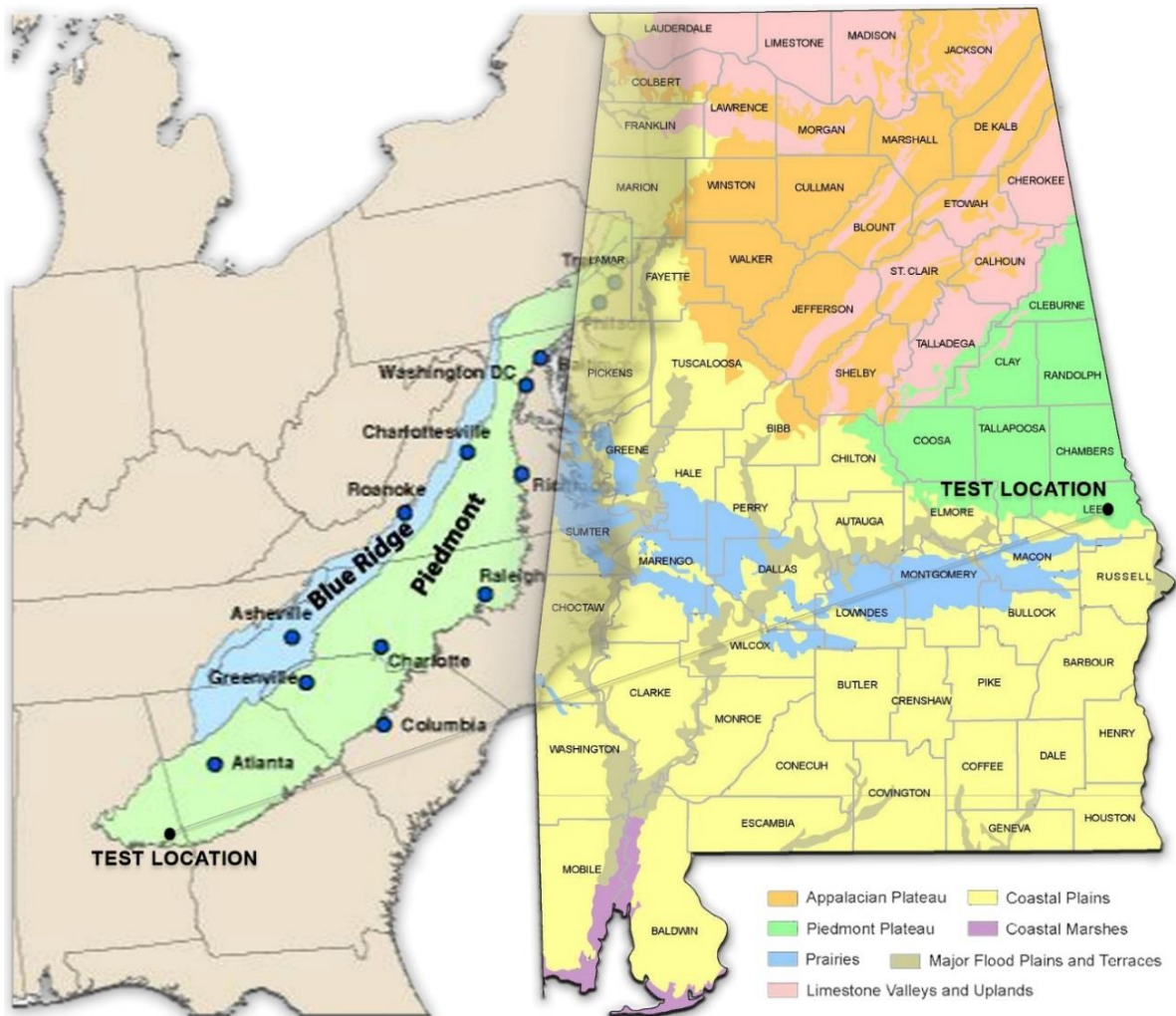


Figure 11 - (a) Map of Piedmont province (USGS, 2001); (b) Alabama soil map (University of Alabama, 2012).

## 4.1 Site Schematic Plans

For redundancy, two excavations were made in consecutive years at the Auburn NGES. The schematic plans for these excavations varied slightly because of changes that were made at the end of the first excavation in order to provide better results. Figure 12 shows the approximate excavation locations overlain on an aerial photo of the Auburn NGES. The excavations were located in an undisturbed portion of the site to the west of the area where previous foundation testing had been conducted.



**Figure 12 - NGES aerial with approximate excavation locations overlaid (Pictometry, 2012).**

### 4.1.1 Excavation #1 (2011)

Figure 13 shows a plan and cross section view of the proposed Excavation #1. Excavation #1 was approximately 1.8m in width, 6.1m deep, 30.5m in length, and included a sump pit at the end of the trench where water could be collected and pumped out of the

excavation if drainage was insufficient. The instrumentation plan for this excavation included 4 slope inclinometer casings, and 10 Watermark suction sensors coupled with temperature sensors. A designated location was also selected to measure volumetric water content via a dielectric water content reflectometer (WCR), which would provide a means of developing a soil-water characteristic curve (SWCC) insitu. Detailed information regarding the overall purpose and technical aspects of the instrumentation plan are presented in the "Instrumentation" section of this dissertation.

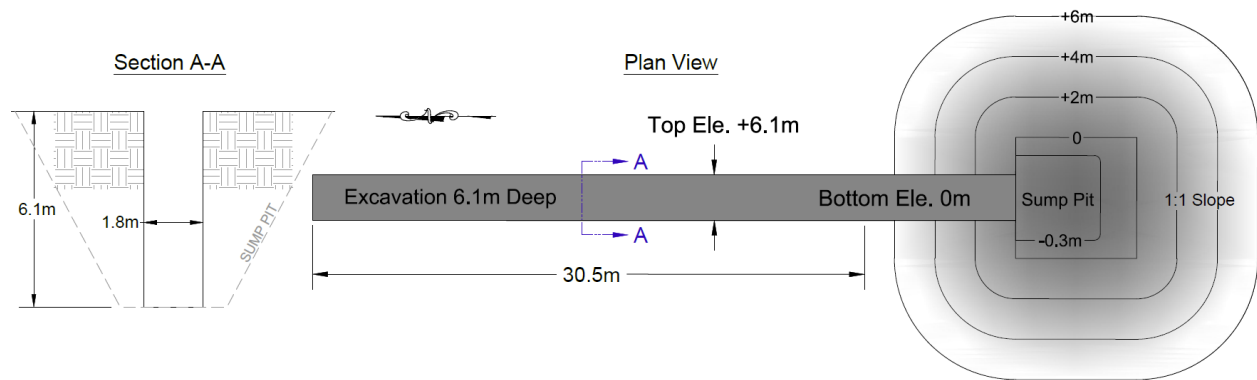


**Figure 13 - Excavation #1 schematic.**

#### 4.1.2 Excavation #2 (2012)

Figure 14 shows plan and profile views of the proposed Excavation #2. Excavation #2 differed slightly from Excavation #1, because during the observation period of Excavation #1, several weaknesses were identified which could easily be corrected. Excavation #2 was approximately 1.8m in width, 6.1m deep, 36.6m in length, and included a 0.5:1 slope on the non-instrumented side to prevent premature failure on that side of the excavation. The instrumentation plan for this excavation included 2 slope inclinometer casings, and 15 Watermark suction sensors coupled with temperature sensors. For redundancy, two designated locations were selected to measure volumetric water content via a dielectric water content reflectometer (WCR), in order to develop a soil-water characteristic curve (SWCC) insitu.

Although more instrumentation was installed on Excavation #2, the number of boreholes was reduced to prevent disturbance of the soil mass. This was based on an observation from Excavation #1 where a tension crack opened up through several boreholes, and eventually became the entry point for a failure surface. Detailed information regarding the overall purpose and technical aspects of the instrumentation plan, as well as the changes made based on observations in the first excavation are presented in the "Instrumentation" section of this dissertation.

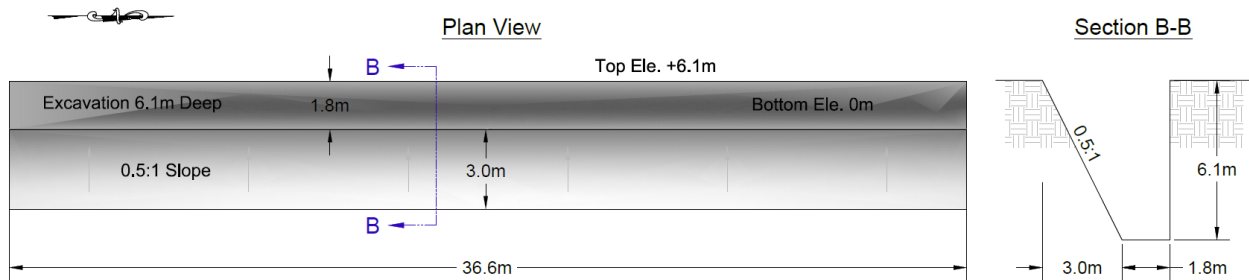


**Figure 14 - Excavation #2 schematic.**

## **CHAPTER 5: INSTRUMENTATION**

### **5.1 Overview / Objectives**

The main goals of the instrumentation plan were to (1) determine with reasonable certainty the boundary conditions at failure for the test excavations, and (2) monitor movement in the soil mass throughout the observation period. The instrumentation plan for this test included a combination of sensors that were connected to an automated data acquisition system (DAQ) to continually measure pore pressures and other boundary conditions for the excavation, as well as the use of slope inclinometers and surveying equipment periodically to determine movement, and cameras to determine the time and other site conditions at failure. Weather data was also collected at nearby weather stations (KALAAUBR4, and MTKGA1) in order to determine weather conditions throughout the duration of the experiment, particularly the time period just before failure.

### **5.2 Instrumentation Equipment**

The instrumentation for the test excavations included soil matric potential sensors, soil temperature sensors, soil piezometers, soil tensiometers, dielectric water content reflectometers (WCR), piezometers, and an automated DAQ (powered by a solar panel). This instrumentation setup was designed to measure pore pressure and water content over long periods of time without having to perform maintenance on the sensors. To monitor movement in the soil mass, slope inclinometer casing was installed, and a slope inclinometer was used periodically. Time-lapse cameras were also used to monitor the movement and failures of the soil mass, as well as to

collect observational data on the conditions at failure. , Figure 16, and Figure 17 illustrate the instrumentation equipment used for this project.



**Figure 15 - Sensors.**

### *5.2.1 Suction Sensors*

To account for the effects of negative pore pressure on the stability of the embankment, instrumentation was used to measure suction within the soil mass. The Watermark 200SS sensor was selected to measure suction because of its robust design, extended range (0-200kPa) and maintenance free operation. These sensors are manufactured by Irrometer Company, Inc. Unlike tensiometers, they provide a maintenance free method of measuring suction for extended periods of time. Since tensiometers measure suction through a ceramic high-air-entry (HAE) medium, they must remain saturated in order to measure properly. Diffusion of air through the air-water interface can cause the sensors to dry out, which will result in erroneous readings over time if not maintained. The Watermark sensors infer the water content of an internal matrix

material whose soil-water characteristics are known. This is achieved by measuring the resistance across electrodes that are embedded in the sensor media. Then a calibration curve is used to determine the water content of the sensor based on the resistance between the electrodes inside the sensor. Since the soil-water characteristics are known for the internal matrix material, the corresponding water content can be used to determine the suction within the sensor. This concept is based on the fact that the suction in the soil surrounding the sensor will equalize with the media within the sensor, which will in-turn force the flow of water in or out of the sensor therefore changing its water content. For the Watermark sensor, this process happens relatively quickly, which makes this sensor suitable for taking simultaneous measurements with a WCR. A detailed analysis of the equalization time for this sensor is presented in the data analysis section of this paper.

The Watermark Model 200 sensor was originally designed, and most commonly used for agricultural purposes to aid in irrigation schedules for various types of plants. The more recent models (200SS, and 200SSX) have incorporated improvements that increase the sensor response time, and reduce sensor to sensor variation (Shock et al., 1998), making them more suitable for engineering applications. These sensors are available for purchase from Irrometer Company Inc, and Campbell Scientific Inc. Campbell Scientific has published a manual for the Watermark sensors, which includes installation instructions, datalogger connection instructions, and calibration equations (Campbell Scientific Inc., 2009). In addition to the manufacturer's calibration, several other calibrations have been performed for the sensor including Thompson and Armstrong (1987), Eldredge et al. (1993), and Shock et al. (1998). In general, the manufacturer's calibration equation should be sufficient for making estimates of suction, but

when higher levels of accuracy are desired, the sensor should be calibrated using site-specific soils.

### *5.2.2 Piezometers*

Geokon 4500 piezometers were used alongside the Watermark sensors to perform a site-specific calibration (presented in the "Sensor Calibrations" section). While the Geokon 4500 piezometer has a reliable calibration curve, there are several disadvantages to solely relying on the Geokon 4500 sensor for suction measurements. The first is that because the sensors are measuring suction through a high air entry (HAE) material, the measurement range is limited to 100kPa. Also, the water compartment behind the HAE disk can dry out over time, making them unable to measure suction. The amount of time required for the sensor to lose its saturation is not very predictable making it less suitable for long-term measurements and permanent installations. Another disadvantage is that the cost of the Geokon 4500 is over ten times that of the Watermark, and it requires a special vibrating wire interface to allow connection to a DAQ.

In addition to the Geokon sensors that were used for calibration, a Geokon 4500 piezometer was also used to measure the water level in the bottom of the excavation throughout the duration of the experiment. Since the piezometers were not vented, a second Geokon 4500 piezometer was placed near the DAQ to measure the atmospheric pressure so that corrections could be made. The method for making these corrections are presented in the data analysis section of this paper.

### *5.2.3 Tensiometers*

Similar to the Geokon 4500 piezometers, tensiometers were used for redundancy in order to aid in the calibration of the Watermark sensors. The tensiometers used in this experiment were the Model "R" tensiometers, manufactured by Irrrometer, Inc. These tensiometers were

equipped with pressure gages that were able to be connected to a DAQ and measured automatically. The disadvantages of the tensiometers are similar to the Geokon 4500 Piezometers in that they also measure suction through a HAE material, and must remain saturated in order to measure properly. Also, the top of the tensiometer must remain above ground to allow for the refilling of the water compartment behind the HAE material. Therefore, the maximum depth that the Model "R" tensiometer can be installed is limited to the length of the sensor itself. Currently, the longest sensor available is 150cm.

#### *5.2.4 Water Content Reflectometers*

The volumetric water content of the soil was measured using the Campbell Scientific CS616 water content reflectometer. This sensor consists of two differentially-driven probe rods that form a transmission line in which the wave propagation velocity can be measured. Because water has a dielectric permittivity significantly larger than soil, the resulting oscillation frequency is an accurate measurement of the water content of the soil surrounding the rods (Campbell Scientific, Inc., 2006). Due to variations in soil types and mineralogy, the calibrations supplied by the manufacturer are generally accurate to  $\pm 2.5\%$  volumetric water content for a range of 0-50%. For applications where higher levels of accuracy are desired, the sensor should be calibrated using site specific soil. The calibrations method for the CS616 WCR is shown in the Data Analysis section of this paper.

#### *5.2.5 Soil Temperature Sensors*

Both the 200SS, and the CS616 sensors require temperature corrections to ensure accurate measurements. For the Watermark sensor, the resistance between the electrodes within the sensor is sensitive to temperature change. Therefore the resistance measurements need to be corrected to account for the temperature change within the sensor before computing the matric

potential. Similarly, the CS616 WCR period measurement varies slightly with the temperature of the soil between the electrodes. The amount of influence that the temperature has on the sensor measurements can vary based on the type of soil between the electrodes, therefore the temperature calibration for the CS616 sensors can vary from one soil to another.

There are many different types and manufacturers of sensors that can effectively measure soil temperature. For this experiment, thermistors from Geokon 4000 series vibrating wire strain gage pluckers were salvaged from a previous research project. The robust weatherproof design of these thermistors makes them suitable for use in soils.

#### *5.2.6 Slope Inclinometer*

A slope inclinometer was used to periodically measure the movement of the instrumented soil mass throughout the duration of the tests. The slope inclinometer that was used in this experiment was the Geokon Model 6000 (). This inclinometer is capable of measuring the amount of inclination (or tilt) on two axes. The inclinometer probe is attached to a readout box, and measurements are taken at specific depth intervals. The total amount of movement of an embankment or slope can be calculated by taking a baseline reading, and comparing the subsequent readings. The process for calculating this movement is presented in the data analysis section of this paper.

#### *5.2.7 Data Acquisition System*

The data acquisition system used in this test comprised of one Campbell Scientific CR1000 datalogger equipped with a CFM100 compact flash memory module. The data acquisition system was powered by the Campbell Scientific PS100 Battery Supply / Charging Regulator, and was also equipped with a Solar Panel for long-term data acquisition. A Campbell Scientific AVW 200 vibrating wire interface was used to connect the Geokon 4500 vibrating

wire piezometers, and two AM 16/32B multiplexers were used to connect the Watermark sensors, and temperature sensors. The components of the DAQ used in this experiment are shown in Figure 16. Wiring diagrams for the individual components and sensors are shown in Appendix A.



**Figure 16 - Data acquisition system.**

A program was developed for the datalogger using the Campbell Scientific CRBasic software. In order streamline the installation process and for the sake of simplicity, the datalogger was programmed to record the raw data from the sensors, and the data was later reduced via spreadsheet. A copy of the datalogger programs used in this experiment can be found in Appendix B.

### 5.2.8 Time-lapse Cameras

Time-lapse cameras were used to visually monitor the excavation for failures, as well as the site conditions at failure. The time-lapse cameras used for this project were the ProjectCam by Wingscapes. These cameras were connected to Moultrie Digital Game Camera (solar) Power Panels for long-term maintenance free operation. The pictures were taken on 1-hour intervals for

the duration of the test, and stored on SD memory cards which were periodically copied. Figure 17 shows the time-lapse cameras and solar panels used in this experiment.



**Figure 17 - Time-lapse camera.**

## **5.3 Instrumentation Installation**

### *5.3.1 Borehole Sensor Installation*

The majority of the sensors used in this experiment were installed in boreholes alongside the excavations. The boreholes were created via a SPT drill rig during the initial characterization. The sensors were installed in the boreholes by first backfilling the borehole to the appropriate depth (if necessary) and then inserting the sensor into the borehole suspended by the wires until the sensors reach the bottom of the borehole. The depth to each sensor location was measured from the surface via a tape measure, and soil was added and compacted in the borehole if necessary to adjust the depth. After the sensors were inserted into the boreholes, soil was added in lifts of approximately 20cm, and compacted using a piece of 1" (2.54cm) Sch. 40 PVC pipe with a PVC cap on the end. The PVC cap had smooth edges which helped to compact the soil without damaging the sensor wires. When the elevation of a new sensor location was reached, this process was repeated until all of the sensors were installed in the borehole, and the borehole was completely filled. The density of the boreholes was controlled by simply

compacting all of the soil that was removed from the borehole back into the borehole. The soil around the borehole was portioned off, and observations were made at the corresponding depths to see when approximately 25%, 50%, 75%, and 100% of the soil was replaced in the borehole. Since the sensors installed in boreholes were measuring suction and temperature, it was determined that this method of backfilling was sufficient, because slight inconsistencies in the density should not affect the readings of the sensors. Figure 18 illustrates the sensor installation process.



**Figure 18 - Instrumentation installation.**

### *5.3.2 Insitu SWCC Installation*

The installation method for the Watermark sensors consisted of the following steps:  
First, an excavation was made in the soil to the desired sensor depth. A hole was then made in

the soil approximately 2mm smaller than the diameter of the sensor. The hole was inspected for rocks or other debris that might result in erroneous suction measurements and cleaned or relocated if necessary. The sensor was inserted in the hole ensuring that good soil contact was provided around the sensor. According to the manufacturer, a piece of 3/4" (1.91cm) diameter PVC pipe can be placed around the collar of the sensor, providing a handle-like extension to help push it into stiff soils. After the Watermark sensor was installed, the temperature sensor was laid at the base of the Watermark sensor approximately 2-5 cm away from the sensor media.

The WCR was then installed in a similar fashion by first making two pilot holes for the electrodes and then installing the sensor in the holes. An installation tool specially designed to make the pilot holes for the sensor should be used, and is available from the manufacturer. It is important not to bend the electrodes while installing the dielectric sensor; doing so can result in erroneous data measurements. The WCR was installed vertically in the soil approximately 10-15 cm away from the Watermark sensor. Figure 19 shows a schematic for the SWCC sensor installation.

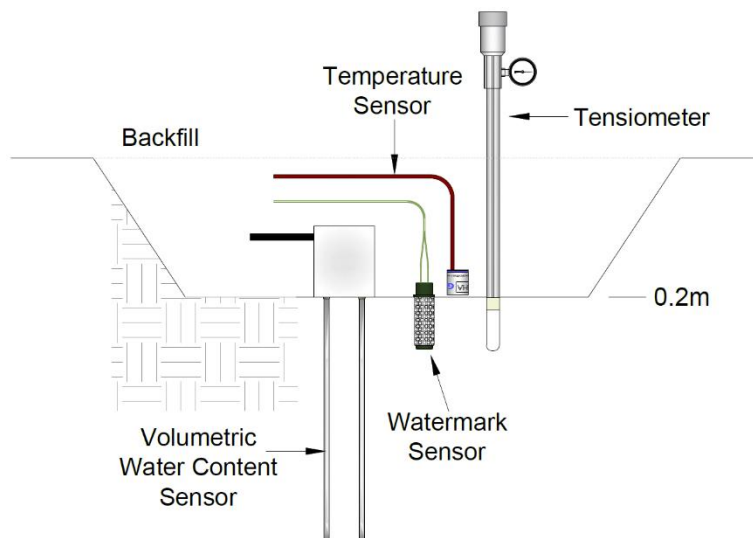


**Figure 19 - Sensor installation schematic for insitu SWCC.**

To calculate the gravimetric water content from the volumetric water content sensor, the density of the soil surrounding the sensor must be known. To accomplish this, a field density test was conducted using the drive-cylinder method (ASTM D 2937-10). The specimen was taken approximately 15-20 cm away from the volumetric water content sensor.

After all of the sensors were installed and the density test was performed, the excavation was backfilled and compacted to the approximate insitu density by replacing all of the excavated soil, and controlling the surface level. The surface of the soil was smoothed and leveled so that surface water would not puddle over the sensor and therefore alter the water content of the surrounding soil.

### *5.3.3 Inclinometer Casing Installation*

The inclinometer casing was installed by first checking the borehole depth to ensure that a portion of the casing would remain above the ground surface. If the borehole was too deep, soil was added and compacted similar to the borehole sensor installation technique. The inclinometer casings were then inserted into the borehole, and they were grouted in place using a mixture of Portland cement and water. Caps were installed on the inclinometer casings to prevent soil and other debris from entering the casing. Once the casings were installed, and the grout had set, baseline readings were taken with the Geokon Model 6000 slope inclinometer.

### *5.3.4 Water Level Piezometer Installation*

After the excavation was complete, the water level piezometer was installed by simply dropping it into the bottom of the excavation so that it was laying flat on an area near the center of the excavation. The barometric pressure piezometer was hung by the cable such that it was suspended about 1m off the ground behind the DAQ.

## 5.4 Instrumentation Plans

### 5.4.1 Excavation #1 (2011)

The first excavation was installed in August of 2010, and was observed for a period of one year. The instrumentation plan for Excavation #1 (Figure 20) comprised of 11 Watermark suction sensors, two CS616 Dielectric sensors (WCR), and 4 inclinometer casings (6.1m deep). The two WCR's were paired with suction sensors at two separate locations (Figure 20 location 6 and 15) in order to develop an insitu SWCC for the soil. The Watermark suction sensors were installed at depths ranging from 0.2-6.1m at approximately 1.5m increments. Excavation #1 included two rows of sensors and inclinometer casings; the first row was 1.8m from the face of the excavation, and the second row was 4.6m from the face.

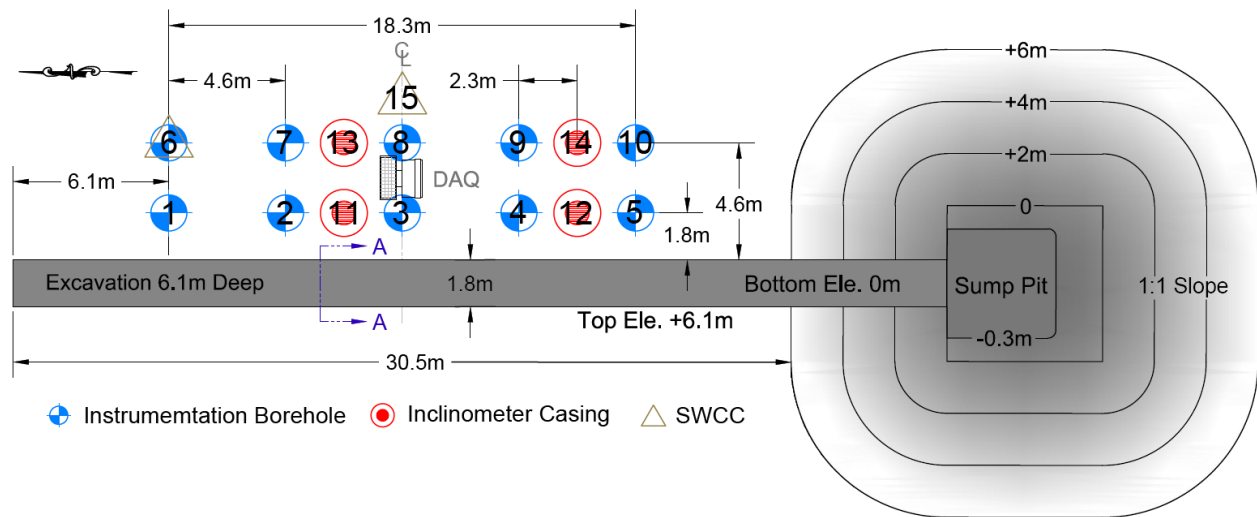
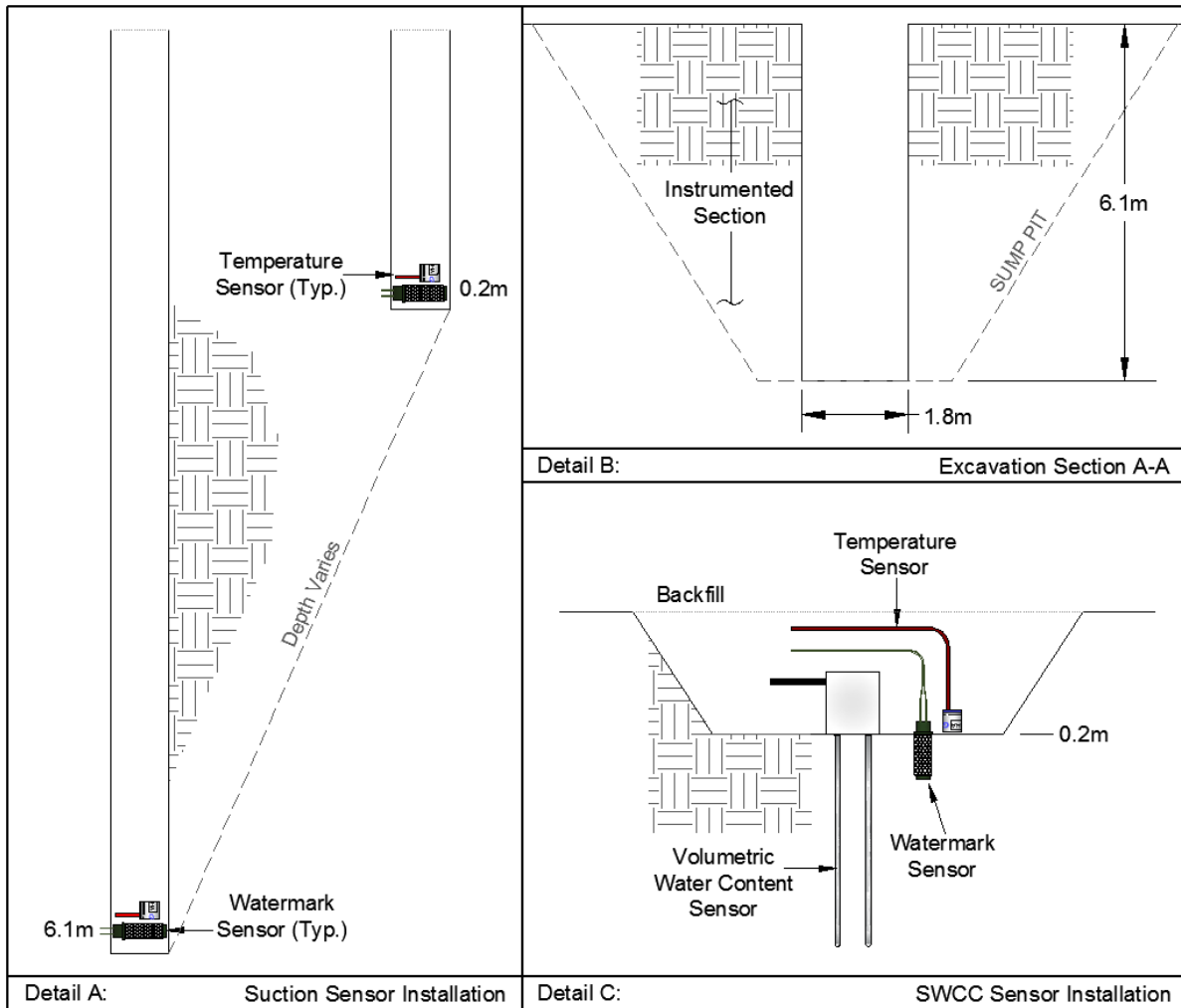


Figure 20 - Excavation #1 instrumentation plan.

Figure 21 shows the details of the instrumentation installation for Excavation #1. The suction sensors were each installed in their own borehole, and the depth of the borehole was made so that the sensor could be located in the bottom (partially in contact with the residual soil). In order to install the sensors in this fashion, a total of 13 boreholes were required (including those drilled for inclinometers). These are shown as Locations #1-14 in Figure 20, excluding

Location #6 which was used for SWCC. The SWCC sensors were installed in two excavated pits of 0.2m depth each (Figure 21C). Location #6 is marked as both an instrumentation borehole, and a SWCC location on the instrumentation plan because the suction sensor at the 0.2m depth was paired with a WCR to develop a second SWCC for redundancy.



**Figure 21 - Excavation #1 instrumentation / construction details.**

Table 4 summarizes the details for each sensor, including the field measured installation depth, the borehole location, and the DAQ channel in which the sensor was connected. Since the Watermark sensors required a soil temperature measurement in the data reduction process, a temperature sensor was installed alongside each Watermark sensor. The corresponding channel in the DAQ where the paired temperature data was collected is also shown in Table 4.

**Table 4 - Instrumentation location and details (Excavation #1).**

Sensor ID	Location ID	Sensor Depth (m)	Measurement Type	Sensor Description	Datalogger Channel	Temperature Channel
WM1	6	0.2	Suction	Watermark 200SS	kOhms(1)	kOhms(12)
WM2	3	3.0	Suction	Watermark 200SS	kOhms(2)	kOhms(13)
WM3	8	6.1	Suction	Watermark 200SS	kOhms(3)	kOhms(14)
WM4	2	4.6	Suction	Watermark 200SS	kOhms(4)	kOhms(15)
WM5	4	1.5	Suction	Watermark 200SS	kOhms(5)	kOhms(16)
WM6	5	0.3	Suction	Watermark 200SS	kOhms(6)	kOhms(17)
WM7	7	3.0	Suction	Watermark 200SS	kOhms(7)	kOhms(18)
WM8	1	6.1	Suction	Watermark 200SS	kOhms(8)	kOhms(19)
WM9	9	4.6	Suction	Watermark 200SS	kOhms(9)	kOhms(20)
WM10	10	1.5	Suction	Watermark 200SS	kOhms(10)	kOhms(21)
WM11	15	0.9	Suction	Watermark 200SS	kOhms(11)	kOhms(22)
WCR1	6	0.2	Moisture	Campbell CS616	VWC	--
WCR2	15	0.2	Moisture	Campbell CS616	VWC2	--
NW	11	6.1	Displacement	Digitilt 50302599	--	--
SW	12	6.1	Displacement	Digitilt 50302599	--	--
NE	13	6.1	Displacement	Digitilt 50302599	--	--
SE	14	6.1	Displacement	Digitilt 50302599	--	--

#### 5.4.2 Excavation #2 (2012)

The instrumentation plan for Excavation #2 was similar to Excavation #1; however it was modified slightly based on some observations made during the first excavation. Because the failure surface observed in Excavation #1 intersected the boreholes closest to the excavation, Excavation #2 was designed to minimize the number of boreholes within 2 meters of the excavation, therefore minimizing the disturbance of the soil in that region. The instrumentation plan only included one borehole 1.8m from the face of the excavation, and it was used to install an inclinometer casing. From the data collected in Excavation #1, it was determined that the suction measurements in the boreholes 4.6m from the excavation face were not substantially different from those in the boreholes 1.8m from the face, and therefore measurements taken 4.6m from the excavation face would be sufficient to determine the negative pore pressures in the soil.

The total number of boreholes was also reduced in the instrumentation plan for the second excavation so as to not to raise the question whether or not the failure was initiated by the boreholes themselves. It was determined that installing the sensors in re-compacted soils would not introduce significant error in the measurements, because the small diameter of the borehole would result in a relatively low fluctuation in pore pressure with respect to the soil surrounding the borehole. (i.e. the pore pressure would equalize with the soil surrounding the borehole at each depth). This same concept is the basis for the Watermark sensor design, and the filter paper method for determining suction (ASTM D5298).

Because the site was not visited on a daily basis, the exact date and time of failure was difficult to determine during the first excavation. Therefore the instrumentation plan for Excavation #2 included time-lapse cameras that were set to take photographs every hour. Although the photographs could not be taken at night, it would still ensure that the failure would be documented within a 12hr timeframe in case the failure is not detectable by the pore pressure sensors.

Another weakness in the instrumentation plan from the first excavation was that the water level in the bottom of the trench was not measured continuously, so the water level at the time of failure was unknown. The excavation was designed so that the water could be collected in a sump pit, and pumped as necessary, but because the site did not have access to a power source, an automatic pumping system was not feasible, and therefore the pumping was intended to be periodically. It was noticed during the first excavation that that the bottom of the trench drained relatively quickly (the soil was permeable enough to allow the water to drain in less than 1 day). so the sump pit was deemed unnecessary for the second excavation.

The second excavation was installed in August of 2011, and was observed for a period of one year. The instrumentation plan for Excavation #2 (Figure 22) comprised of 16 Watermark suction sensors, 8 Geokon piezometers, two CS616 Dielectric sensors (WCR), two Irrometer tensiometers, two inclinometer casings (6.1m deep), and two time-lapse cameras. The Watermark suction sensors were installed at depths ranging from 0.2-6.1m at approximately 1.5m increments. Excavation #2 included a single row of sensors (offset 4.6m from the face of the excavation), and two inclinometer casings; the first was 1.8m from the face of the excavation, and the second was offset 4.6m from the face.

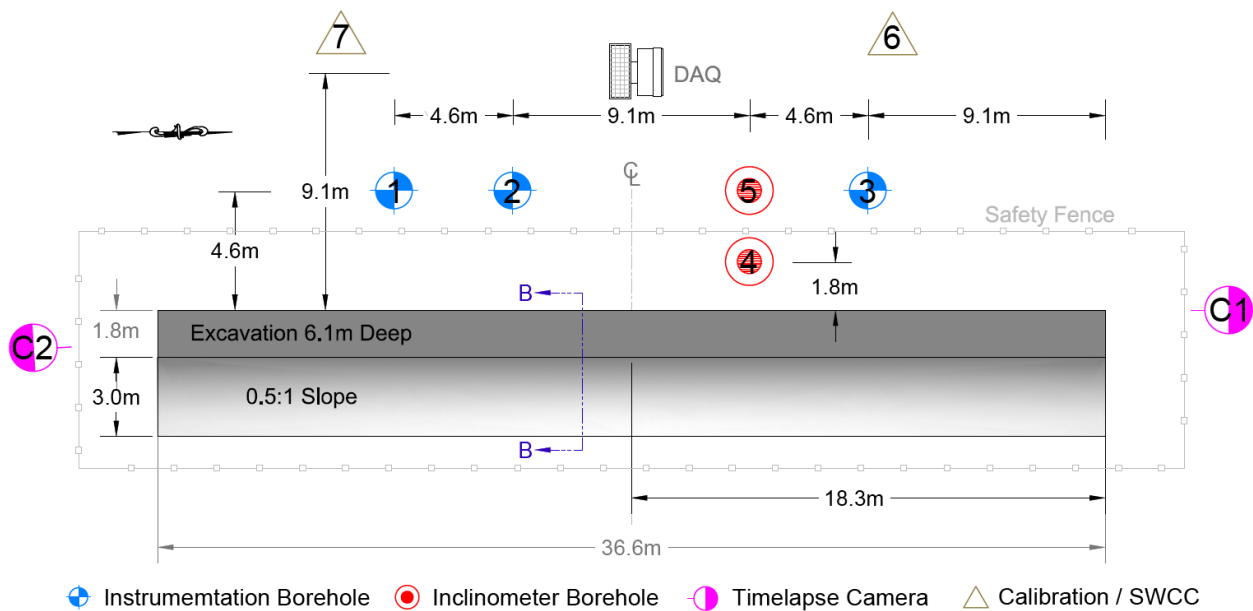


**Figure 22 - Excavation #2 instrumentation plan.**

Figure 23 shows profile views and details for the Watermark / Geokon sensor installation (Figure 23A) as well as the modified sensor installation plan for the SWCC (Figure 23B). The suction sensors were installed in three separate boreholes (5 sensors per borehole). In order to install the sensors in this fashion, a total of 5 boreholes were required (including those drilled for inclinometers), reducing the total number of boreholes by 8 in comparison to the first excavation. The boreholes are shown as Locations #1-5 in Figure 22. The SWCC sensors were installed in

two excavated pits of 0.2m depth each (Figure 23C), and are represented by Locations #6-7 in Figure 22.

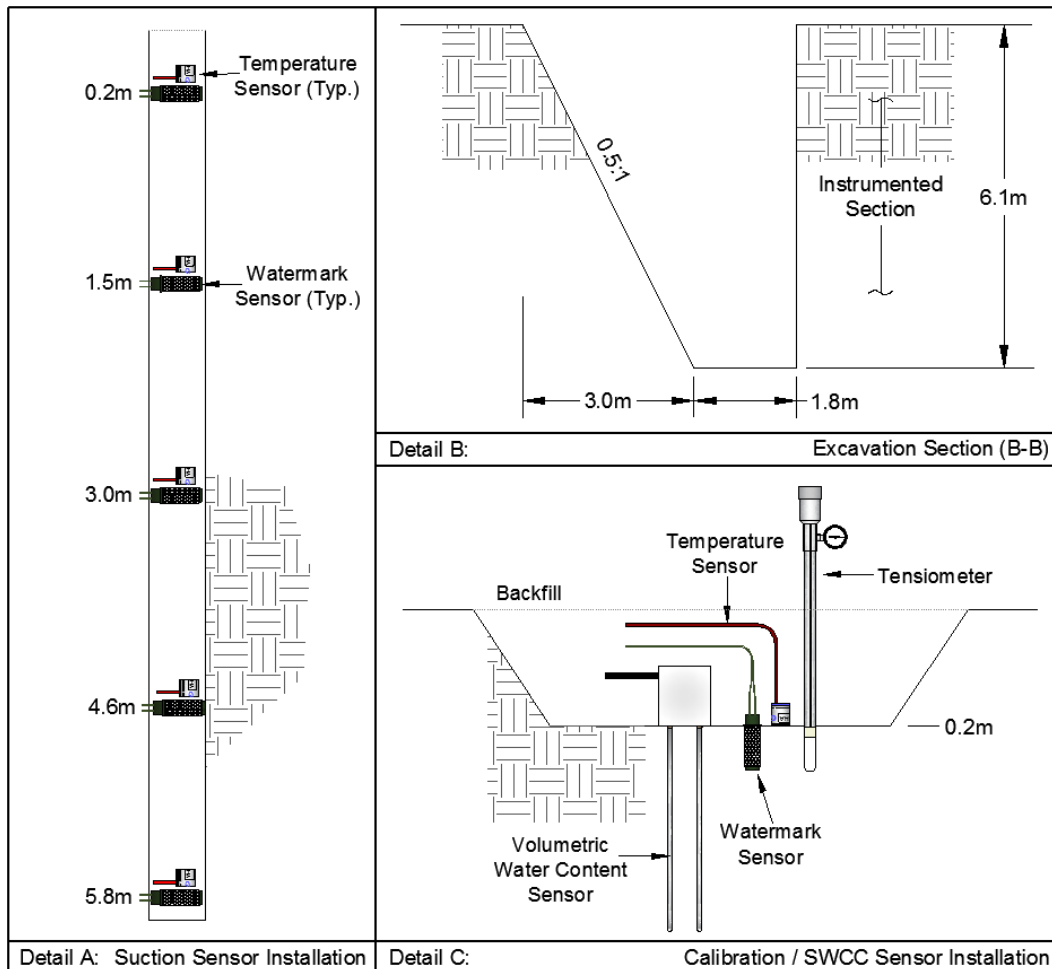


**Figure 23 - Excavation #2 instrumentation / excavation details.**

Table 5 summarizes the details for each sensor, including the field measured installation depth, the borehole location (Figure 22), and the DAQ channel in which the sensor was connected. Since the Watermark sensors required a soil temperature measurement in the data reduction process, a temperature sensor was installed alongside each Watermark sensor. The corresponding channel in the DAQ where the paired temperature data was collected is also shown in Table 5.

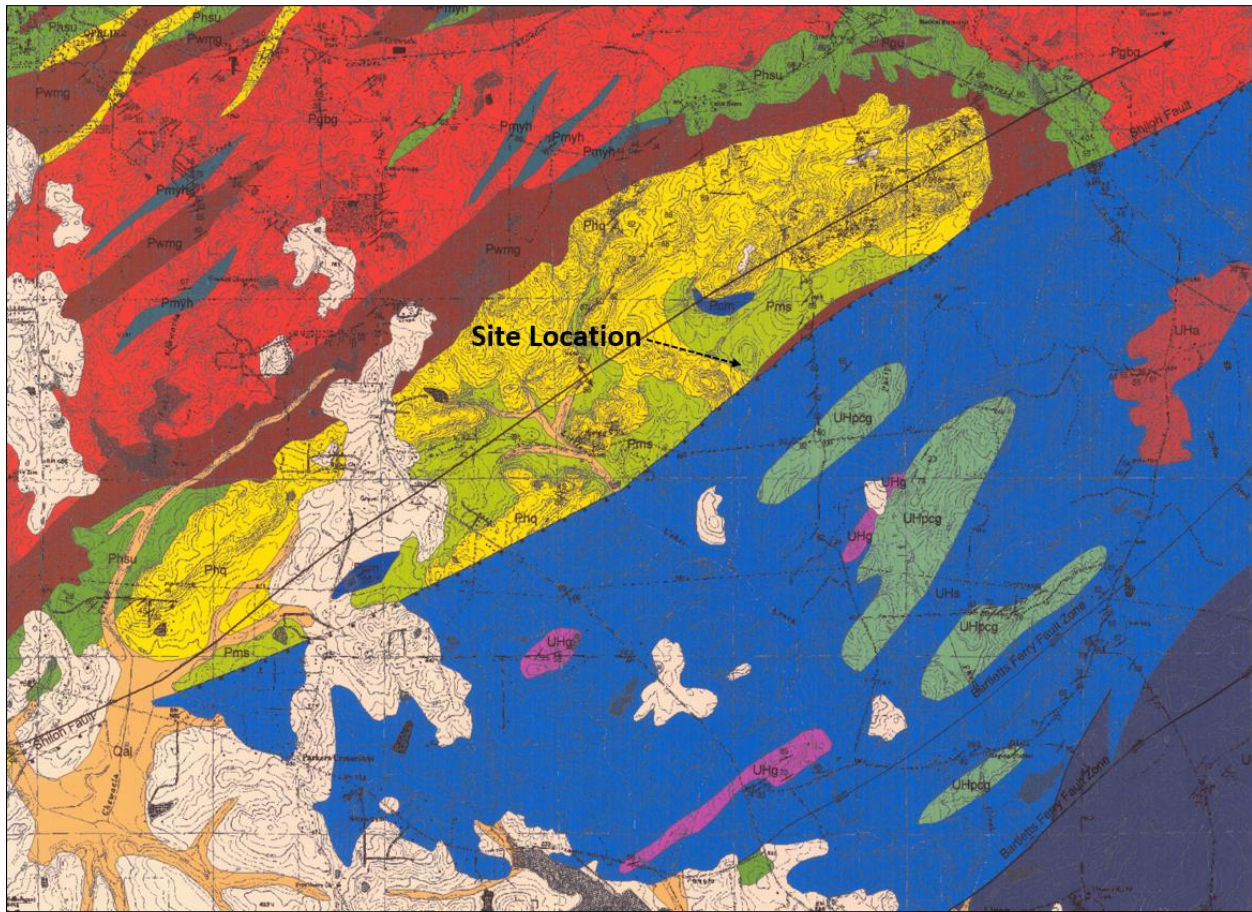
**Table 5 - Instrumentation location and details (Excavation #2).**

Sensor ID	Location ID	Sensor Depth (m)	Measurement Type	Sensor Description	Datalogger Channel	Temperature Channel
WM1	1	5.8	Suction	Watermark 200SS	kOhms(1)	kOhms(2)
WM2	1	4.6	Suction	Watermark 200SS	kOhms(3)	GKTemp(1)
WM3	1	3.0	Suction	Watermark 200SS	kOhms(5)	kOhms(6)
WM4	1	1.5	Suction	Watermark 200SS	kOhms(7)	kOhms(8)
WM5	1	0.2	Suction	Watermark 200SS	kOhms(9)	GKTemp(2)
WM6	2	5.8	Suction	Watermark 200SS	kOhms(11)	kOhms(2)
WM7	2	4.6	Suction	Watermark 200SS	kOhms(13)	kOhms(14)
WM8	2	3.0	Suction	Watermark 200SS	kOhms(15)	kOhms(16)
WM9	2	1.5	Suction	Watermark 200SS	kOhms(17)	GKTemp(3)
WM10	2	0.2	Suction	Watermark 200SS	kOhms(19)	kOhms(20)
WM11	3	5.8	Suction	Watermark 200SS	kOhms(21)	kOhms(22)
WM12	3	4.6	Suction	Watermark 200SS	kOhms(23)	kOhms(24)
WM13	3	3.0	Suction	Watermark 200SS	kOhms(25)	GKTemp(4)
WM14	3	1.5	Suction	Watermark 200SS	kOhms(27)	kOhms(28)
WM15	3	0.2	Suction	Watermark 200SS	kOhms(29)	kOhms(30)
WM16	6	0.3	Suction	Watermark 200SS	kOhms(31)	GKTemp(5)
WM17	7	0.3	Suction	Watermark 200SS	kOhms(32)	GKTemp(6)
GK1	1	4.6	Suction	Geokon 4500(3bar)	GKFreq(1)	GKTemp(1)
GK2	1	0.2	Suction	Geokon 4500(3bar)	GKFreq(2)	GKTemp(2)
GK3	2	1.5	Suction	Geokon 4500(3bar)	GKFreq(3)	GKTemp(3)
GK4	3	3.0	Suction	Geokon 4500(3bar)	GKFreq(4)	GKTemp(4)
GK5	6	0.3	Suction	Geokon 4500(3bar)	GKFreq(5)	GKTemp(5)
GK6	7	0.3	Suction	Geokon 4500(3bar)	GKFreq(6)	GKTemp(6)
GK7	EXC	--	Pressure	Geokon 4500	GKFreq(7)	GKTemp(7)
WCR1	6	0.2	Moisture	Campbell CS616	VWC	--
WCR2	7	0.2	Moisture	Campbell CS616	VWC2	--
TENS1	6	0.3	Suction	Irrrometer "R"	SEVolt1	--
TENS2	7	0.3	Suction	Irrrometer "R"	SEVolt2	--
EAST	4	9.1	Displacement	Digitilt 50302599	--	--
WEST	5	9.1	Displacement	Digitilt 50302599	--	--

## CHAPTER 6: SITE CHARACTERIZATION

### 6.1 Site Geology

The Auburn University NGES is located in the Southwest portion of the Piedmont region of the United States (32°35'39" N, 85°17'50" W). According to Vinson and Brown (1997), The Southern Piedmont region was primarily formed from Precambrian to Paleozoic era high-grade metamorphic and igneous rocks, and the residual soils are primarily of the Wacoochee complex; the site geology can be further classified and being either Halawaka Schist or Phelps Creek Gneiss. Halawaka Schist contains feldspathic muscovite-biotite schist and quartz-diorite gneiss; it can locally contain lenses of muscovite-graphite schist and amphibolite, and is commonly cut by feldspathic veins and pegmatites (Vinson and Brown, 1997). Phelps Creek Gneiss is made up of quartz monzonite and granite gneiss in dikes and sheets with wide migmatite zones at contacts (Osborne et al., 1988). Boring logs from previous borings performed at the site note that the recovered samples are commonly sandy and micaceous with veins of weathered rock (schist, gneiss), and quartz sand. Figure 24 shows a geologic map of the Parkers Crossroad quadrangle, in Lee County, Alabama (Carter and Steltenpohl, 2002). The underlying rock in the test location is predominately foliated metamorphic bedrock, and it underlies a thick deposit of saprolite that was formed over time through a chemical weathering process. The foliated nature of the parent rock can clearly be seen in the excavation photographs in Chapter 10.



<b><u>PINE MOUNTAIN TERRANE</u></b>		
	Pgu	Granitic rock of uncertain origin
<b><u>Basement Complex</u></b>		
	Pgbg	Basement Complex
	Pwmg	Whatley Mill Gneiss
<b><u>Pine Mountain Group</u></b>		
	Pms	Manchester Schist
	Pm	Chewacla Marble
	Phq	Hollis Quartzite
	Phsu	Halawaka Schist undifferentiated
	Pmyh	Mylonitized Halawaka Gneiss
<b><u>GULF COASTAL PLAIN</u></b>		
	Qal	Quaternary Alluvium
	Ke	Eutaw Formation
	K	Upper Cretaceous Gulf Coastal Plain
<b><u>UNCERTAIN HERITAGE</u></b>		
	UHpcg	Phelps Creek Gneiss
	UHg	Granodiorite intrusion
	UHa	Schist - Amphibolite
	UHs	Schist undifferentiated
<b><u>UCHEE TERRANE</u></b>		
	Umg	Motts Gneiss
	Uag	Hornblende Gneiss
	Ubg	Unnamed Biotite Gneiss
	Us	Unnamed Schist
<b><u>MYLONITE ZONES</u></b>		
	GRFZ	Goat Rock Fault Zone

Figure 24 – Geologic map of the Parkers Crossroads quadrangle (Carter and Steltenpohl, 2002).

## 6.2 Previous Auburn NGES Characterization

Previous researchers have conducted a variety of insitu and laboratory tests at the NGES. Vinson and Brown (1997) published site characterization data that was to aid in further geotechnical experiments on the site. Their insitu tests included the standard penetration test (SPT), cone penetration test (CPT), piezocone penetration test (PCPT), pressuremeter test (PMT), cone pressuremeter test (CPMT), dilatometer test (DMT), and the Iowa borehole shear test (BST). Other insitu testing included the seismic dilatometer test (SDMT), the seismic cone penetration test (SCPT), and the crosshole seismic test (CHT). The laboratory tests included Atterberg limits, grain size distribution, specific gravity, consolidated undrained triaxial tests (CU), consolidated drained triaxial tests (CD), and unconsolidated undrained triaxial tests (UU). Table 6 shows a summary of the tests performed by Vinson and Brown (1997), and Figure 25 shows the corresponding locations of the tests in relation to the test excavations performed in this project.

**Table 6 - Testing Summary (Vinson and Brown, 1997).**

Test Type	Locations	Depth Range
Triaxial CU	B-2, B-5, B-7, B-8	4m - 15m
Triaxial UU	B-2, B-5, B-6, B-7, B-8	1m - 3m
Triaxial CD	B-8	10m
CPMT	C-41, C-42, C-43, C-44	1m - 12m
PMT	B-2, B-5	1m - 15m
DMT	AU1, AU2, AU3	< 1m - 8m
SDMT	AU1, AU2, AU3	<1m - 8m
SCPT	C-41, C-42	<1m - 15m
CPT	C-11→C-18, C-21→C-27, C-32, C-41→C-44	<1m - 25m
PCPT	C-23, C-43, C-44	7m - 17m
SPT	B-2, B-5	1m - 15m
CHT	Array#1: B-1→B-3, Array#2: B-4→B-6	<1m - 15m
BST	B-7, B-8	2m - 9m



Figure 25 - Vinson and Brown (1997) test locations (Pictometry, 2012).

### 6.2.1 Previous Index Tests

Table 7 summarizes the index properties of the Auburn NGES as reported by Vinson and Brown (1997). Based on the index tests, the USCS classification for the soils on this site was found to be predominately SM, ML, or MH (AASHTO A-4, A-5, or A-7-5), indicating a high variability in soil properties with location and depth. This variability in the index properties is a characteristic of Piedmont residual soils in general, which is one reason that laboratory characterization is difficult for these types of soils (Sowers, 1954, 1963). The average specific gravity with depth as reported by Vinson and Brown (1997) is presented in Table 8.

**Table 7 - Summary of index testing (Vinson and Brown, 1997).**

Property	Number of Tests	Average	Standard Deviation
Water Content (%)	64	34.0	7.5
Liquid Limit (%)*	22	46.3	10.0
Plastic Limit (%)*	22	38.1	6.5
Plasticity Index (%)*	22	8.2	5.9
Wet Unit Weight (kN/m <sup>3</sup> )	35	18.3	0.5
Dry Unit Weight (kN/m <sup>3</sup> )	35	13.3	0.9
Sand Content (%)	48	46.7	17.2
Silt Content (%)	22	33.0	8.4
Clay Content (%)	22	9.5	6.4

\*20 samples were reported as "nonplastic" and are not included.

**Table 8 - Specific gravity (Vinson and Brown, 1997).**

Location	Depth (m)	Specific Gravity
Boring B-7	6	2.84
Boring B-7	8	2.73
Boring B-7	10	2.77

To identify the changing of soil type with depth, the grain size distributions, and Atterberg limits recorded by Vinson and Brown (1997) were averaged for equivalent depths, and are presented in Figure 26 and Figure 27. These figures summarize the index properties of the soil throughout the range of depths that were influential in this experiment. Based on these summaries, the upper zone samples tended to show a greater range of plasticity (plasticity index) than the deeper samples. It was also evident that the percentage of clay-sized particles was significantly higher in the upper zone and tended to decrease with depth.

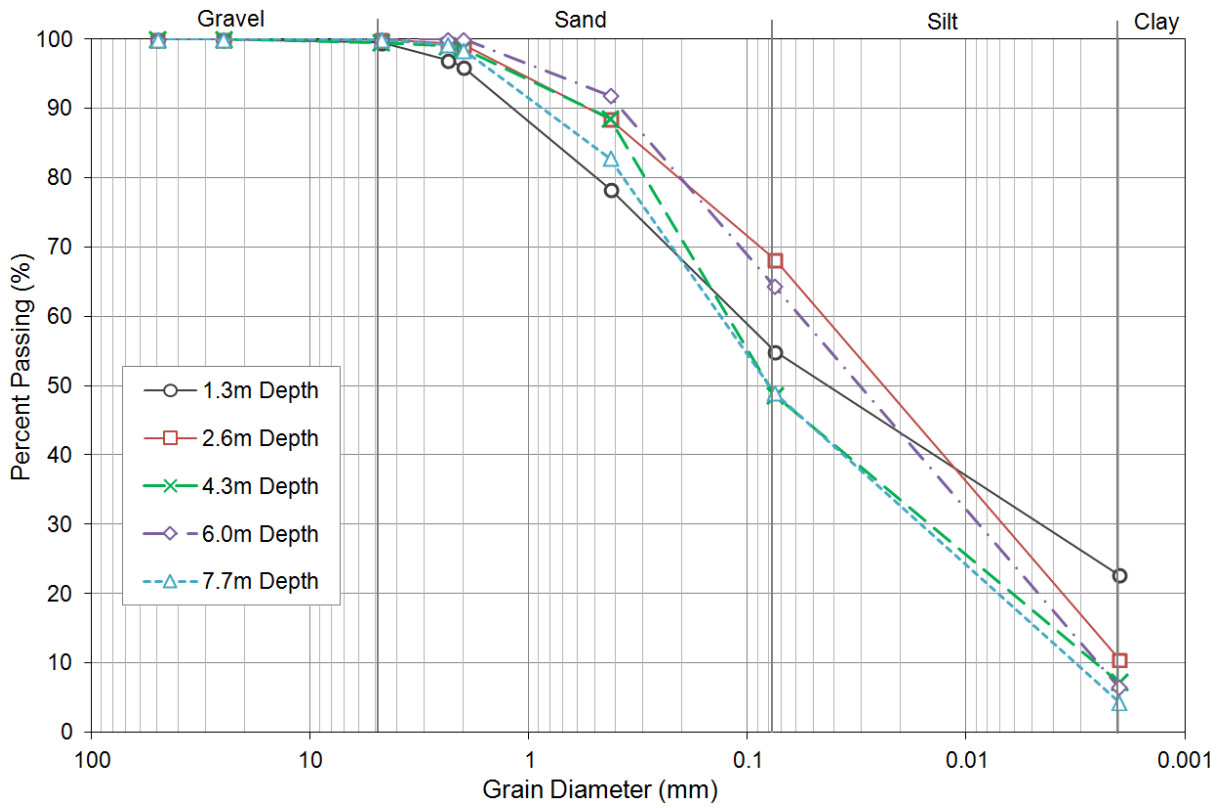


Figure 26 - Grain size distribution summary (Vinson and Brown, 1997).

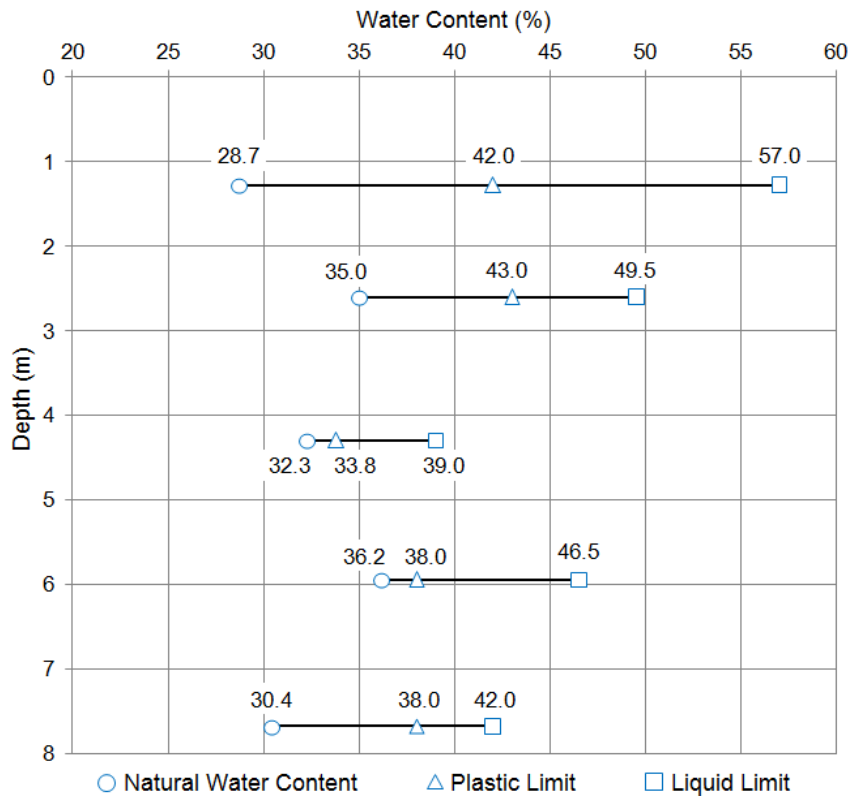


Figure 27 - Atterberg limits summary (Vinson and Brown, 1997).

### 6.2.2 Previous Triaxial Tests

The results of the triaxial shear tests performed by Vinson and Brown 1997 are summarized below. The calculated values for  $\phi'$  and  $c'$  presented in these tables are based on linear p-q regressions.

**Table 9 - Triaxial results (Vinson and Brown, 1997).**

Test Type	Number of Tests	$c'$ (kPa)	$\phi'$ (deg)	$R^2$
CU and CD Tests	23	17	31	0.91
CU Tests	22	10	34	0.93
Multi-Stage CU	8	17	32	0.99

**Table 10 - Triaxial results with depth (Vinson and Brown, 1997).**

Depth Range	Number of Tests	$c'$ (kPa)	$\phi'$ (deg)	$R^2$
4 to 8 meters	10	8	36	0.83
10 to 15 meters	14	14	31	0.96

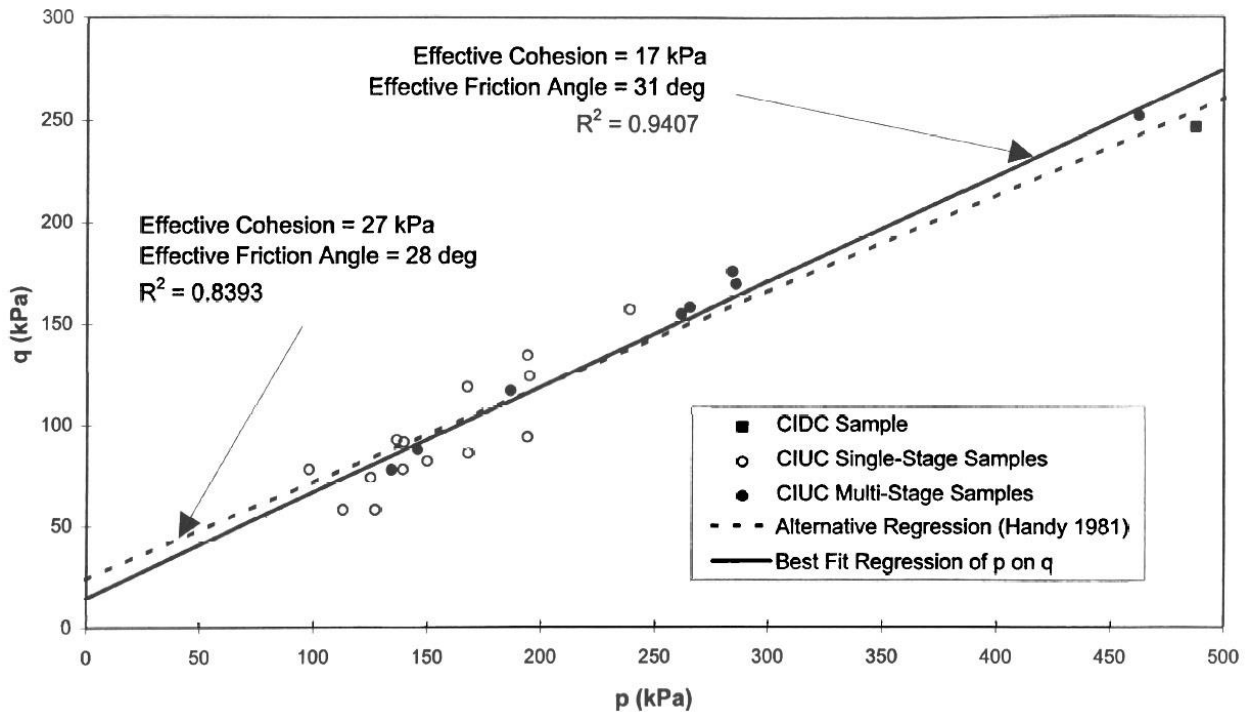


**Figure 28 - Triaxial summary (Vinson and Brown, 1997).**

### 6.2.3 Previous Insitu Test Results

Selected data from previous insitu tests (conducted by Vinson and Brown 1997) was used in conjunction with the site characterization performed in this experiment to aid in the definition of the material properties with depth. The modulus values from the PMT were selected to reflect the average modulus over the expected levels of strain anticipated in the test. These modulus values are presented in Table 11.

**Table 11 - PMT modulus results (Vinson and Brown, 1997).**

Depth (m)	Average E (kPa)
1	8,750
2	8,350
4	4,350
6	6,100
8	5,200
10	6,150

## 6.3 Insitu Testing

In addition to the testing that was performed by Vinson and Brown (1997), site specific testing in close proximity to the excavation was also performed in order to develop a profile of the site stratigraphy directly under the excavation location, and to retrieve samples for laboratory testing.

### 6.3.1 Standard Penetration Test

The Standard Penetration Test (SPT) was performed in three of the instrumentation boreholes located on the West side of Excavation #2. Because the standard penetration test is so widely used in the United States, it was performed in order to aid in future correlations of data. Another benefit of the standard penetration test is that additional samples were retrieved for laboratory analysis and classification. Detailed results of the SPT are presented in Appendix C.

### 6.3.2 Cone Penetration Test

Cone penetration tests were performed in close proximity to the location of Excavation #1 to provide data for future comparisons of data. The results of the CPT are presented in Appendix C.

## 6.4 Laboratory Testing

### 6.4.1 Shear Strength Testing

The shear strength for the instrumented soil mass was estimated by the use of consolidated drained (CD) triaxial shear tests. Drained tests were selected because they most accurately represent the long term strength of the soil. In order to accurately model the unsaturated properties of the soil, both saturated and unsaturated triaxial shear tests were performed. The procedure used for the CD test were based on ASTM D7181-11, "Standard Test Method for Consolidated Drained Triaxial Compression Test for Soils." A new method was proposed for unsaturated triaxial shear testing, and is presented in the following chapter, along with the results of the unsaturated tests. The results of the saturated, consolidated drained triaxial shear tests are summarized in and Figure 30- Figure 32.

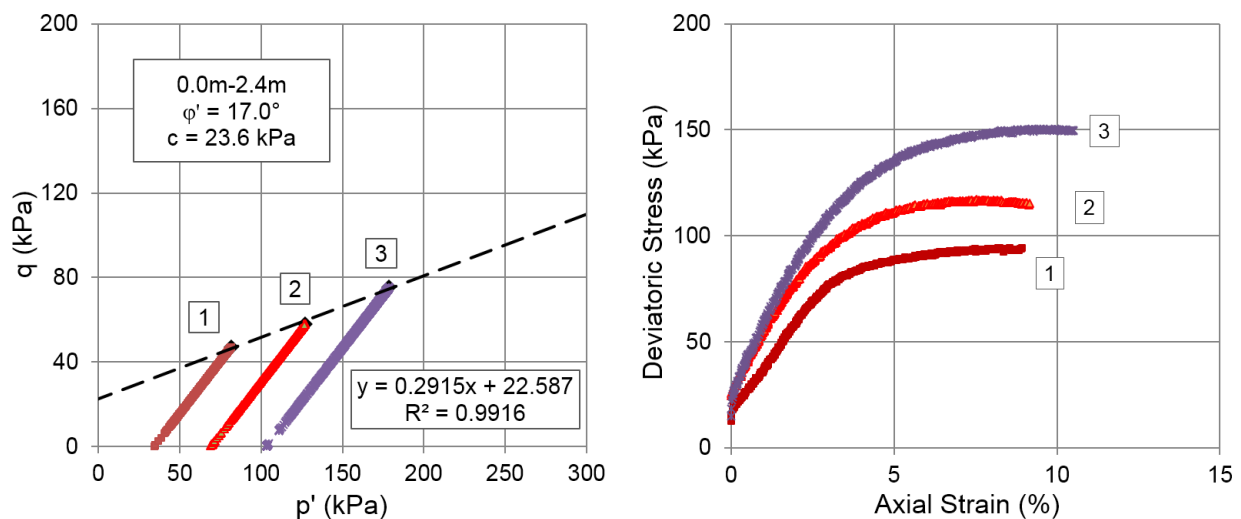


Figure 29 - Failure criterion for consolidated drained triaxial tests at 0m-2.4m depth.

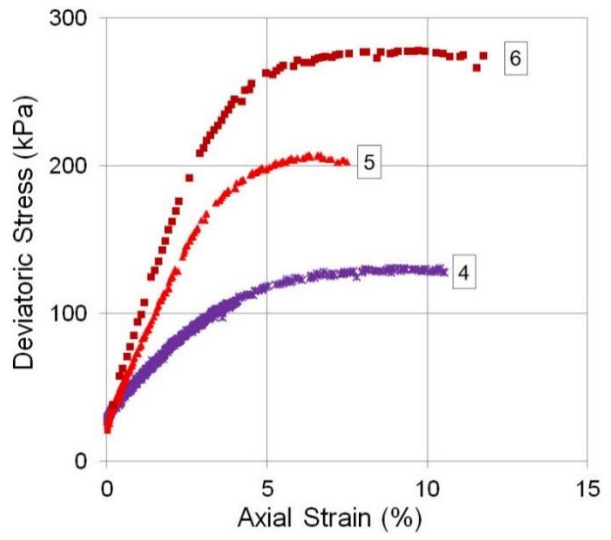
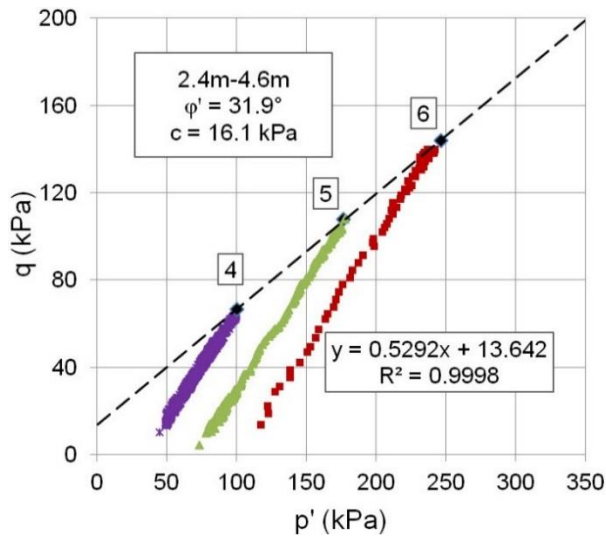


Figure 30 - Failure criterion for consolidated drained triaxial tests at 2.4m-4.6m depth.

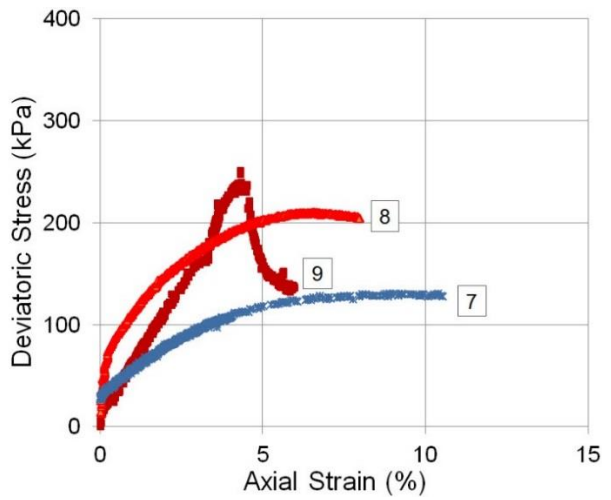
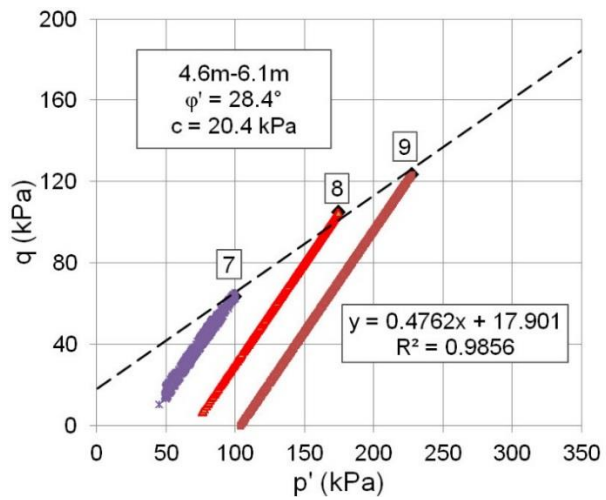


Figure 31 - Failure criterion for consolidated drained triaxial tests at 4.6m-6.1m depth.

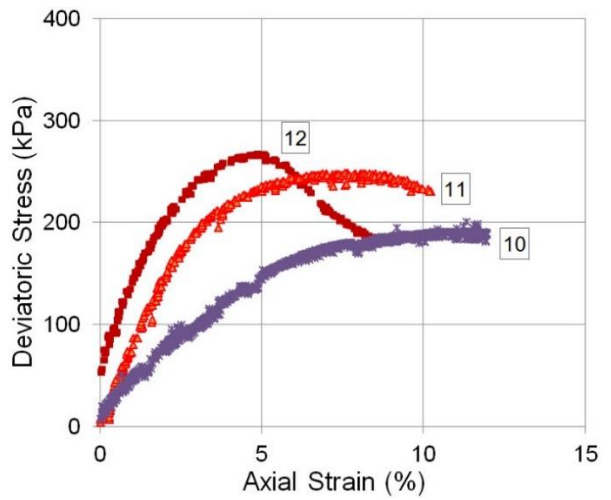
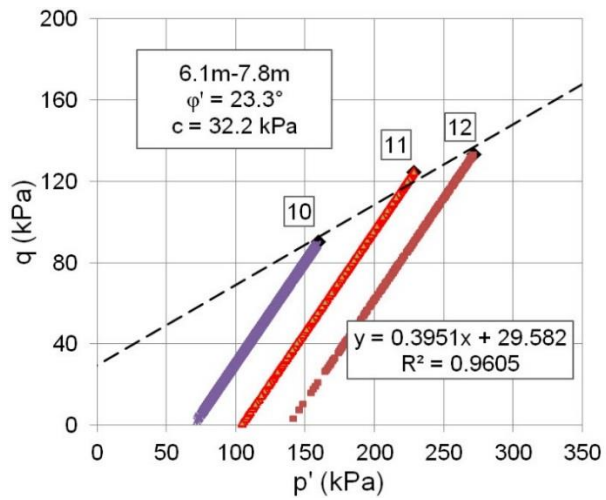


Figure 32 - Failure criterion for consolidated drained triaxial tests at 6.1m-7.8m depth.

**Table 12 - Triaxial test conditions at failure.**

Test #	$\gamma_d$ (kN/m <sup>3</sup> )	B-Value	$\sigma_d$ (kPa)	$\sigma_3$ (kPa)	$\sigma_1$ (kPa)	$u_w$ (kPa)	$\sigma'_3$ (kPa)	$\sigma'_1$ (kPa)
1	15.2	0.90	94	345	439	310	34.5	129
2	14.1	0.93	116	338	454	269	69	185
3	14.3	0.88	151	365	516	262	103	254
4	11.3	0.96	133	379	512	345	34	167
5	11.9	0.95	216	414	630	345	69	285
6	12.8	0.94	288	448	736	345	103	391
7	11.3	0.96	133	379	512	345	34	167
8	15.0	1.00	211	421	632	352	69	280
9	13.9	0.96	248	345	593	241	104	352
10	13.5	0.91	181	345	526	276	69	250
11	13.1	0.84	250	345	595	241	104	354
12	13.8	1.00	268	379	647	241	138	406

In situ testing, and observational results from the excavation suggested the presence of weak layers within the excavation, therefore shear strength parameters were calculated for each soil layer individually instead of averaging the values for the full depth range. For modeling purposes, it was necessary to accurately define these weakened layers to assess their impact on the overall stability of the excavation. The results of the shear strength calculations for the various depths are summarized in Table 13.

**Table 13 - Shear strength with depth based on triaxial test results.**

Depth (m)	Samples	Effective Friction, $\phi'$	Effective Cohesion (kPa)
0.0 - 2.4	1, 2, 3	17.0	23.6
2.4 - 4.6	4, 5, 6	31.9	16.1
4.6 - 6.1	7, 8, 9	28.4	20.4
6.1 - 7.8	10, 11, 12	23.3	32.2

### 6.4.2 Pressure Plate Test

A pressure plate test was performed in order to determine the moisture retention curve for the site specific soils, and to validate the results of the insitu SWCC test. The procedures and results for the insitu SWCC test are presented in the chapter entitled "Insitu SWCC Test." The procedures for the pressure plate test were followed based on ASTM D6836-02, "Standard Test Methods for Determination of the Soil Water Characteristic Curve for Desorption Using Hanging Column, Pressure Extractor, Chilled Mirror Hygrometer, or Centrifuge." The results of the pressure plate extractor test are shown in Figure 33 below.

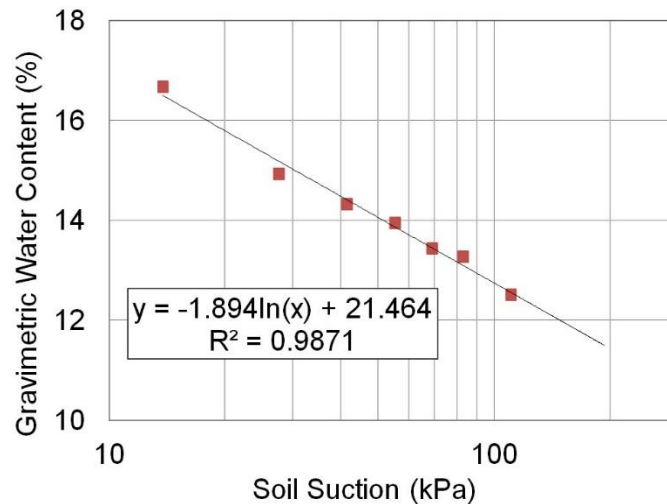


Figure 33 - Primary drying curve for pressure plate test.

### 6.4.3 Permeability Test

Permeability tests were performed on undisturbed samples taken from the excavation location in order to determine the flow properties of the soil surrounding the excavation. The procedures for the permeability test were followed according to ASTM D5084-00, "Standard Test Methods for Measurement of Hydraulic Conductivity of Saturated Porous Materials Using a Flexible Wall Permeameter." The results of the permeability tests are summarized in Table 14.

**Table 14 – Permeability results.**

Sample #	Sample Depth (m)	Hydraulic Gradient, i	Permeability, k (m/s)
1	0.0 - 2.4	4.6	$1.3 \times 10^{-5}$
2	2.4 - 3.0	4.6	$3.7 \times 10^{-6}$
4	3.0 - 4.6	4.6	$1.2 \times 10^{-5}$
8	4.6 - 6.1	4.6	$6.8 \times 10^{-6}$
11	6.1 - 7.8	4.6	$2.1 \times 10^{-7}$

## CHAPTER 7: UNSATURATED TRIAXIAL METHOD

To accurately model the unsaturated properties of the soil, a method was developed to determine the unsaturated strength parameter  $\phi^b$  using standard triaxial testing equipment with several low cost modifications. This method was published in the ASTM Geotechnical Testing Journal, Volume 35, Issue 1 (Burrage et al., 2011).

Several triaxial testing devices have been proposed and developed for unsaturated soils including Padilla et al. (2006), Wulfsohn et al. (1998), Thom et al. (2008), Cabarkapa and Cuccovillo (2006), Jotisankasa et al. (2007), Cui et al. (2007), and Sivakumar et al. (2006). These devices range in complexity and level of automation, and as mentioned earlier, most of these are often very expensive and require users with ample experience and training. In order to determine the unsaturated properties of the soil used in this experiment within a reasonable budget, a method was devised that can be used to evaluate the shear strength properties of unsaturated soils using a traditional triaxial testing apparatus. The proposed procedure is based on the axis translation technique, which is used in conjunction with many unsaturated soil testing devices, including the pressure plate extractor (ASTM D 6836-02).

### 7.1 Modifications to the Standard Triaxial Apparatus

The main goal of this method was to develop a simplified procedure for triaxial testing of unsaturated soils that can be implemented with ease and minimal cost, to obtain shear strength parameters of unsaturated soils. The testing apparatus consisted of a triaxial cell, a triaxial pressure panel, a load frame, a load cell, two pressure transducers, one displacement transducer,

one volume change transducer (optional), and a data acquisition system. Most of the components were unaltered with the exception of the triaxial cell, which was modified in order to apply matric suction to the soil sample using the axis translation technique. A schematic diagram of the proposed testing system is shown in Figure 34.

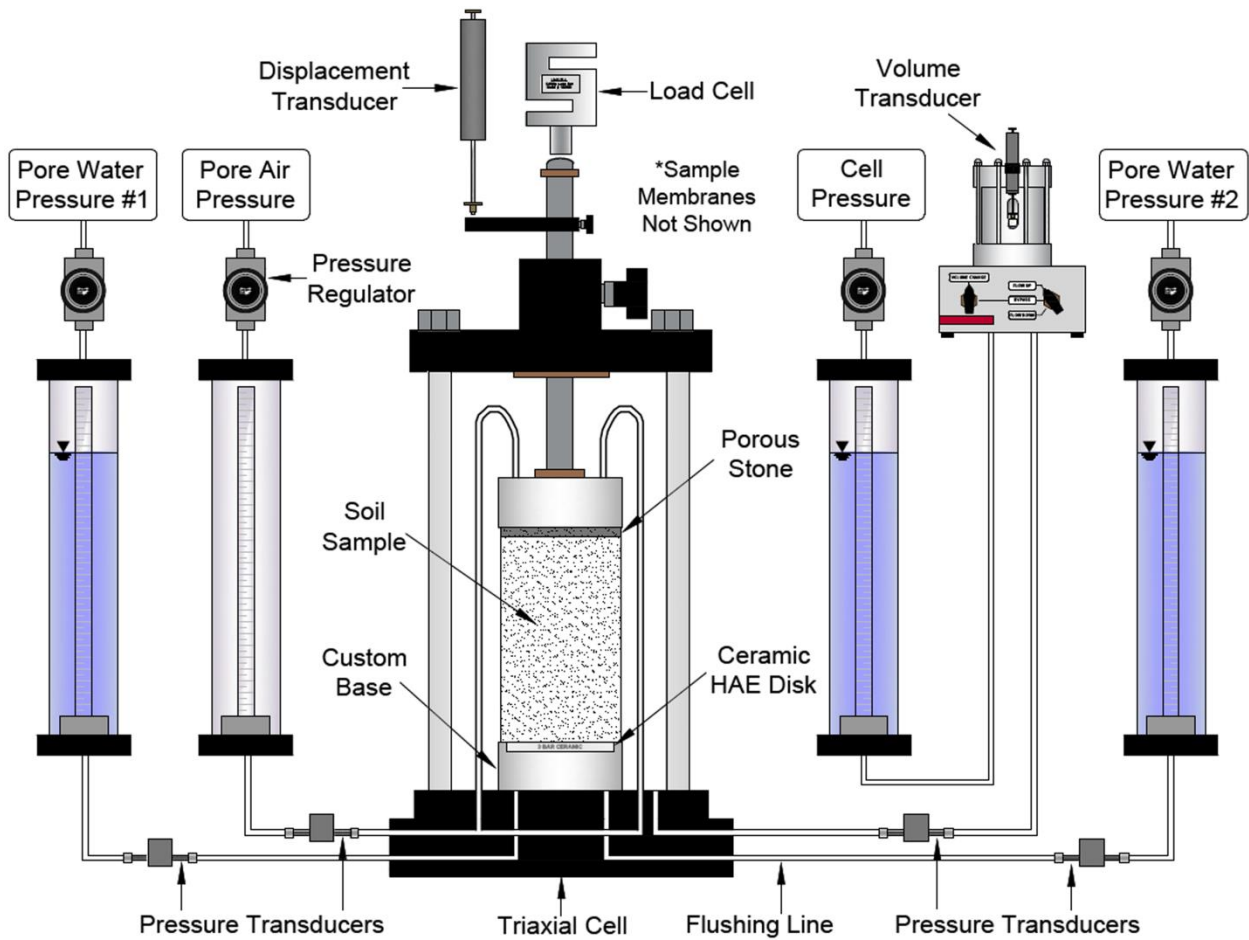


Figure 34 - Schematic diagram of the modified triaxial apparatus.

### 7.1.1 Triaxial Cell Modification

To control the matric suction during testing, a high-air-entry (HAE) disk was used to separate the air phase and the water phase of the soil so that differential pressures could be applied to impose a matric suction ( $u_a - u_w$ ). The disk used in this experiment was the 600 series (1-bar standard), from Soilmoisture Equipment Corporation. The only modification to the triaxial cell consisted of fabricating a modified base pedestal that would accommodate the HAE

disk and provide a water compartment below the disk for saturation. Figure 35(a) shows a dimensioned drawing of the customized triaxial base that was made. Note that this base is made for use with 2.8 inch (71.1 mm) diameter Shelby tube specimens, but a similar design can be used for a specimen of any diameter. Also, different HAE disks may be substituted for the 1-bar disk to allow testing at higher levels of matric suction. This base was constructed so that the location of the mounting screw and pressure lines would fit the Durham Geo Slope Indicator model S-511 triaxial cell.

When dealing with high air entry materials, it is important for them to remain saturated in order to prevent the flow of air. To accomplish this, a groove was cut under the disk compartment to allow for a sufficient amount of water to remain in contact with the disk. While high air entry materials create an air-water interface that prevents the transfer of phases, it is normal for a small amount of air to diffuse through the disk causing air bubbles to accumulate under the disk (Wulfsohn et al., 1998). Depending on the duration of the test, the diffused air could become problematic if enough air becomes trapped under the disk to cause it to lose saturation. In order to prevent this, the grooved compartment under the disk was routed in a way that water could flow from one of the pore pressure lines connected to the bottom base to the other pore pressure line connected to the bottom of the base by creating a pressure differential between the two lines. This flow of water would cause any trapped air bubbles to be flushed out of the water compartment below the disk.

The flushing groove is typical for several unsaturated triaxial systems that have been used in the past such as Padilla et al. (2006), and Wulfsohn et al. (1998). These systems use a spiral groove that starts in the center of the disk, and spirals to the outside edge of the disk. However, since the pore pressure lines in the cell used for this research were not located in the center and

the edge, the groove was cut to direct the water from one line to the other covering as large of an area on the disk as possible. Figure 35(b) shows a scaled drawing of the groove pattern used in this experiment. The light shaded area represents the 3.18 mm groove that was cut to a depth of 1.59 mm in the acrylic base. The black circles represent the location of the two existing pore pressure lines on the cell base. These holes were labeled as "1" and "2" to correspond with the pore water pressure cell connections shown in Figure 34. The dark gray shading shows the outer lip of the base that the HAE disk will fit inside.

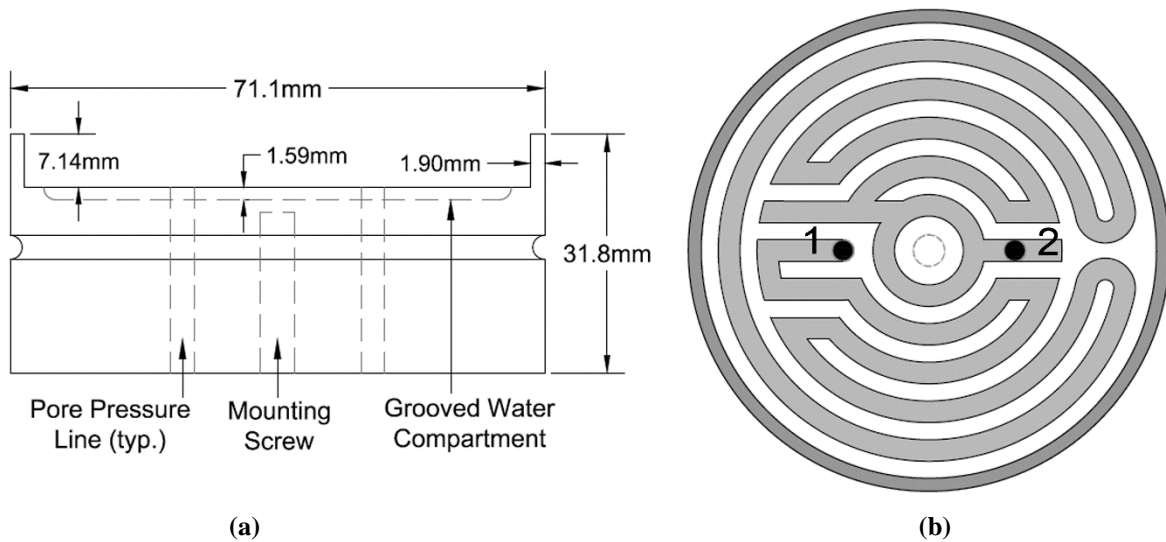


**Figure 35 - Modified triaxial cell base (a) side view, (b) top view showing groove pattern.**

The HAE disk was mounted in the base using silicone adhesive and tested for leaks before a triaxial test was performed using the cell.

### 7.1.2 Modification to Apply Matrix Suction

Similar to other unsaturated test methods, matrix suction was applied to a sample using the axis translation technique. In order to impose a desired level of matrix suction to the sample, the pressure line that connects to the top of the sample was connected to an empty burette in the pressure board to control the pore air pressure, and the pressure line that connects to the bottom of the sample (below the HAE disk) was connected to a pressure chamber filled with water to

control the pore water pressure (pore water pressure #1). The matric suction was applied by creating a pressure differential between the pore air pressure and the pore water pressure. To allow for the flushing of diffused air, the second pore pressure line that connects to the bottom of the sample was also connected to a pressure chamber filled with water (pore water pressure #2). Figure 34 illustrates the connections used for the proposed unsaturated triaxial apparatus.

### *7.1.3 Volume Change Measurement*

In a typical triaxial test, the sample would be saturated so that the volume change could be determined by the amount of water that extrudes from the sample. However, the volume change in an unsaturated test is equal to the total amount of water that is extruded from the sample plus the total amount of air that is extruded from the sample during testing. Although it is possible to quantify the total amount of air and water extruded from the sample during testing, devices used to measure extruded air and diffused air (Padilla et al., 2006b, and Wulfsohn et al., 1998) are not commonly found in a typical triaxial lab. These devices can also add significant cost and complexity to a triaxial apparatus. Alternate methods have been proposed for the measurement of volume change during unsaturated testing such as the use of strain gages attached to the sample (Thom et al., 2008), or the use of radial strain belts and submersible displacement transducers attached to the specimen (Cabarkapa and Cuccovillo, 2006). These methods can also add significant cost and complexity to the apparatus.

In the proposed method, the volume change measurement was determined by filling the triaxial cell completely with deaired water and measuring the total volume change of the cell fluid during the test. This method is considered to be one of the simplest methods of measuring volume change during testing (Leong et al., 2003), but can introduce error from various sources including, cell expansion and temperature fluctuation. Various researchers have developed

methods of perfecting this technique, one of the first being Bishop and Donald (1961) who developed a double cell device in which the volume measurement could be taken from a smaller internal cell to minimize errors caused by cell expansion.

To simplify the proposed apparatus and retain the cost effectiveness, the standard triaxial cell was used to measure the volume change and the amount of error was quantified for the apparatus through a series of calibration tests. The first calibration was performed on an undisturbed soil sample taken from the same site as the soil used in the unsaturated triaxial tests. The sample was saturated, consolidated, and tested to failure while recording both the change in pore water volume, and the change in cell water volume. The volume change for the cell fluid was then corrected to account for the loading ram entering the cell, and the two volumes were plotted versus axial strain (Figure 36-a). This figure shows the volume change during consolidation, the resetting of the loading ram for the height change during consolidation ( $h_c$ ), and the volume change during the loading phase. The difference in the two volume measurements was plotted versus axial strain and is shown in Figure 36-b. The results of this calibration show that the maximum difference in volume between the two methods was  $1.2 \text{ cm}^3$  during consolidation and  $0.5 \text{ cm}^3$  during shear.

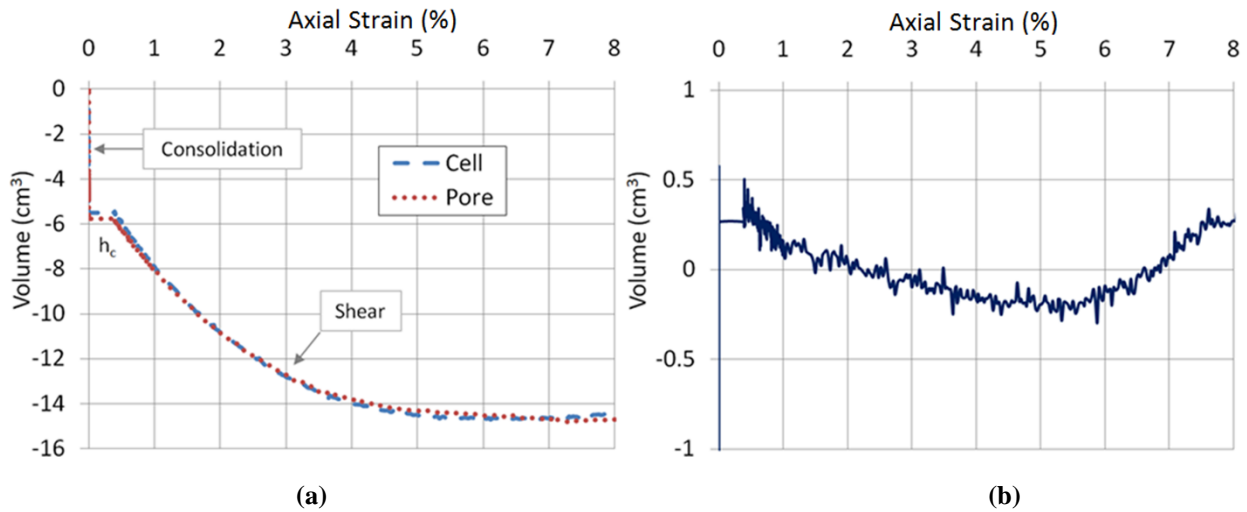


**Figure 36 - Volume change method comparison #1 (a) volume change vs. strain (b) difference in volume methods.**

To test the accuracy using the burettes on the triaxial cell, a second calibration was performed on a sample of clean sand which was prepared and tested in a similar manner. The volume change versus strain for this test is shown in Figure 37-a, and the difference between the two methods was also plotted versus strain (Figure 37-b). From this calculation the maximum difference between the two volume methods was found to be  $0.4 \text{ cm}^3$ .

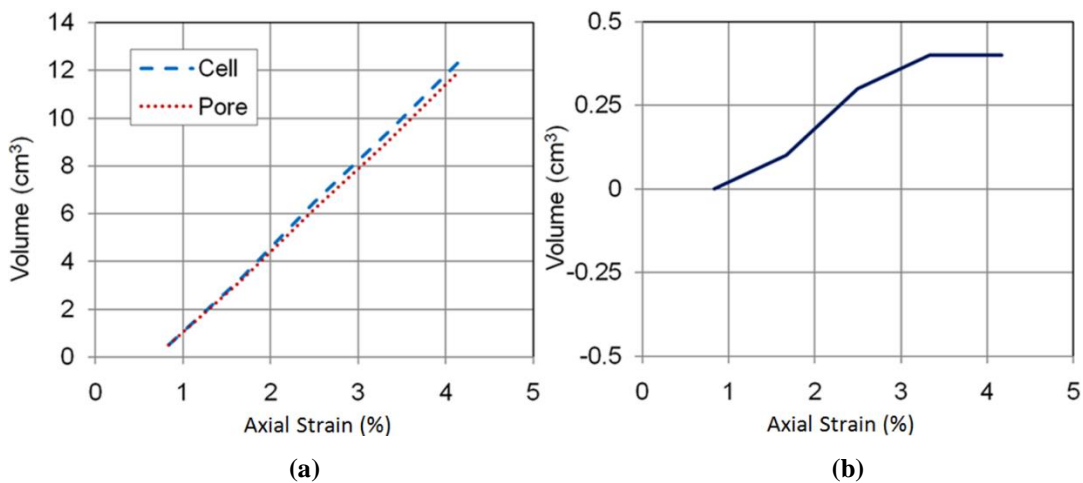


**Figure 37 - Volume change method comparison #2 (a) volume change vs. strain (b) difference in volume methods.**

In order to quantify the amount of error in this method of recording volume change, the volume measurements for the pore water were assumed to be accurate (since that is the

traditional method of recording volume change in a saturated test). The difference in the cell volume change readings were assumed as error and were used to calculate the percent error for the tests based on the average area of the specimen at failure. The highest error was found to be 0.3% for the apparatus used in this experiment, but this value may not be typical for all equipment in all environments, therefore when using this technique to determine volume change, similar calibrations should be performed to ensure larger errors are not induced. If larger errors are present, it may be possible to form a calibration equation from the results of multiple calibration tests, however since the errors measured for the equipment used in this experiment were very low, such calibrations were not applied to the data.

## **7.2 Test Procedure**

To test the functionality of the proposed apparatus, triaxial tests were performed on undisturbed soil samples from the Auburn NGES. The procedures for these tests were followed based on traditional consolidated-drained (CD) triaxial testing methods for undisturbed soil samples, with the exception of the matric suction application and volume change measurement. Note that the procedures described in this paper are based on the tests that were performed to test the functionality of the apparatus. Procedures for different testing methods, (constant water content, multi-stage, or others) may also be used with the proposed apparatus, but are not presented in this paper.

### *7.2.1 Sample Preparation / Mounting*

The initial sample preparation was followed based on ASTM D4767-04 method for undisturbed specimens. Soil samples were extruded from 2.8 inch (71.1 mm) thin walled Shelby tubes, and trimmed to a height of approximately 153 mm. Prior to mounting the specimen, the ceramic disk was saturated by opening the valves on the pore water pressure lines, and allowing

water to flow through the disk from the bottom to the top. A porous stone was placed on top of the soil specimen, and two membranes were installed around the sample to prevent air leakage during testing (Ho and Fredlund, 1982, Wulfsohn et al., 1998). According to ASTM D4767, membrane corrections should be applied when calculated error from membrane application is greater than 5%. However such corrections were not deemed necessary in this experiment because the calculated errors were less than 5%. After mounting the specimen, the triaxial cell was completely filled with deaired water to allow for volume change measurement using the cell fluid.

### *7.2.2 Matric Suction Application*

To apply the matric suction to the sample, the cell was connected to the pressure panel as shown in Figure 34. The chamber pressure and the pore pressures (air and water) were increased simultaneously, keeping the cell pressure approximately 5-10 kPa above the pore pressures until the pore pressures reached approximately 69kPa. The suction was then applied by increasing the pore air pressure, keeping the chamber pressure approximately 5-10 kPa above the pore air pressure, until the desired level of matric suction was reached.

### *7.2.3 Suction Equalization*

An important consideration for this experimental setup is to make sure that the external air and water pressures are applied to the sample long enough to ensure the matric suction within the sample has been achieved. The time required for this matric suction to be achieved within the sample is often referred to as equalization time. Typically the boundary conditions are chosen such that the sample undergoes drying during the equalization time and hence water is collected beneath the HAE disk during this period. The equalization time can be very long depending on the type of soil sample being tested, the dimensions of the sample, and the

difference between the initial conditions of the sample, i.e., its initial values of moisture and matric suction compared to the imposed levels of matric suction. Typically clay samples will require longer equalization times than silts or sandy samples. Furthermore, the larger the change of matric suction (i.e., initial versus final matric suction) the longer the equalization time.

For planning purposes it is useful to have an estimate of the required equalization time as some unsaturated soils may require several days to achieve the target matric suction. During the matric suction application, the user can assess whether equalization has been achieved from a plot of accumulated volume of expelled water coming from under the HAE disk versus time. For the experiments carried out in this paper, the volume of water exiting the sample during matric suction application was monitored via an internal pipette on the pressure panel. The samples were allowed to equalize until the readings in the pipette became stable. On average, this took approximately 48 hours per sample.

In order to ensure that ample time was allowed for equalization of the unsaturated specimens, the software Seep/W by Geo-Slope International was used to model the equalization rate of the specimens. The boundary conditions of the model were set to represent the average unsaturated specimen used in this experiment with respect to the sample dimensions, and the axis translation boundary conditions that were imposed on the specimen (138 kPa of air pressure applied to the top of the specimen, and 69 kPa of water pressure applied to the bottom of the specimen). The HAE disk was also input into the model at the bottom of the specimen. The initial matric suction for the model was estimated by relating the initial moisture content of the tested samples to a soil-water-characteristic curve that was previously obtained for the test soil using a pressure plate extractor (ASTM D 6836-02). From this relation, the initial matric suction that was input into the model was 35 kPa. The soil-water characteristic curve was also input into

the model, along with average values for the saturated soil permeability which were estimated based on consolidation results ( $10^{-4}$  cm/s). Unsaturated permeability was also input into the model based on standard curves for ML soils. Figure 38 shows a plot of water extrusion versus time generated by Seep/W.

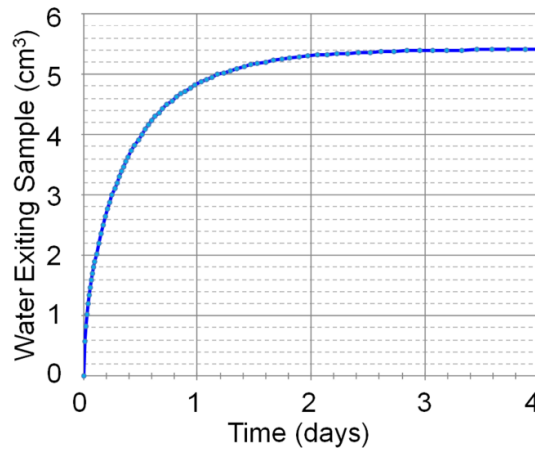


**Figure 38 - Sample equalization time based on Seep/W modeling software.**

The results of this model showed that 98% of the equalization had occurred in 48 hours, indicating that the matric suction level in the samples in this experiment was within approximately 0.35 kPa of the desired level. Through this model verification, it was determined that the internal pipette readings were sufficient for determining when the equalization had occurred in the sample.

#### *7.2.4 Flushing the HAE Disk*

After the suction was applied, the HAE disk was initially flushed to remove any air bubbles that might have been trapped under the disk. In order to flush the disk, the pressure regulator for the second pore water pressure port (labeled as pore water pressure #2 in Figure 34) was set to a pressure approximately 1-2 kPa lower than the first pore water pressure port (pore water pressure #1), and the valve was opened allowing water to flow through the groove under the disk (Figure 35b). The burettes were monitored and the valves were closed when air bubbles

stopped appearing in the burette (approximately 1 minute). The process was performed at least once every 18-24 hours to ensure that the disk remained saturated. Since the outer cell fluid was being used to determine the volume change of the specimen, the diffused air can be flushed without impacting volume change measurements during testing.

#### *7.2.5 Consolidation*

Before the sample was consolidated, the volume change device was connected in-line with the cell pressure line so that the total volume change of the cell fluid could be measured and used to calculate the total volume change of the soil specimen. If a volume change device is not available, burette readings may be taken instead to determine the total volume change of the specimen during consolidation and shear. Note that when using the cell volume change to measure the specimen volume change during shear, the measurement for cell volume change must be corrected to account for the loading ram entering the cell during the test. After connecting the volume change measurement device, the confining pressure was applied to the system with the valve closed on chamber to allow the volume change measurement device to become pressurized. Then the data acquisition process was started and the cell pressure valve was opened so that the volume change of the specimen could be measured during consolidation.

#### *7.2.6 Shear*

After the matric suction was equalized within the sample and the consolidation was complete, the samples were sheared under drained conditions at a displacement controlled rate of 0.167 mm/min. This rate of displacement was considered to be adequate for the soil samples tested in this experiment because it ensured drained conditions during testing.

### 7.3 Unsaturated Triaxial Test Results

The initial degree of saturation was determined for each sample and is recorded in Table 15. In order to minimize the amount of time required for the unsaturated samples to equalize, they were selected from Shelby tubes where the initial matric suction was close to the imposed suction (69 kPa). The initial matric suction for the samples used in the unsaturated tests (samples 4-6) was estimated using a soil-water characteristic curve that was previously conducted on the soil at the NGES site. These estimated initial values are also presented in Table 15.

**Table 15 - Initial sample conditions for triaxial tests.**

Sample	Degree of Saturation (%)	Estimated Matric Suction (kPa)
1	83.3	--
2	83.0	--
3	87.8	--
4	55.9	59
5	55.6	60
6	56.3	58

Table 16 and Table 17 summarize the conditions at failure for each specimen. In these tables,  $\gamma_d$  represents the dry unit weight of the soil,  $\sigma_d$  represents the deviatoric stress,  $\sigma_3$  represents the confining stress,  $\sigma_1$  represents the major principal stress ( $\sigma_3 + \sigma_d$ ),  $u_w$  represents the pore water pressure, and  $u_a$  represents the pore air pressure. The B-values obtained for the saturated samples are also shown in Table 16, indicating the level of saturation achieved.

**Table 16 - Saturated triaxial test conditions at failure.**

Test #	$\gamma_d$ (kN/m <sup>3</sup> )	B-Value	$\sigma_d$ (kPa)	$\sigma_3$ (kPa)	$\sigma_1$ (kPa)	$u_w$ (kPa)	$\sigma'_3$ (kPa)	$\sigma'_1$ (kPa)
1	11.3	0.96	133	379	512	345	34	167
2	11.9	0.95	216	414	630	345	69	285
3	12.8	0.94	288	448	736	345	103	391

**Table 17 - Unsaturated triaxial test conditions at failure.**

Test #	$\gamma_d$ (kN/m <sup>3</sup> )	$\sigma_d$ (kPa)	$\sigma_3$ (kPa)	$\sigma_1$ (kPa)	$u_a$ (kPa)	$u_w$ (kPa)	$u_a-u_w$ (kPa)	$\sigma_3-u_a$ (kPa)	$\sigma_1-u_a$ (kPa)
4	13.5	226	172	398	138	69	69	34	260
5	13.6	316	207	523	138	69	69	69	385
6	14.4	365	241	606	138	69	69	103	468

Deviatoric stress versus axial strain, and volumetric strain versus axial strain plots for the samples are shown in Figure 39a and Figure 39b respectively. The test numbers that correspond with Table 16 and Table 17 are labeled in Figure 39.

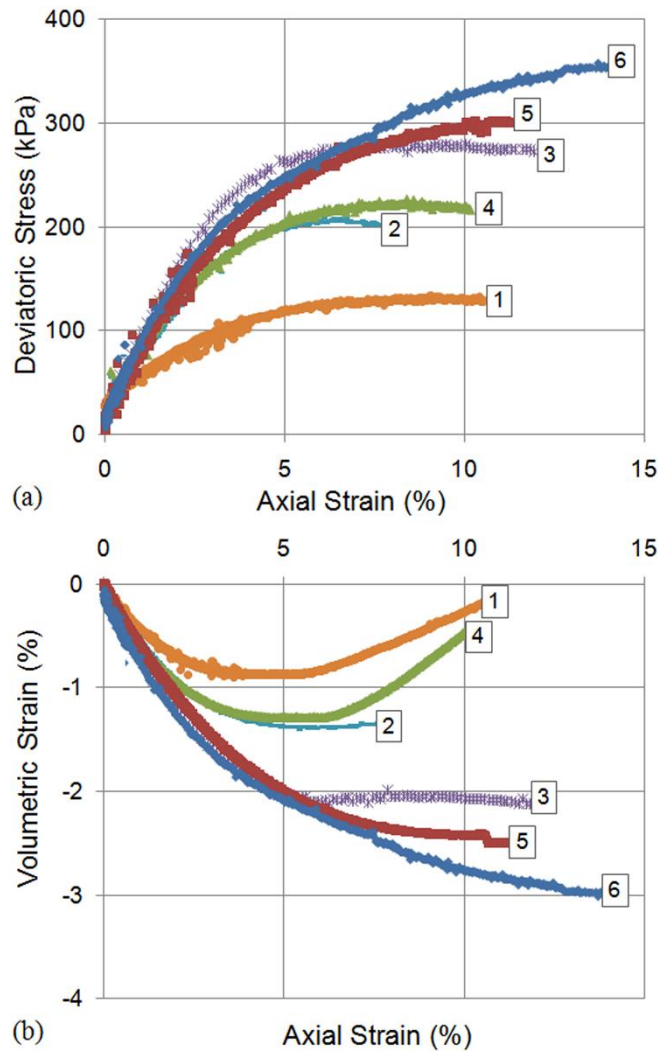


**Figure 39 - (a) Deviatoric stress vs. axial strain (b) volumetric strain versus axial strain.**

In order to test samples close to their initial matric suction values, the unsaturated samples were taken from Shelby tubes in a depth range of 2.5-3.0 m, because the moisture content at that depth corresponded with the desired initial suction value. The saturated samples were taken from the same borehole at a depth of 4.1-4.6 m. Because the soils were taken from two different depths, the dry unit weight of the samples varied slightly. This difference in unit weight could have a slight impact on the comparison between the saturated and unsaturated tests, but the impact was considered to be minimal in comparison to the effects of the 69 kPa of matric suction imposed on the samples. The index testing and insitu tests both showed that the soil

properties were relatively constant throughout this range of depth indicating that large amounts of error should not be present due to variations in soil properties.

The results of the triaxial tests were plotted in  $p'$ - $q$  space (MIT definition) to determine the values for the effective friction angle ( $\phi'$ ) and the effective cohesion ( $c'$ ) for the soil (Figure 40). A linear trendline was fit through the failure points of the saturated samples, and a trendline of equal slope was fit to the unsaturated tests to determine the increase in cohesion for the unsaturated tests.

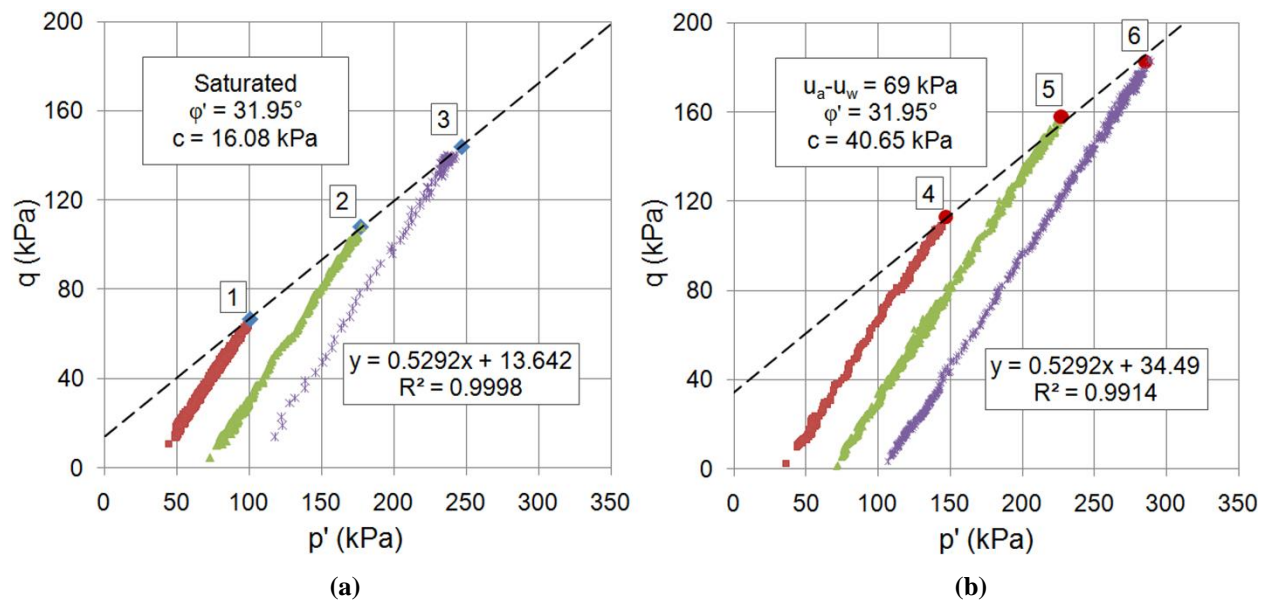


**Figure 40 - Failure criterion for (a) saturated samples and (b) unsaturated samples.**

The trendlines displayed in Figure 40 are presented in the format shown in Equation 14.

Using this equation,  $\phi'$  and  $c'$  can be calculated using the relations shown in Equations 15 and 16.

$$q_f = \tan(\alpha') p'_f + a' \quad (14)$$

$$\sin \phi' = \tan \alpha' \quad (15)$$

$$c' = \frac{a'}{\cos \phi'} \quad (16)$$

Equation 17 defines  $p'$  for the saturated tests, and Equation 18 defines  $p'$  for the unsaturated tests. Equation 19 defines  $q$  for both the saturated and unsaturated tests.

$$p' = \frac{(\sigma_1' + \sigma_3')}{2} \quad (17)$$

$$p' = \frac{(\sigma_1 + \sigma_3)}{2} - u_a \quad (18)$$

$$q = \frac{(\sigma_1 - \sigma_3)}{2} \quad (19)$$

The calculated values for the effective friction angle and cohesion are shown in Figure 40. From this plot, the samples tested at a suction of 69 kPa showed on average an increased cohesion of approximately 24.6 kPa over the saturated samples, indicating that apparent cohesion was present during the unsaturated tests.

#### 7.4 Method Comparison

For the purpose of comparing these test results to previous tests in similar soils,  $\phi^b$  was calculated using the relationship shown in Equation 20 (Lu and Likos, 2004), and was found to be 19.6° for a matric suction range of 0 to 69 kPa. It is important to note that because this equation assumes linear behavior, it is only valid at matric suctions near saturation. Current research has shown the rate of change in apparent cohesion at different levels of matric suction to be non-linear over a wide range of suctions (Lu and Likos, 2006). However, this non-linear behavior could still be defined using the proposed apparatus by testing multiple samples at various levels of matric suction.

$$c'_1 = c' + (u_a - u_w) \tan \phi^b \quad (20)$$

In this equation,  $c'_1$  represents the effective cohesion for the unsaturated specimens with imposed matric suction ( $u_a - u_w$ ),  $c'$  represents the effective cohesion from the saturated tests, and  $\phi^b$  is an angle that represents the rate of increase in shear strength as the matric suction increases.

The value calculated for  $\phi^b$  in this experiment was compared to values presented by previous research in similar soil types. Table 18 was modified from Fredlund and Rahardjo (1993) to show shear strength parameters for soils similar those used in this experiment.

**Table 18 - Shear strength parameters for relevant unsaturated soils.**

Soil Type	$c'$ (kPa)	$\phi'$ (deg)	$\phi^b$ (deg)	References
Undisturbed Decomposed Granite	28.9	33.4	15.3	Ho and Fredlund (1982b)
Boulder Clay; $w = 11.6\%$	9.60	27.3	21.7	Bishop et al. (1960)
Madrid gray clay; $w = 29\%$	23.70	22.5	16.1	Escario (1980)
Tappen-Notch Hill silt; $w = 21.5\%$	0.00	35.0	16.0	Krahn et al. (1989)

Fredlund and Rahardjo, (1993)

The soils tested in Ho and Fredlund (1982b) comprised of decomposed granite that was described as slightly clayey, sandy silt with some fine gravel. The effective friction angle for this soil was assumed to be  $33.4^\circ$ , and the effective cohesion was assumed to be 28.9 kPa. The average  $\phi^b$  value for the tests was  $15.3^\circ$  with a standard deviation of  $\pm 5.7^\circ$  (Ho and Fredlund, 1982b). Since the soil tested in this experiment was also decomposed granite with similar properties, an expected value for  $\phi^b$  would be in the same range.

Index testing by Vinson and Brown (1997) also concluded that the soils at the Auburn NGES site classified as primarily silts with some clay. Based on the values presented in Table 18, expected  $\phi^b$  values for silts and clays could be in the range of  $16.0$ - $21.7^\circ$ .

Due to these results, the calculated  $\phi^b$  value of  $19.6^\circ$  falls within an expected range for similar soil types, indicating that large errors were not introduced by the proposed apparatus and methodology.

## 7.5 Limitations

Several limitations exist and must be considered when using this testing method. The first limitation is the time required for equalization within the sample after imposing a matric

suction. Although this limitation exists whenever unsaturated tests are performed, the use of a larger 2.8 inch (71.1 mm) diameter specimen will result in a greater amount of equalization time. In this test, soil samples were selected that were already close to the imposed matric suction values, therefore only 48 hours was required for the samples to equalize. However, when large matric suction differentials are applied to samples, the time can be greatly increased and since this method does not provide a means of automatically flushing the diffused air from beneath the disk, the sample might require attention during this equalization phase.

The volume change method used in this test was calibrated for the conditions in the laboratory, and was shown to have a maximum of 0.3% error. However, different equipment and laboratory conditions might result in higher levels of error. The pressure cell used in this experiment was equipped with metal bands that wrapped around the acrylic cell, providing additional support, and keeping cell expansion to a minimum. Also, the temperature in the laboratory remained relatively constant ( $\pm 1^\circ\text{C}$ ) during testing, therefore the expansion and contraction of the cell due to temperature fluctuation was minimized. In environments with large temperature fluctuations, the expansion and contraction of the cell could introduce additional error in the volume change measurement. As noted in the procedure section, two membranes were placed on the specimen to prevent leaks. Since the viscosity of air is much less than that of water, there is a higher probability of leaks when testing unsaturated soils. Leaks, through the membranes, around the cell base, or around the HAE disk may also contribute to additional error in the volume change if encountered. Because of these limitations, calibrations similar to those presented in this paper should be conducted to determine the potential error associated with the simplified volume change measurement procedure.

Because of the heterogeneous nature of soil (in general), many tests are needed to properly assess the limitations of an apparatus. Although the example tests performed in this experiment indicate that the apparatus functioned properly, additional testing is needed to prove its effectiveness when using other soil types, and laboratory equipment.

Because of these noted limitations, this method is intended to be a simplified approach with adequate precision levels for applied conventional geotechnical engineering practice. Advanced research applications may require higher levels of precision and thus may require use of specialized, more expensive, unsaturated soil testing systems.

## CHAPTER 8: INSITU SWCC METHOD

Soil-water characteristic curves (SWCC) are commonly used when performing finite element models in unsaturated residual soils. Although limited research exists, previous attempts at defining SWCC in residual soil have proven to be cumbersome and time consuming due to the heterogeneous nature of residual soil and its high susceptibility to disturbance. For this reason, Agus et al. (2001) suggested empirical parameters that could be used to estimate the SWCC. Agus et al. (2001) and Aung et al. (2001) also evaluated the impact of weathering and porosimetry on the SWCC in residual soils. The main focus for the SWCC measurement used in this paper was to validate empirical methods used in modeling unsaturated residual soil.

Insitu measurements of soil-water relationships have been conducted by numerous researchers in the past including Nielsen et al. (1973), Dane and Hruska (1983), Greminger et al. (1985), and Paquet et al. (1993). One of the benefits of insitu SWCC determination is that soil water relationships can be measured with minimal disturbance. Various researchers such as Box and Taylor (1962), Campbell and Gardner (1971), Vanapalli et al. (1999), Ng and Pang (2000), Miller et al. (2002), Zhou and Yu (2005), and Birle et al. (2008) concluded that the SWCC can be affected by numerous parameters including the bulk density, void ratio, initial water content, and stress state, indicating that traditional laboratory test methods may introduce significant error due to the disturbance involved with sampling and preparing laboratory samples. Other researchers such as Gallipoli et al. (2003), Wheeler et al. (2003), Miller et al. (2008), Muraleetharan et al. (2009), Sheng and Zhou (2011), and Salager et al. (2013) have studied the

coupling effects of mechanical behavior with hydraulic behavior. Because of these findings, laboratory devices have been developed that allow the SWCC to be measured at various stress states. Malicki et al. (1992) developed a method of determining the soil-water characteristics within a core sample tube. Devices were also developed by Ng and Pang (2000), and Padilla and Perera (2005) which allow the simulation of confining pressure while determining the SWCC. Although substantial research has been performed on determining the SWCC of soil insitu, it is still an area full of challenge and worth studying further as changes in technology lead to the enhancement of equipment and sensors.

In this experiment, a field instrumentation technique was developed to generate a SWCC for residual soil insitu. The aim was to develop a cost-effective method that could easily be implemented, and could be conducted over a long period of time with minimal maintenance, and thus overcome some of the difficulties that have been confronted in the aforementioned research. This method would enable the collection of insitu soil-water relationships at many locations simultaneously, which would be particularly useful in residual soils, because of the heterogeneous nature.

The Watermark 200SS sensor was selected to measure suction because of its robust design, extended range (0-200kPa) and maintenance free operation. The Campbell Scientific CS616 Water Content Reflectometer (WCR) was selected to measure volumetric water content because of its accuracy, fast response time, and its ability to measure long-term unattended water content. Both manufacturers provide instructions for the installation of these sensors insitu, as well as generic calibration equations. However, previous research such as Benson and Wang (2006) and Shock et al. (1998) suggest that these sensors be calibrated using site specific soils to

ensure accuracy. Such calibrations were performed for the sensors used in this experiment, and are presented in the Data Analysis section of this paper.

### 8.1 Data Analysis

The insitu SWCC test was conducted from August 5<sup>th</sup>, 2010 until November 10<sup>th</sup>, 2010. The suction and volumetric water content were both measured on 30 minute time intervals. The range of the soil water content was solely dependent on the local weather conditions for the duration of the test (the soil was not wet or dried to extend the range of the SWCC). Because the sensors were installed during period where the soil was drying rapidly, the initial equalization time for the suction sensor could not be determined and therefore the data for the first drying curve was discarded (August 5<sup>th</sup> - August 27<sup>th</sup>). Figure 41 shows the time series for gravimetric water content, suction, and soil temperature, along with the measured precipitation for the duration of the test.

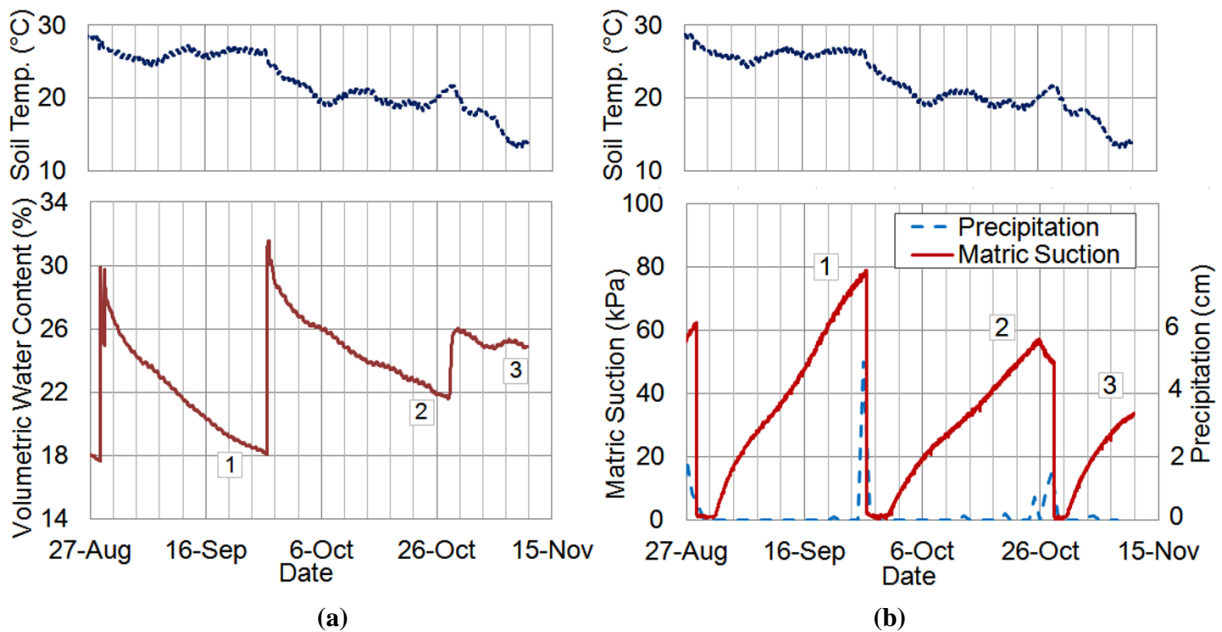


**Figure 41 - (a) Volumetric water content and soil temperature vs. time, (b) Suction, precipitation and soil temperature vs. time.**

### *8.1.1 Unresponsive Data*

When reducing the data, it was observed that with every storm event, there was a certain number of readings in which the Watermark sensor was unresponsive (only reading 0 kPa), indicating that internal matrix within the sensor became saturated with each storm event and required some time to equalize after each saturation. This behavior was seen with every substantial storm event that was recorded, regardless of the water content change of the surrounding soil during that event. One possible cause of this could be that water was able to reach the sensor more easily than the surrounding soil. Because this sensor was only 30 cm deep, and the wire was buried near vertical, a likely path for water to flow would be around the buried sensor wire, and perhaps through the backfilled soil material. An alternate sensor configuration to prevent this from occurring is presented in the recommendations section of this paper. In order to clearly see the drying curves measured during the test, the data points from the unresponsive sensor measurements were manually located and discarded.

### *8.1.2 Sensor Lag*

In periods where the soil suction is changing rapidly, it is possible for the sensor to not have enough time to equalize properly, therefore creating a "lag" in the suction data with respect to the WCR data. In order to prevent erroneous data, any such points should be identified and removed from the data set. To fully assess the equalization rate for the Watermark sensor, two additional sensors were installed on the same site at depths where the suction was relatively constant (1.5m and 3.0m). Because the suction was constant at that depth, it was easy to see exactly when sensor equalization had occurred. Figure 42a shows the initial equalization curve for the 1.5m sensor (Sensor 1), and the 3.0m sensor (Sensor 2). The instantaneous equalization rate was then plotted for the sensors by fitting polynomial trendlines to the initial equalization

curves, and plotting the first order derivatives of these trendlines. The R-squared values for these trendlines were both greater than 0.99 indicating that the trendlines were an accurate representation of the equalization curve. The first order derivatives of the equalization curves for sensors 1 and 2 are illustrated in Figure 42b.

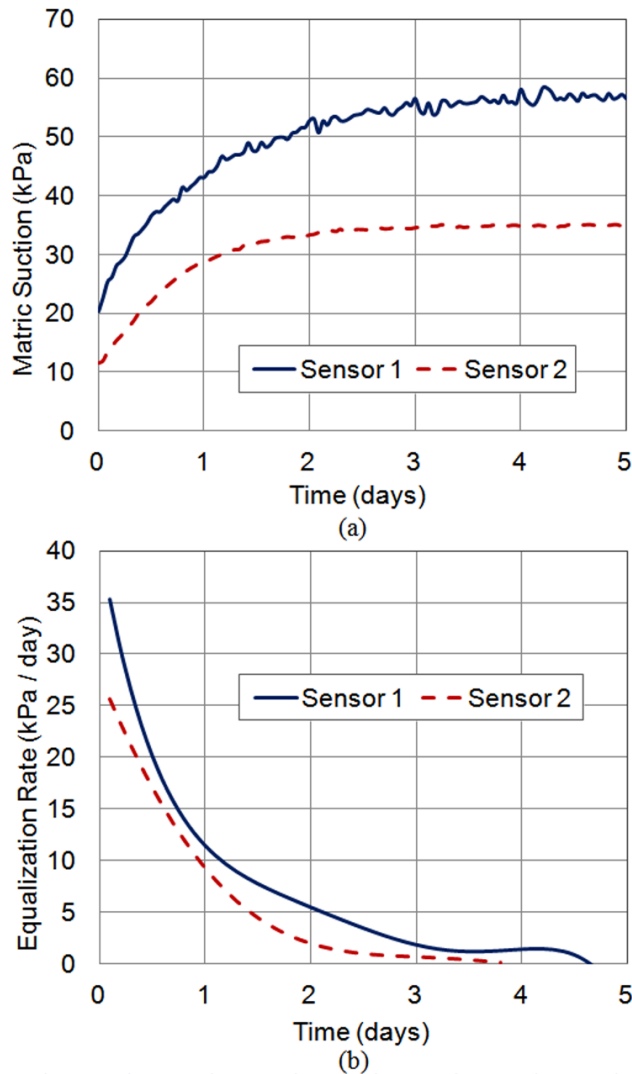


**Figure 42 - (a) Measured equalization curves. (b) calculated instantaneous equalization rate (first order derivative of equalization curves).**

To assess the error introduced by the sensor lag, it was assumed that the equalization rate is a function of the suction differential between the sensor, and the surrounding soil. Figure 43 shows a plot of the instantaneous equalization rate versus the pressure differential between the

Watermark sensor and the surrounding soil (sensor lag). This is based on the assumption that if the Watermark sensor measurements are changing, they are being driven by a pressure differential between the sensor media and the surrounding soil. Therefore if the Watermark sensor equalization rate is greater than zero, the suction in the surrounding soil must be slightly different than the suction within the sensor, creating a "lag" in the data recording.

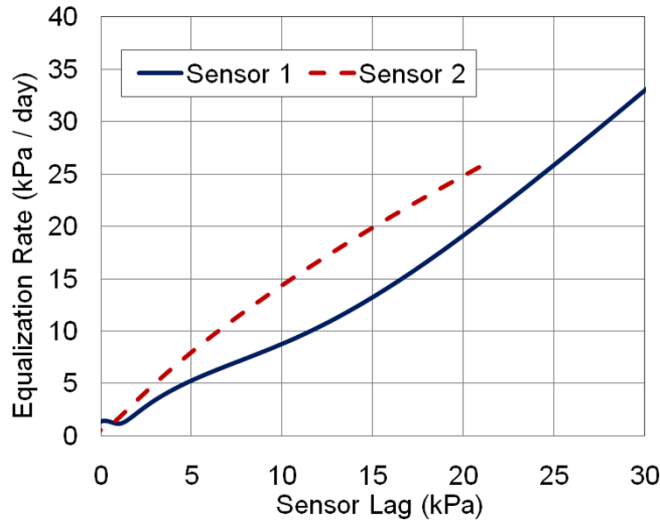


**Figure 43 - Equalization rate versus sensor lag (error).**

To quantify the amount of error encountered during the SWCC generation, the instantaneous equalization rate was plotted for the sensor used in the SWCC measurement throughout the entire duration of the test (Figure 44). From this figure, the peak equalization rate was approximately 5.5 kPa/day, while the majority of measurements taken when the equalization rate was between 1 and 3 kPa/day. Substituting this data into Figure 43, the maximum error during the SWCC measurement was determined to be approximately 4kPa, while the majority of readings had less than 2kPa lag error. The maximum error should not have a large impact on the curve development, because since only a few points were recorded with 4kPa error, they would be considered outliers on the curve. Therefore, the average error (due to sensor lag) for the suction measurements generated by the Watermark sensor was approximately 2kPa. In

applications where this error is not tolerable, the accuracy could be improved by removing the data points with the highest equalization rates (errors), leaving only those that are closer to equalization with the surrounding soil. Also, corrections could be applied to the data set to shift the entire curve and therefore correct for the sensor lag. For the purpose of this experiment, however, the 2kPa average error was tolerable, and such corrections were not applied to the data.

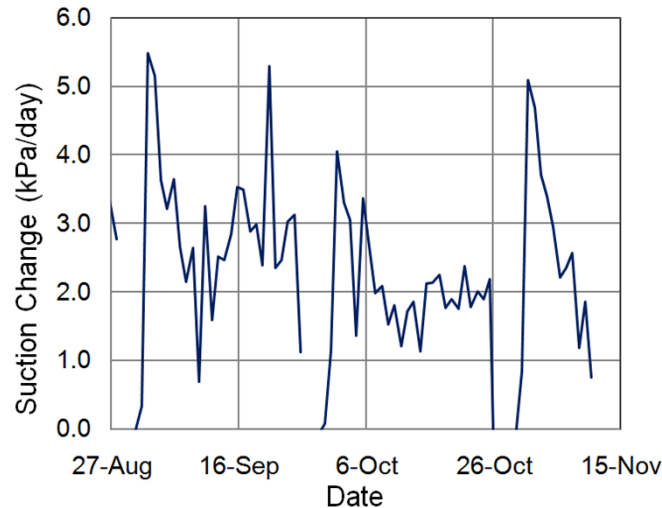


**Figure 44 - Instantaneous equalization rate throughout duration of SWCC measurement.**

## 8.2 Results

During the duration of the test, a total of three drying curves were recorded (labeled as 1, 2, and 3 in Figure 41). A plot of gravimetric water content versus matric suction was formed with the data and is shown in Figure 45. The three drying curves were labeled on Figure 45 to correspond with the time series shown in Figure 41. Because substantial rain events caused the saturation to occur very quickly (usually within one or 2 data intervals), sufficient data points for wetting curves were not recorded in this test. However, other research such as Chard (2002) and Shock et al. (2001) suggest that obtaining wetting data with the Watermark sensors is possible if the water content does not increase as rapidly. The recommendations section of this paper discusses an alternate sensor configuration and techniques that may improve the collection of wetting data.

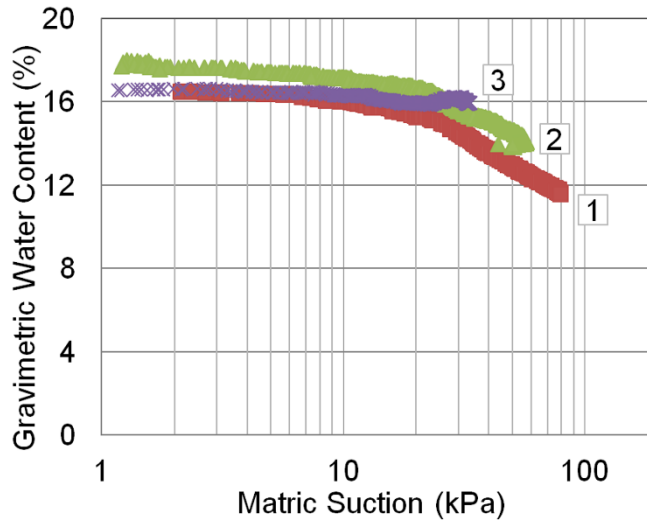


**Figure 45 - Drying curves recorded during insitu SWCC test (0.3m depth).**

Based on this plot, curve 1 on Figure 45 represents the first drying curve which occurred from August 28th to September 25th, curve 2 represents the second drying curve which occurred from August 30th to September 27th, and curve 3 represents the final drying curve which occurred from October 28th to November 15th, 2010.

### *8.2.1 Primary Curve Approximation*

Pham et al. (2003) defines the different types of soil-water characteristic curves as bounding curves, and scanning curves, illustrated by (Figure 46). Primary curves are most commonly measured and consist of the bounding curves that form the hysteresis. Scanning curves begin at a point on the wetting curve, travel through the hysteresis, and connect to the drying curve (or vice versa). They are created when the beginning water content of the soil is less than fully saturated. Theoretically the primary drying curve of the soil could be estimated by taking the upper boundary of all the data collected for a given sensor location (assuming the soil is completely saturated at some point during the measurement process). With enough data, it may also be possible to approximate the wetting curve in a similar fashion by drawing a lower-

bound curve that connects the lowest data points (assuming wetting data is recorded by the Watermark sensors).

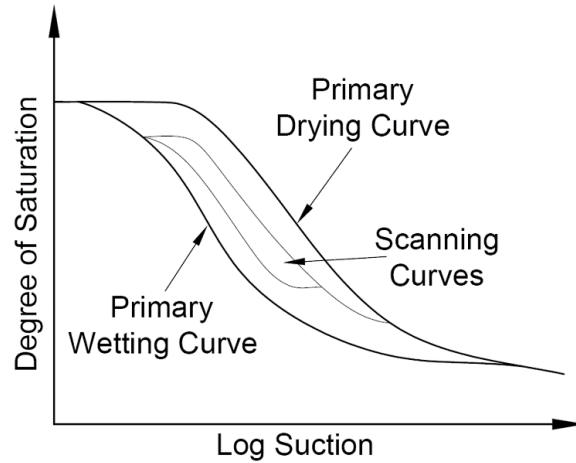


**Figure 46 - Bounding and scanning curves.**

For the three curves measured in this experiment, curve 2 was the closest to the primary drying curve, because the soil was able to reach the highest level of saturation before the drying began (approximately 80%). However, since the surrounding soil did not reach 100% saturation during this experiment, all of the curves measured were still considered to be scanning curves.

Figure 47 shows the approximate location of the primary drying curve based on the data that was obtained during the experiment (0-100kPa range).

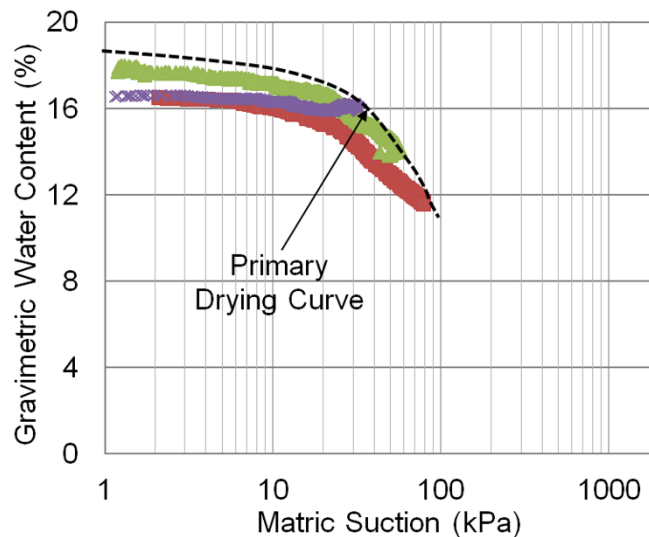


**Figure 47 - Approximate location of primary drying curve based on insitu data.**

### **8.3 Limitations**

One of the greatest limitations when using the method presented in this paper is that the water contents of the insitu soil are not easily controlled, therefore limiting the range of the soil-water relationships that can be obtained. Environmental factors such as temperature and precipitation can greatly increase the amount of time required to form a soil water relationship over a desired range of water contents. Because suction values generally become more constant with depth, this insitu method is also limited to soil depths above the water table in which the change in water content is great enough to form a curve. Based on suctions recorded from other sensors in the field, the depth range for this site would be in the range of 0-0.6 meters.

#### *8.3.1 Sensor Limitations*

It is important to note that the Watermark sensor is not able to accurately measure changes in suction when the surrounding soil is close to saturation. When the soil is near saturation, the water content of the substrate material within the Watermark sensor does not change significantly because it will be below the air entry value of the substrate material within the sensor. This type of behavior was identified by Flint et al. (2002) in a paper that focused on thermal dissipation sensors. Another limitation of the Watermark sensor is that it takes some time to equalize after initial installation and after every substantial storm event, therefore creating some erroneous data points. Also, the calibration coefficients for the Watermark sensor can vary based on the properties of the surrounding soil, which might make it necessary to perform a site specific calibration depending on the tolerable range of error.

Similar to the Watermark sensor, the Campbell Scientific CS616 WCR calibration can vary based on the type of soil surrounding the sensor. The manufacturer's calibrations may be suitable for estimates, but calibrations should be performed to ensure accuracy, especially when

taking measurements in residual soils. This is also important when dealing with soils that may have high metal content (and thus high dissipation of energy during measurements of dielectric permittivity), which can lead to significant errors.

#### 8.4 Recommendations

Due to the limitations that were identified during this experiment, an alternate sensor configuration is suggested which should provide less disturbance, and provide more representative results (Figure 48). This configuration will allow the water flux to take place through residual soil directly above the sensors and not through re-compacted soil, which should help to more effectively capture the insitu behavior of residual soil and prevent errors associated with the water flux through the re-compacted soils. This should also prevent the premature saturation of the Watermark sensors with each storm event because water will not have a direct path along the sensor wire into the soil surrounding the sensor.

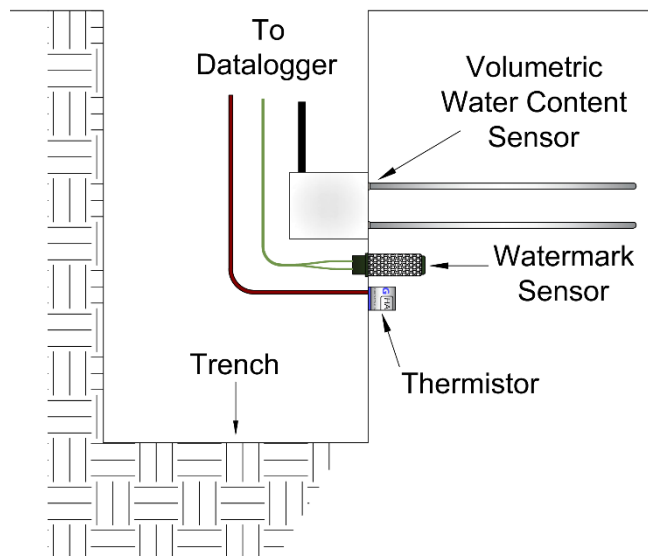


**Figure 48 - Alternate sensor configuration**

In order to measure the primary drying curve more effectively, the soil surrounding the sensor location could be initially saturated upon sensor installation. This will ensure that the

subsequent drying curve obtained will be the primary drying curve and not a scanning curve within the hysteresis. It should also greatly reduce the equalization time for the Watermark sensors, because both the sensor and the surrounding soil will be saturated when the data collection process starts.

In order to extend the range of measured SWCC, it might be beneficial to cover the sensor area (with a tarp or tent), and divert surface runoff to prevent saturation of the surrounding soil during the measurement process. This should also greatly decrease the time required to develop a curve of significant range. If necessary, methods of heating the soil surface could also be used to speed up the evaporation process, and extend the range beyond what is seen by natural soil-atmosphere interaction. Similarly, water could be added to the soil to increase the volumetric water content, and extend the range in the opposite direction. A wetting curve could potentially be measured, if the rate is monitored, and the sensor location is protected from the influence of high intensity storm events. However, altering the moisture content in the soil may not be feasible in soils which are sensitive to changes in water content (i.e. residual soils which might exhibit collapsing, or irreversible hardening effects).

## CHAPTER 9: DATA ANALYSIS

### 9.1 Site Specific Sensor Calibrations

All of the sensors that were used in this experiment were supplied with manufacturer's calibration equations. However, current literature suggests that the calibrations for the Watermark SMP sensors, and the dielectric WCR's can vary based on site-specific soils. Therefore, in order to increase the accuracy of the data, these sensors were calibrated using site specific soils.

#### *9.1.1 Watermark Sensor Calibration*

In order to ensure accurate measurements of suction in residual soil, the Watermark sensors were calibrated insitu to preserve the impacts of the residual soil fabric structure and cementation. A Watermark 200SS sensor was installed side-by-side with a Geokon Model 4500 series vibrating wire piezometer (equipped with a 3 bar HAE ceramic filter) and simultaneous measurements were recorded throughout several wetting and drying cycles. A linear equation was then formed to calibrate the resistance measurements from the Watermark sensor to the suction measurements recorded by the Geokon piezometer. Although the polynomial equation provides a better fit for the calibration data in the range of 0-100 kPa, other popular calibrations suggest that the sensor response throughout the 0-200 kPa range is best represented by a linear equation.

The resistance measurements taken by the Watermark sensor are sensitive to temperature changes within the sensor. Because the sensors were calibrated insitu, the data obtained was not

sufficient to form a site specific temperature calibration. However, the temperature corrections supplied by the manufacturer were deemed to be sufficient because it was assumed that temperature response of the sensor was predominately dependent upon the temperature changes of the internal matrix and electrodes within the sensor, and would not be impacted greatly by the type of soil that surrounds the sensor. The manufacturer's equations for normalizing the Watermark resistance measurements to 21°C are as follows (Campbell Scientific, Inc. 2009).

$$R_{21} = \frac{R_s}{1 - (0.018 \times dT)} \quad (21)$$

$$dT = T_s - 21^\circ C \quad (22)$$

Where:  $R_s$  is the measured resistance (kΩ), and  $T_s$  is the temperature of the soil (°C).

Once the resistance measurements taken by the Watermark sensors were corrected for temperature, the corrected resistance values were plotted versus the suction values measured by the Geokon 4500, and a linear trendline was fit through the data (Figure 49a). The resulting calibration equation is as follows:

$$SWP = 7.5175 \times R_{21} - 17.414 \quad (23)$$

Where:  $SWP$  is the soil water potential (kPa), and  $R_{21}$  is the measured resistance value normalized to 21°C (kΩ). Figure 49b shows the resulting site specific calibration equation (Equation 3) along with other widely accepted calibration equations for the 0-200 kPa range.

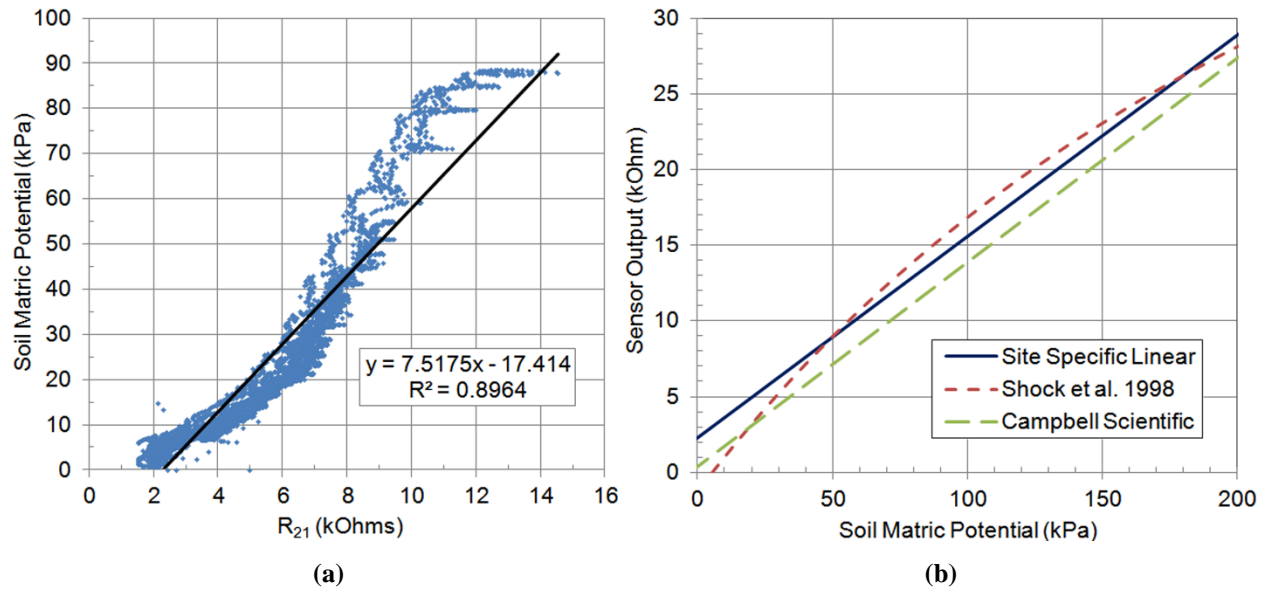


**Figure 49 - (a) Site specific calibration data, (b) calibration curve comparison.**

Figure 50 shows a time series of the data collected by the Geokon sensor along with the Watermark data that was calibrated using Equations 21-23. The data proves to be a good fit with the maximum error being about 5kPa. The accuracy of the data did not show a noticeable change with soil temperature indicating that the manufacturer's temperature calibrations were sufficient.

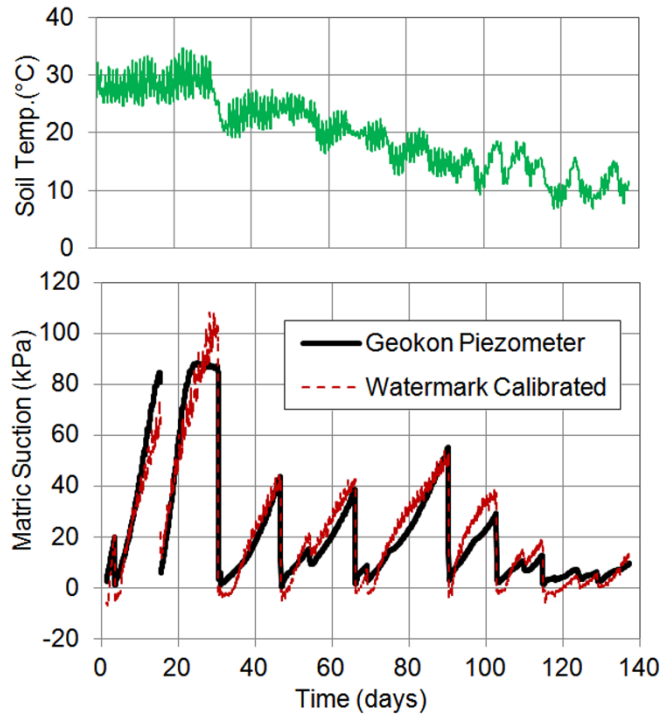


**Figure 50 - Comparison of Watermark linear calibration curve (site specific) with Geokon piezometer data.**

### 9.1.2 CS-616 Dielectric WCR Calibration

The CS-616 WCRs were calibrated based on the procedures outlined in Benson and Wang (2006). Four samples were prepared and compacted into calibration cells at approximately the same density as the measured insitu density. The samples were prepared with volumetric water contents ( $\theta$ ) ranging from approximately 0.05 to 0.30. The samples were placed in an automated temperature control chamber, and the temperature was changed from 5°C to 30°C over a period of 48 hours while taking soil temperature ( $T$ ) and period ( $P$ ) measurements every 10 minutes. The resulting data is presented in Figure 51a. From this plot, it is evident that  $P$  varies linearly with  $T$ , and the linear relationship is defined by Equation 24, where  $\alpha_\theta$  and  $\beta_\theta$  are empirical parameters that that vary with  $\theta$ .

$$P = \alpha_\theta T + \beta_\theta \quad (24)$$

The values determined for  $\alpha_\theta$  and  $\beta_\theta$  were then plotted versus  $\theta$  to determine the relationship between these parameters and  $\theta$  (Figure 51b). It was determined that the relationship between  $\alpha_\theta$  and  $\theta$  follows a second order polynomial (Equation 25), and the relationship between  $\beta_\theta$  and  $\theta$  is linear (Equation 26).

$$\alpha_\theta = a_2\theta^2 + a_1\theta + a_0 \quad (25)$$

$$\beta_\theta = b_1\theta + b_0 \quad (26)$$

Equations 5 and 6 were substituted into Equation 4 to form an expression relating  $\theta$ ,  $P$  and  $T$ . This equation was then solved for  $\theta$ , and is shown as Equation 27.

$$\theta = \frac{-(b_1 + a_1 T) + \sqrt{(b_1 + a_1 T)^2 - 4a_2 T (a_0 T + b_0 - P)}}{2a_2 T} \quad (27)$$

Where:  $\theta$  is the volumetric water content of the soil (unitless),  $P$  is the period measured by the CS-616 sensor ( $\mu\text{s}$ ),  $T$  is the temperature of the soil surrounding the sensor ( $^\circ\text{C}$ ), and  $a_0$ ,  $a_1$ ,  $a_2$ ,  $b_0$ ,  $b_1$  are coefficients determined from the regressions shown in Figure 51. These coefficients are summarized in Table 19.

**Table 19 - Temperature compensating calibration coefficients.**

Coefficient	Value	Units
$a_0$	0.0311	$\mu\text{s}/^\circ\text{C}$
$a_1$	0.5306	$\mu\text{s}/^\circ\text{C}$
$a_2$	-1.0155	$\mu\text{s}/^\circ\text{C}$
$b_0$	17.159	Ms
$b_1$	32.781	Ms

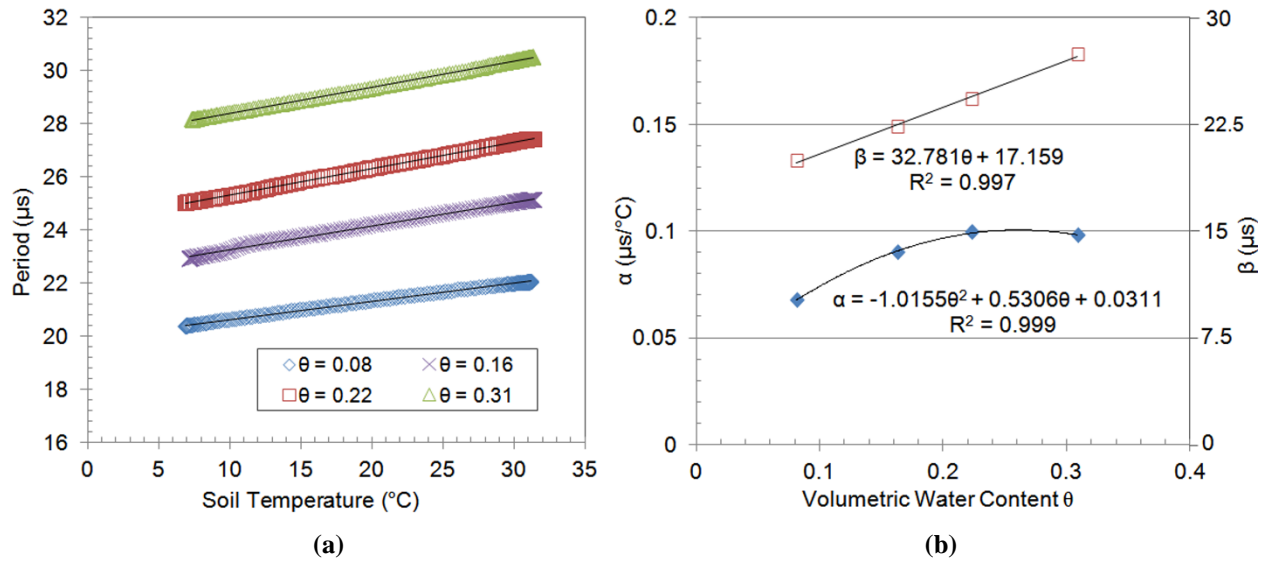


**Figure 51 - (a) Measured period vs. temperature for 4 different volumetric water contents, (b) Calibration parameters  $\alpha$  and  $\beta$  versus volumetric water content.**

## 9.2 Sensor Data Reduction

### 9.2.1 Geokon Suction Sensor Data Reduction

Geokon sensors were all provided with calibration certificated from the manufacturer which were used to convert the raw frequency reading of the vibrating wire to pore water pressure in kPa. The equation used to reduce the Geokon sensor readings is shown in the following equation:

$$P = G(R_0 - R_1) + K(T_1 - T_0) - (S_1 - S_0) \quad (28)$$

Where: P is the calculated pressure in kPa, G is the linear gage factor in kPa/Digit,  $R_0$  is the initial gage reading in Digits,  $R_1$  is the current gage reading, K is the thermal factor in kPa/°C,  $T_1$  is the current temperature reading in °C,  $T_0$  is the initial temperature reading (taken at  $R_0$ ),  $S_1$  is the current barometric pressure reading in kPa, and  $S_0$  is the initial barometric pressure reading. The linear Gage factor (G), and thermal factor (K) for each gage is shown in Table 20.

**Table 20 - Calibration coefficients for Geokon model 4500S sensors.**

Serial #	G kPa/digit	K kPa/°C
1114514	0.1148	-0.07966
1114499	0.1115	-0.09487
1114501	0.1092	-0.005135
1114502	0.1105	-0.06772
1114497	0.1127	-0.09532
1114500	0.1189	-0.08386
1114498	0.1139	-0.02484
1114513	0.1120	-0.06418

### *9.2.2 Excavation Water Level Data Reduction*

According to Geokon, the barometric pressure calibration portion of the equation is only used for unvented pressure transducers which are not buried in soil. In this project, only two of the Geokon 4500s pressure transducers were not buried in soil, and therefore the barometric pressure correction was applied (the last portion of Equation 28). One of these sensors was placed in the bottom of the excavation to measure the water level, and the other sensor was mounted with the DAQ, and was used to measure the barometric pressure. The pressure measurements (in kPa) were multiplied by a factor of 10.1972 to convert them to cm H<sub>2</sub>O.

### *9.2.3 Slope Inclinometer Data Reduction*

In order to reduce the inclinometer data, baseline readings were taken before the excavation process began at depth increments of 0.61m. The raw data output from the inclinometer includes an A+ and A- for each depth increment. The deflection for each depth increment (CA) is then calculated using the following equations:

$$CA = 0.025 \times R_{INT} \times SA \quad (29)$$

$$SA = (PA^+ - PA^-) - (IA^+ - IA^-) \quad (30)$$

In these equations,  $CA$  is the deflection for each reading interval in millimeters,  $R_{INT}$  is the absolute reading interval in meters (0.61m),  $PA^+$  and  $PA^-$  are the present A axis measurements in digits, and  $IA^+$  and  $IA^-$  are the initial A axis measurements in digits.

In order to obtain the total deflection of the inclinometer casing at each depth, the deflections for each reading interval ( $CA$ ) were summed from the bottom up in order to form a cumulative deflection at each depth increment.

## CHAPTER 10: RESULTS

### 10.1 Observational Results

The two test excavations were constructed in subsequent years, and were both observed for a period of 1 year. The following general observations were made based on the outcome of the two excavations:

- The residual soil profile consisted of layers with variable properties. Thin granular layers were also observed (Figure 52) which caused a premature failure on the non-instrumented side of Excavation #1.
- While excavating, tension cracks developed (almost immediately), which ran parallel to the face of the excavation approximately 1.5-2m away from the face. Each failure plane observed intersected one of the existing tension cracks.
- Each failure occurred near a time of heavy rainfall, which implied that the reduction in apparent cohesion with increased soil moisture was a driving force for failure, as well as hydrostatic pressures in the tension crack.
- It appeared that most failures started in the bottom of the trench where water would enter during a rain event, and eventually propagated to the surface approximately 1.5-2m behind the excavation face (along the tension crack). Figure 53 shows undermining that had occurred along the toe of the slope just before failure in Excavation #2.



**Figure 52 - Thin layers present in undisturbed soil samples.**



**Figure 53 - Undermining from water in bottom of trench.**

Figure 54 shows the spoil material being removed from excavation #2 immediately after construction. Figure 55 and Figure 56 show photos of Excavation #1 before and after failure. Figure 55 was taken from the North end of the excavation, and Figure 56 was taken from the

south end of the excavation. The west side of the excavation is where the localized failure occurred while the trench was being excavated, and a portion of this side of the excavation had to be removed to clean out the bottom of the trench so that the total excavation depth remained 5.8m. The main failure occurred on the East side of the excavation approximately 3.5 months after construction.



**Figure 54 – Excavation construction.**

Because of the premature failure on the non-instrumented side of Excavation #1, material was removed from the non-instrumented side of Excavation #2 in order to form a slope so that failure would not occur in that area (Figure 57). Figure 58 shows time-lapse photos of Excavation #2 before and after each significant failure, and Figure 59 is a photograph taken of Excavation #2 just after failure on 9/21/11.



**Figure 55 - Excavation #1 before and after failure (South facing).**



**Figure 56 - Excavation #1 before and after failure (North facing).**



**Figure 57 – Material being removed from non-instrumented side of Excavation #2.**

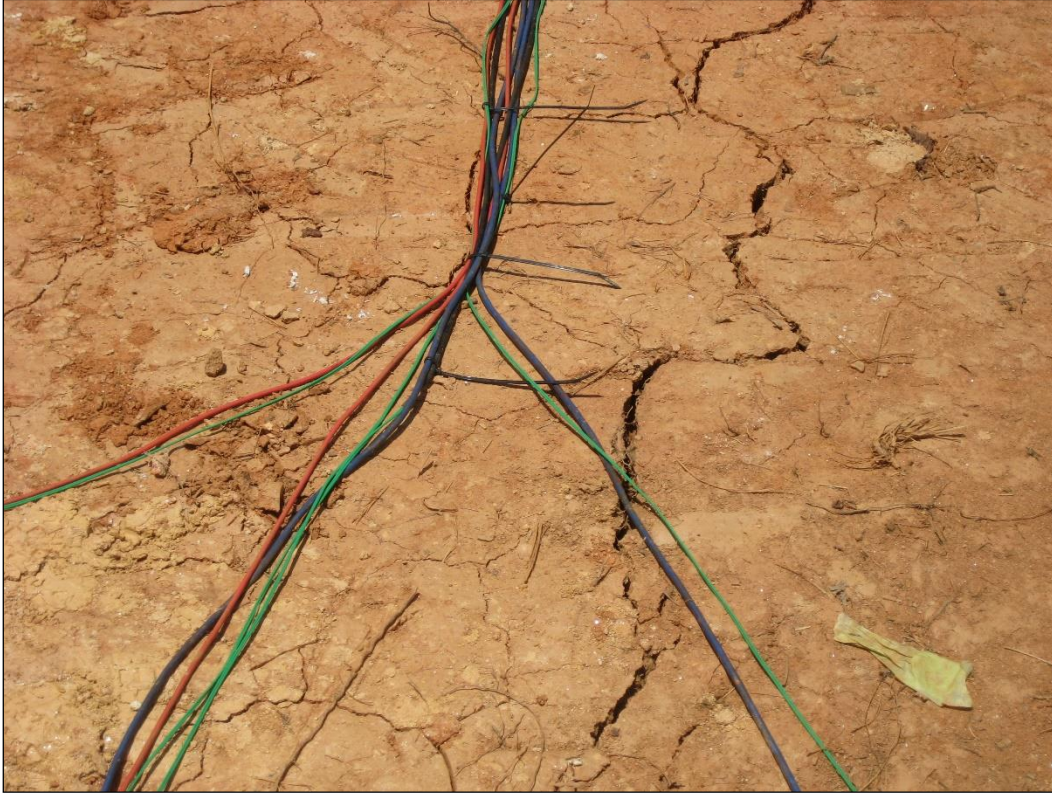


Figure 58 - Excavation #2 time-lapse photos.



**Figure 59 – Excavation #2 after initial failure on 9/21/11.**

Figure 60 and Figure 61 show the tension cracks that developed as a result of the excavation process. For the most part, the tension cracks followed along the path of the 1.8m offset instrumentation boreholes. In order to determine whether or not the drilling of the boreholes created a weakened path for failure, only 1 borehole was made within 1.8m of the excavation face on Excavation #2. Despite the fact that there was only 1 borehole near the face, the initial tension cracks on Excavation #2 still developed approximately 1.8m from the face, and this was the plane along which failure occurred in both excavations. Figure 62 and Figure 63 show the progression of the tension cracks over time for both excavations. In general, the tension cracks started small, and grew larger over time even in areas where failure had not occurred.



**Figure 60 – Tension cracks developed during Excavation #1.**



**Figure 61 – Tension cracks developed during Excavation #2.**



**Figure 62 - Tension crack progression over time (Excavation #1).**

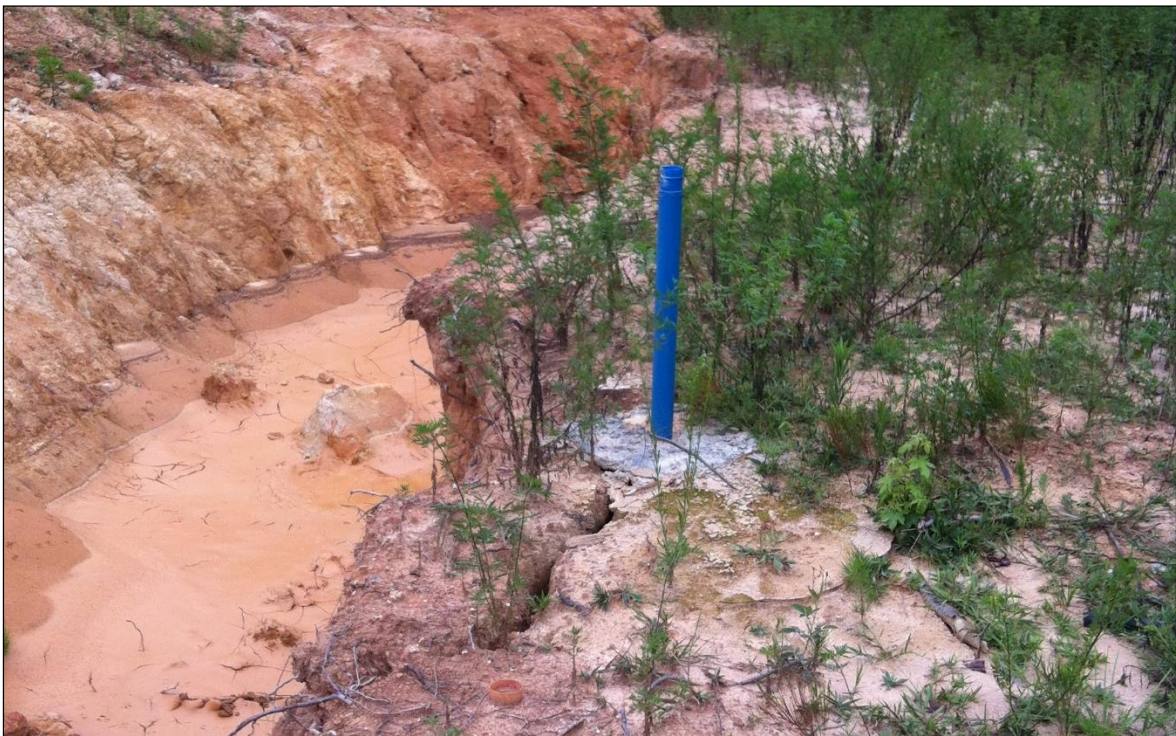


**Figure 63 - Tension crack progression over time (Excavation #2).**

## 10.2 Matric Suction Data

Figure 65 and Figure 66 show the (Watermark sensor) suction measurements and precipitation throughout the entire test period for Excavations #1 and #2 respectively. Figure 64 shows the suction measurements recorded by the Geokon sensors that were used in Excavation #2. A vertical line was drawn at the date and time of each failure for reference. Figure 65 illustrates the difference in the matric suction in the zone closest to the excavation (1.8m) versus the zone that is further away from the excavation (4.6m). The tension cracks that developed along the path of the front row of sensors allowed water to easily penetrate the soil, and therefore saturate to a greater depth than the soil further away from the excavation face. Because the matric suction values remained relatively stable in the soil further away from the excavation face, the tension cracks were thought to be a primary factor in the failure of the excavation.

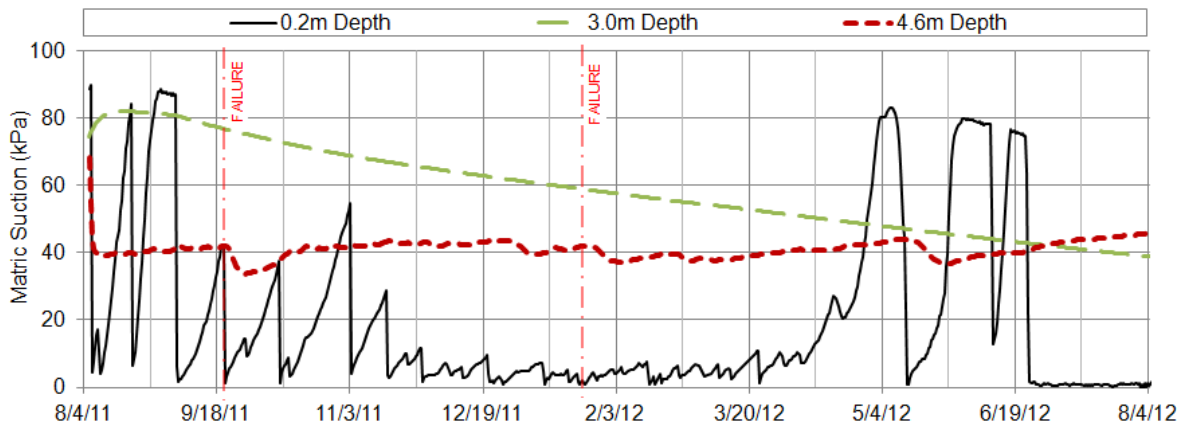


Figure 64 - Geokon piezometer matric suction data (Excavation #2).

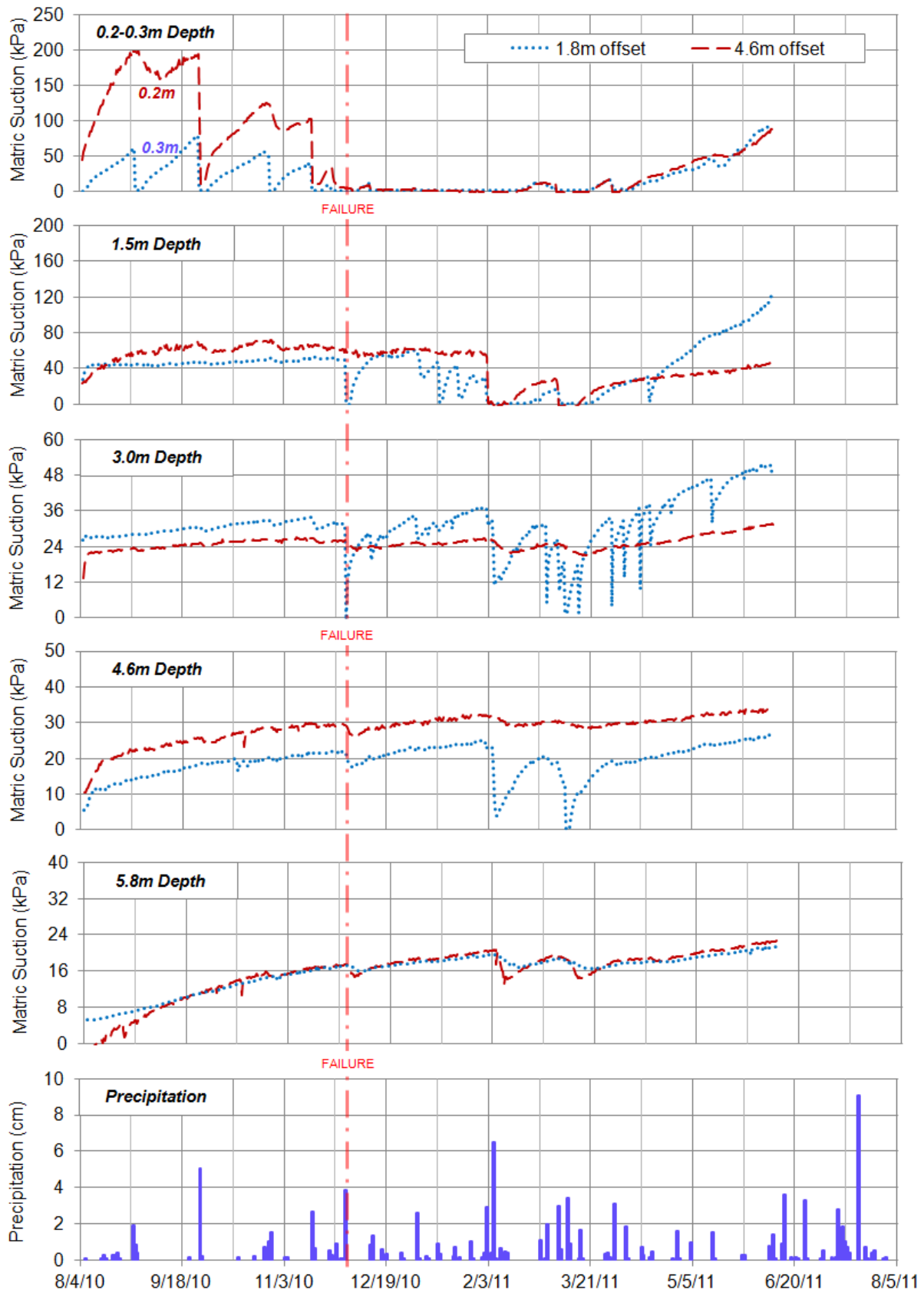


Figure 65 - Matric suction and precipitation vs. time (Excavation #1).

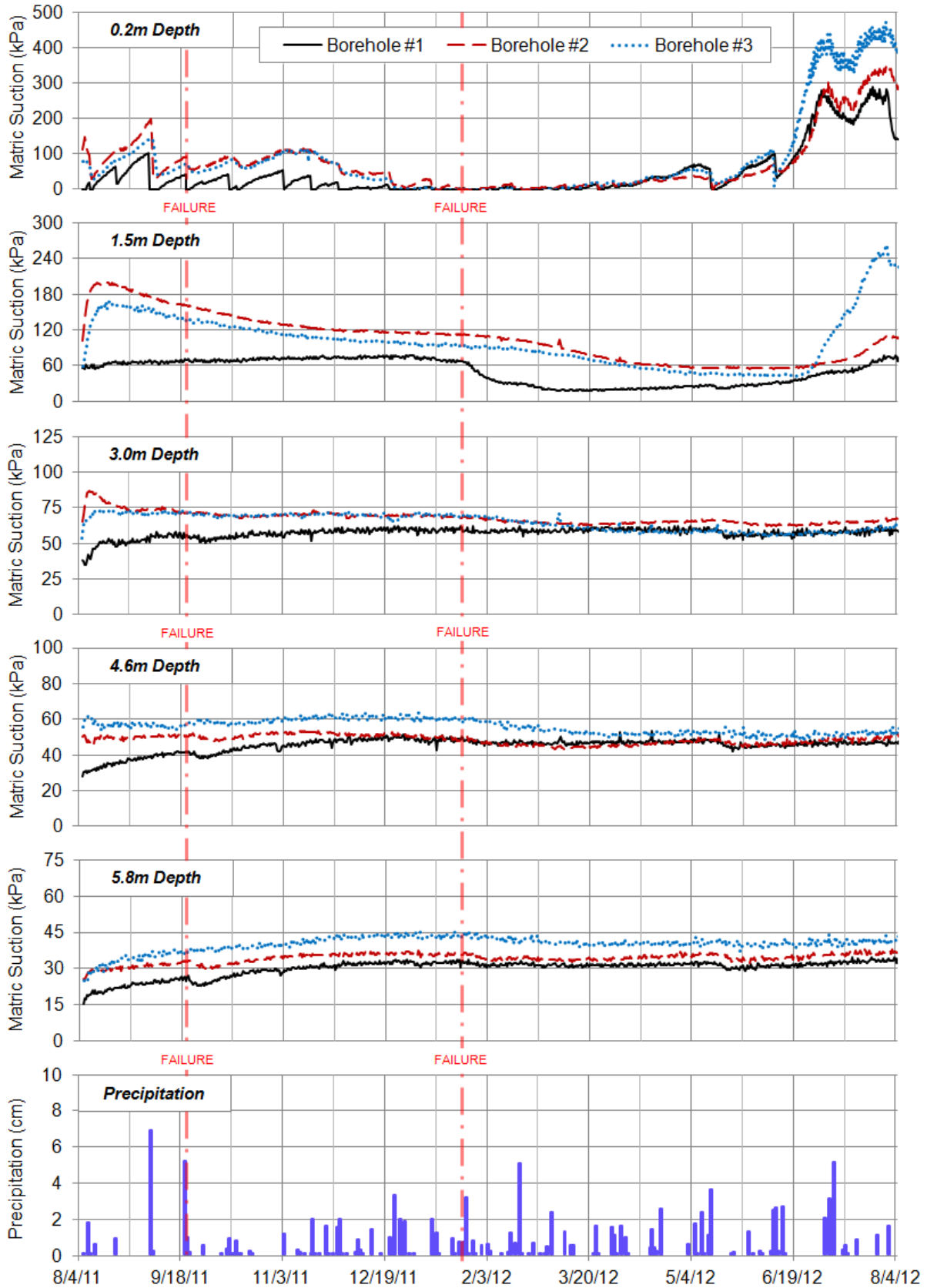


Figure 66 - Matric suction and precipitation vs. time 4.6m offset (Excavation #2).

### 10.3 Site Conditions / Weather Data

Figure 67 and Figure 68 show the daily precipitation throughout the test period for Excavation #1 and Excavation #2 (respectively). Figure 69 shows the water depths recorded by the vibrating wire piezometer located in the bottom of Excavation #2. However, shortly after excavation, the sensor was partially buried by some fine sediment that washed in the bottom of excavation, and the readings were not an accurate representation of the water level in the excavation, and the readings were not an accurate representation of the water level in the excavation due to the low permeability of the soil covering the sensor. However, the water level was able to be approximated for modeling purposes based on the time-lapse photos, and photos from the routine site visits.

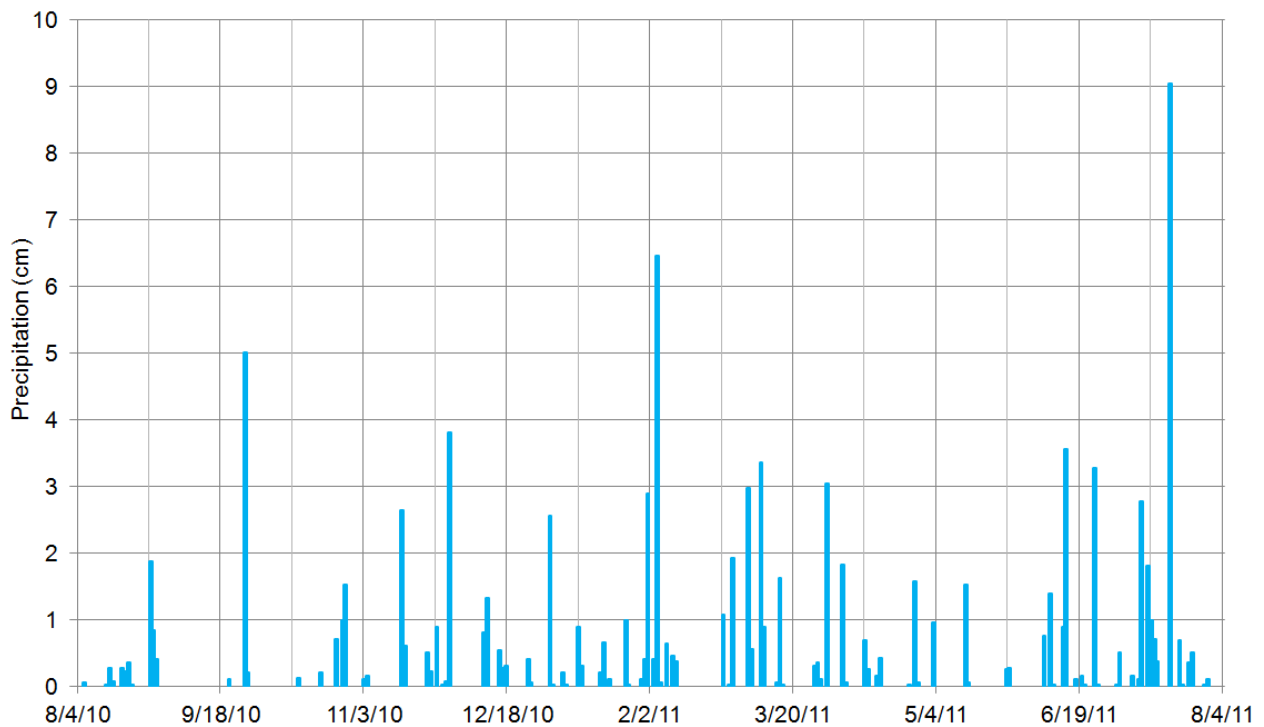
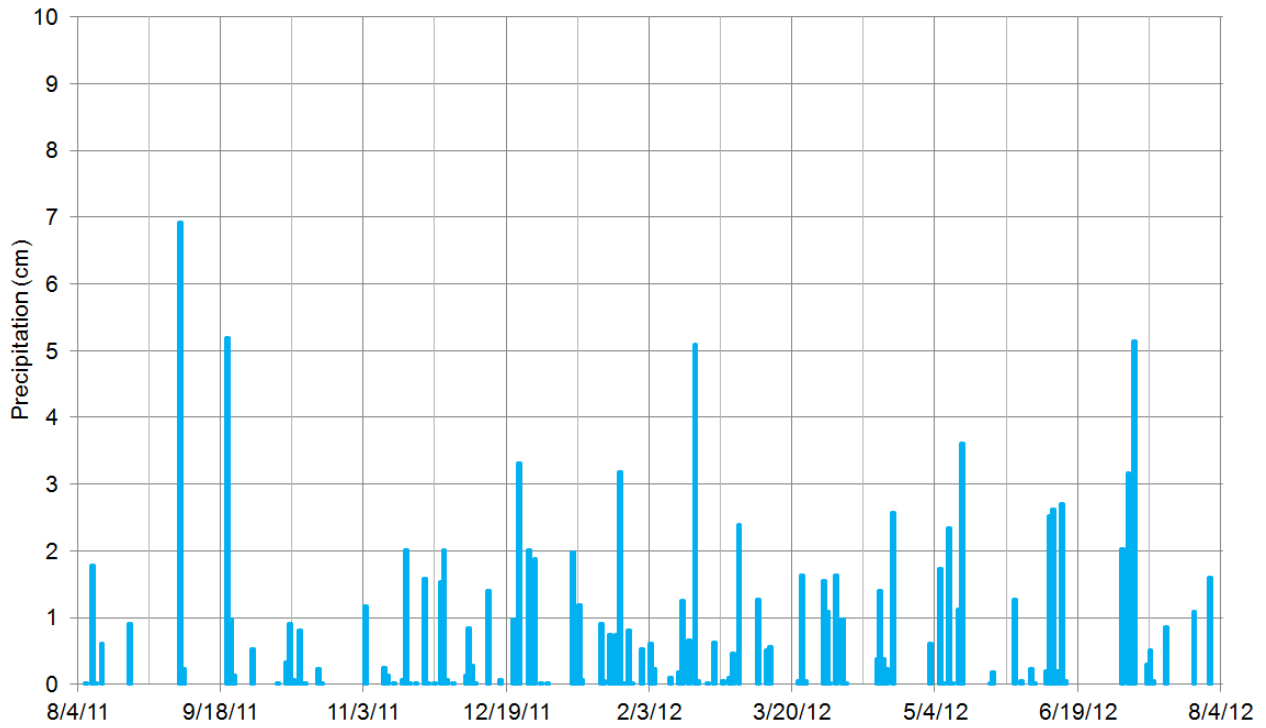
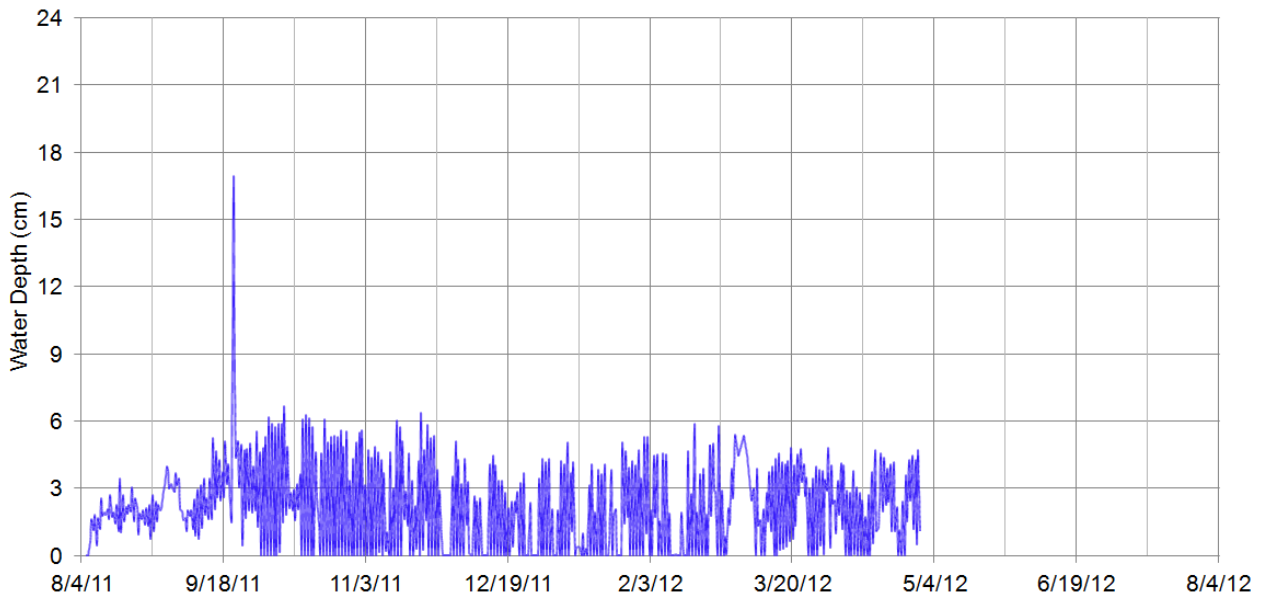


Figure 67 - Daily precipitation (Excavation #1).



**Figure 68 - Daily precipitation (Excavation #2).**



**Figure 69 - Water level in bottom of Excavation #2.**

#### **10.4 Inclinometer Data**

The results of the slope inclinometer readings for Excavation #1 and Excavation #2 are shown in Figure 70 and Figure 72 (respectively). In both excavations the maximum horizontal deflection before failure was approximately 3-5cm at the 1.8m offset. The two 1.8m offset

inclinometer casings on Excavation #1 were undermined by the failure, and showed larger deflections after failure occurred, until the point where they became inaccessible to take measurements. Figure 71 and Figure 73 show the 1.8m offset inclinometer casings for both excavations after failure had occurred.

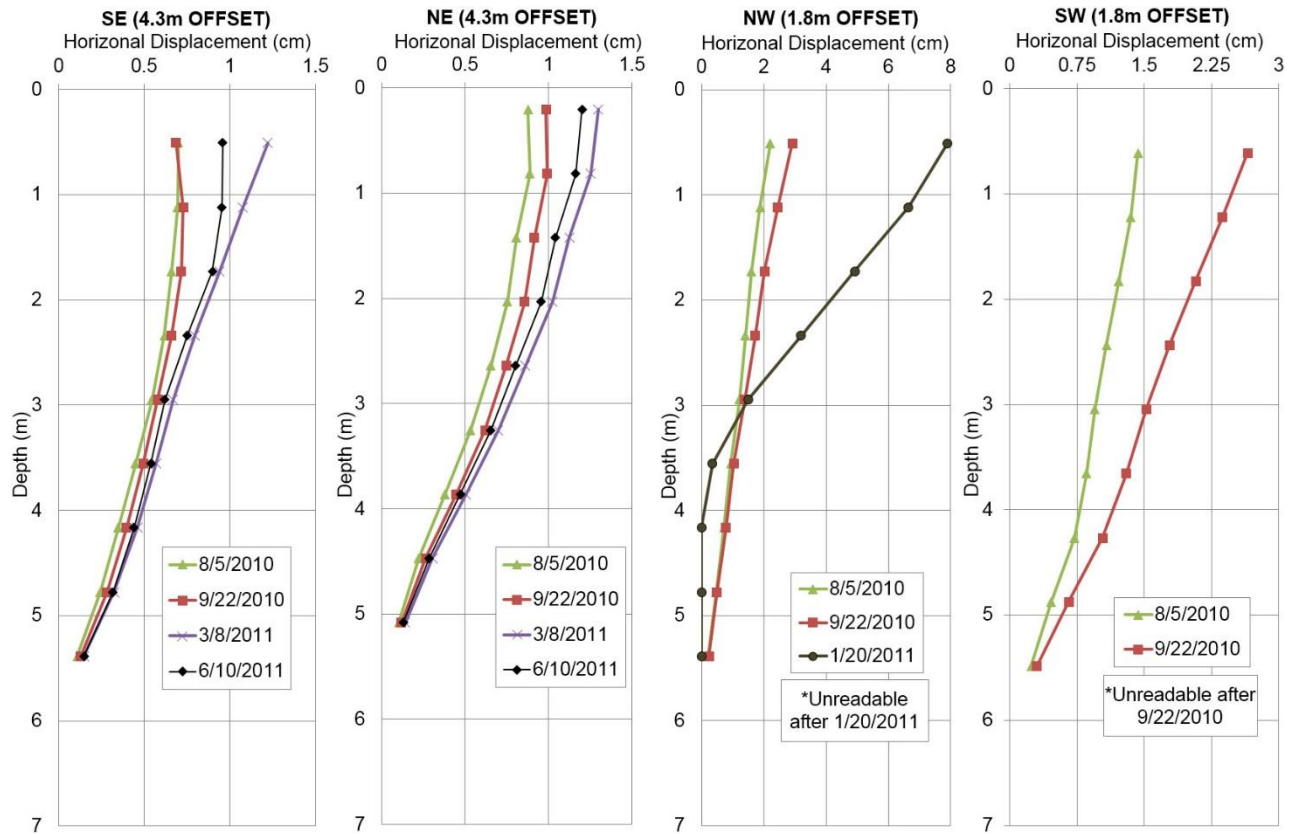


Figure 70 - Inclinometer data (Excavation #1).



Figure 71 - Inclinometer casings after failure (Excavation #1).

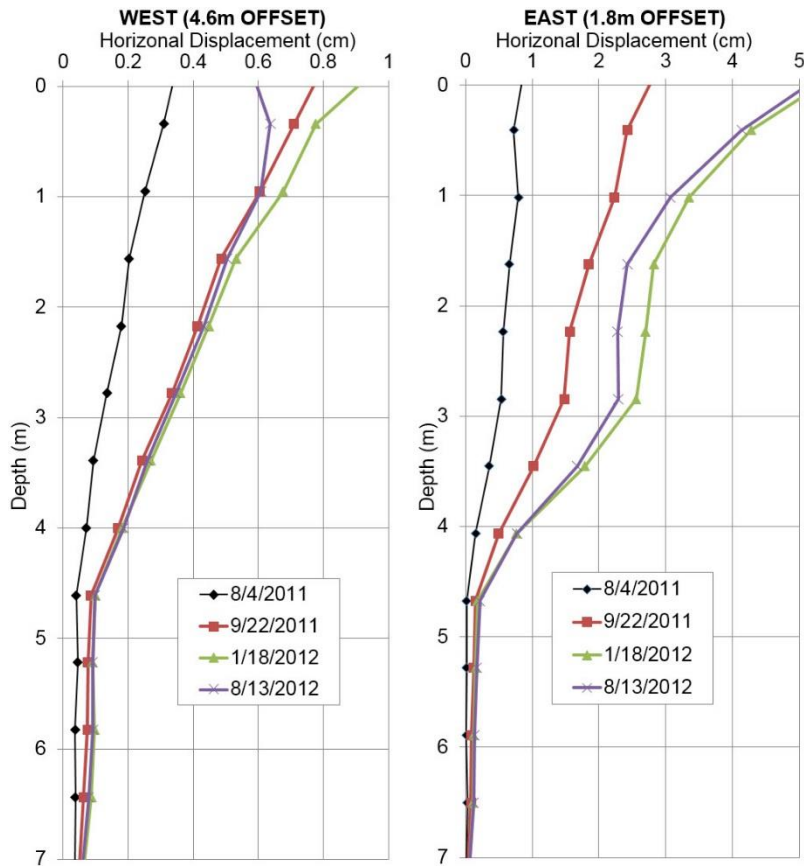


Figure 72 - Inclinometer data (Excavation #2).



Figure 73 – Inclinometer casing after failure (Excavation #2).

## CHAPTER 11: FINITE ELEMENT MODELING

A finite element model was created based on the recorded boundary conditions and material properties that were collected during the test period. The main goal of the finite element model was to provide a connection between the measured strength parameters of the soil, and the observational results in the field. The finite element model was constructed to reflect the field boundary conditions as accurately as possible, so that conclusions could be drawn based on the accuracy of the characterization methods for determining the strength properties of residual soil.

In order to accurately model the field behavior, the finite element model consisted of several analyses. The first analysis was to determine the deformation caused by the excavation process. For this analysis, the material properties from the site characterization were entered along with the average pore pressure values for the period of time from the initial excavation to failure. In doing so, the deformed mesh could be generated and compared to the inclinometer results for that time period. The second analysis was a transient seepage model to generate the pore pressures at the critical state (just before failure). Because water was present in the excavation and the tension crack at the time of failure, the transient model was necessary to estimate the pore pressures between the tension crack, and the toe of the excavation. The third analysis was another deformation analysis to identify any elements that might have yielded at the critical state pore pressures that had not yielded in the initial deformation analysis. The final analysis was a finite element slope stability analysis where the factor of safety was estimated based on the geometry of the deformed mesh, and the pore pressures generated by the transient seepage model.

The software package used for this finite element analysis was GeoStudio 2012 by Geo-Slope International. Within this package, the different analyses are run in sequence by different analysis methods. Sigma/W was used for the time-deformation analyses, Seep/W was used for the seepage analyses, and Slope/W was used for the slope stability analysis. The software allows the individual models to be run in sequence while basing the initial boundary conditions off the boundary conditions of the parent analysis. The sequence for overall finite element analysis is summarized in Table 21, and Figure 74. A combination of a Sigma/W and a Seep/W analysis was needed at each step to model both the deformation, and pore pressures. The Slope/W analysis was then linked to the final Sigma/W analysis for geometry, and the final Seep/W analysis for pore pressures to set the boundary conditions for the slope stability analysis.

**Table 21 - Finite element analysis steps.**

Analysis #	Analysis Type	Analysis Description	Start (days)	End (days)	Parent Analysis
1	Sigma/W	Insitu Conditions	0.00	0.00	--
2	Seep/W	Initial Pore Pressures	0.00	0.00	Insitu Conditions
3	Sigma/W	Excavation Deformation	0.00	30.00	Insitu Conditions
4	Seep/W	Excavation Pore Pressures	0.00	29.75	Initial Pore Pressures
5	Seep/W	Pore Pressures Before Failure	29.75	30.00	Excavation Pore Pressures
6	Sigma/W	Deformation Before Failure	30.00	30.04	Pore Pressures Before Failure
7	Slope/W	Slope Stability Analysis	30.04	30.04	Deformation Before Failure

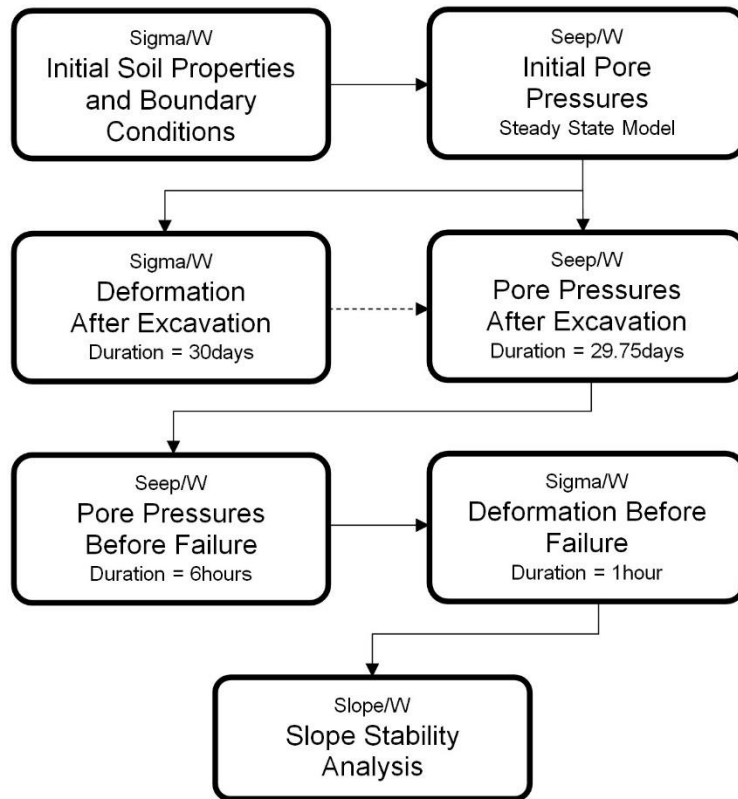


**Figure 74 – Finite element model flow chart.**

### 11.1 Sigma/W Analysis (Before Excavation)

Table 22 shows the material properties that were used for the Sigma/W analyses. The effective friction and cohesion were input based on the results of the consolidated-drained triaxial tests. The effective modulus values were taken from the dilatometer test results (Vinson and Brown, 1999), and the permeability values were taken from the results of the flexible wall permeameter test.

**Table 22 - Material properties for initial Sigma/W analysis.**

Layer ID	Top Depth	Bottom Depth	Effective Friction ( $\phi'$ )	Effective Cohesion ( $c'$ )	Effective Modulus ( $E'$ )	Permeability at Saturation $k$ (m/s)	Moist Unit Weight ( $\gamma$ )
NGES 0.2m	0.0 m	0.8 m	17.0°	23.6 kPa	8,750 kPa	$1.3 \times 10^{-5}$	18.7 kN/m <sup>3</sup>
NGES 1.5m	0.8 m	2.2 m	17.0°	23.6 kPa	8,350 kPa	$1.3 \times 10^{-5}$	17.1 kN/m <sup>3</sup>
NGES 3.0m	2.2 m	3.8 m	31.9°	16.1 kPa	4,350 kPa	$3.7 \times 10^{-6}$	17.5 kN/m <sup>3</sup>
NGES 4.6m	3.8 m	5.2 m	28.4°	20.4 kPa	5,350 kPa	$1.2 \times 10^{-5}$	18.3 kN/m <sup>3</sup>
NGES 5.8m	5.2 m	30 m	23.3°	32.2 kPa	6,100 kPa	$6.8 \times 10^{-6}$	18.7 kN/m <sup>3</sup>

The input dialogue for the Sigma/W analysis (0.2m depth) is shown in Figure 75. The dilation angle was assumed to be zero, and Poisson's ratio was estimated to be 0.3 (Blight and Leong, 2012). The anisotropy ratio was assumed to be 0.50 and load response ratio was assumed to be one. The remaining parameters were entered in for each depth increment as shown in Table 22.

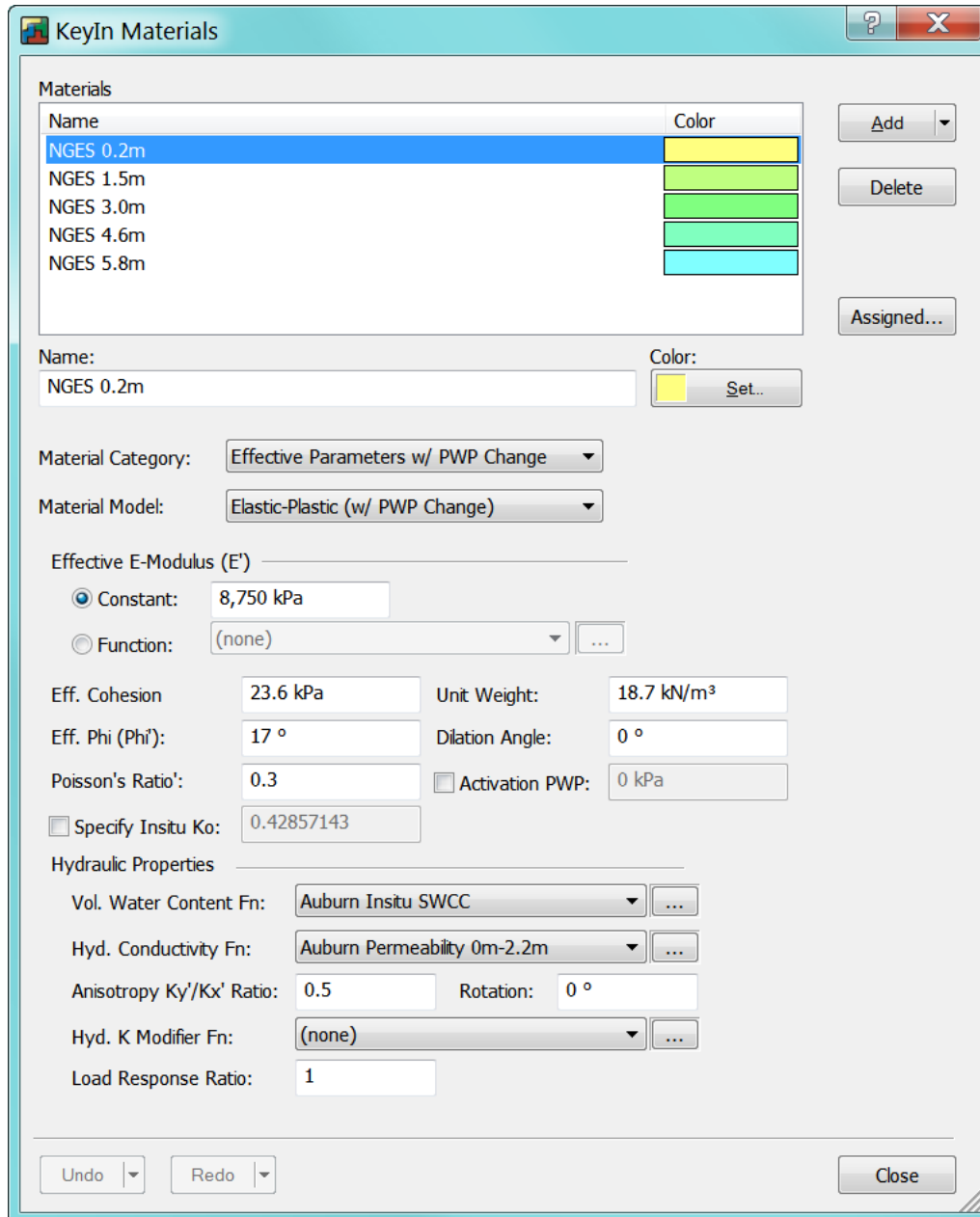
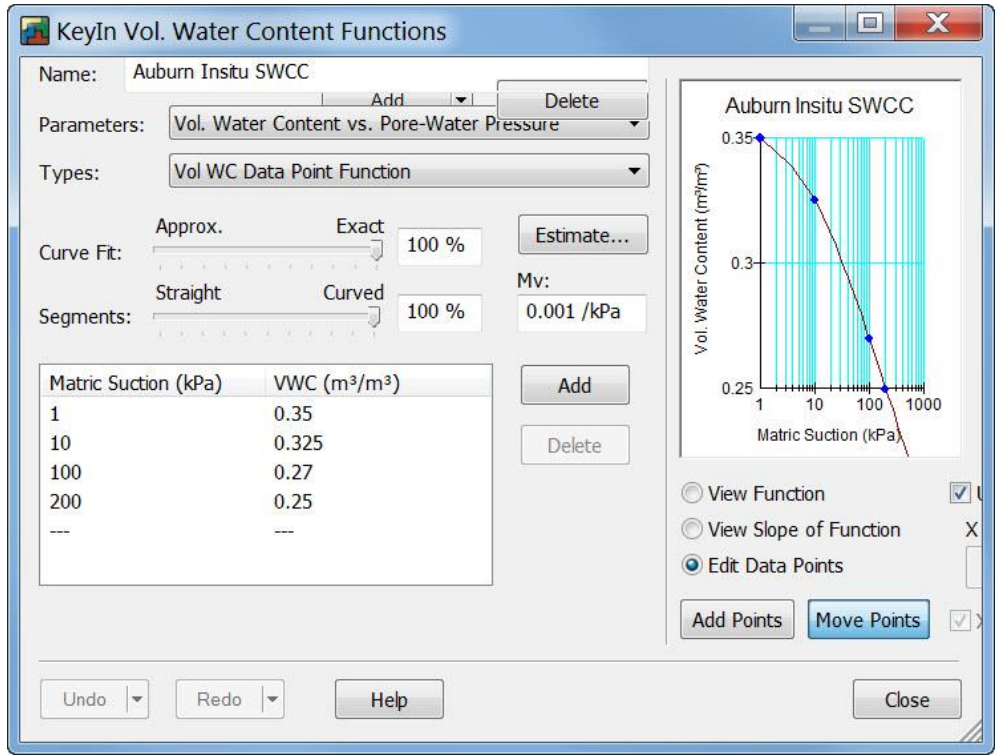
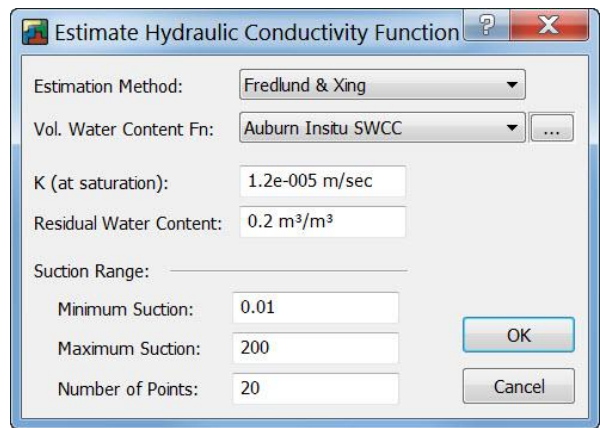


Figure 75 – Key in materials dialogue for initial Sigma/W analysis.

The hydraulic properties that were input in the initial Sigma/W analysis are shown in Figure 76 and Figure 78. The hydraulic conductivity function was approximated for each layer by the Fredlund and Xing method (Fredlund, et al., 1994). The input parameters for this approximation are shown in Figure 77. For each layer, the value for the permeability at saturation was changed to match the values shown in Table 22.



**Figure 76 - Volumetric water content function.**



**Figure 77 - Input parameters for Fredlund and Xing hydraulic conductivity function approximation.**

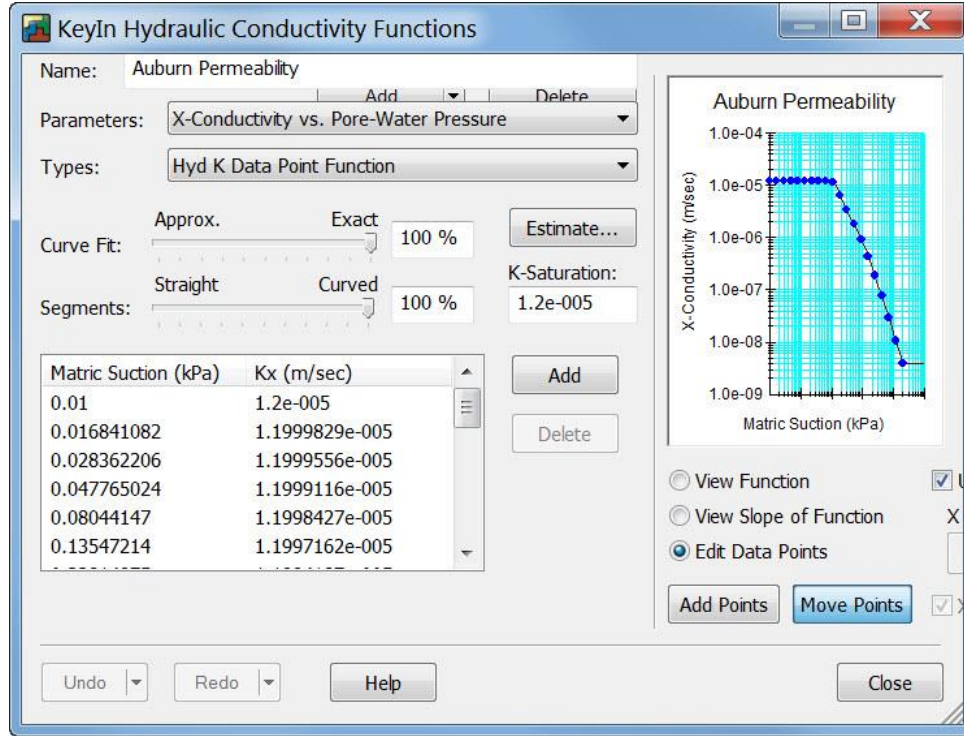


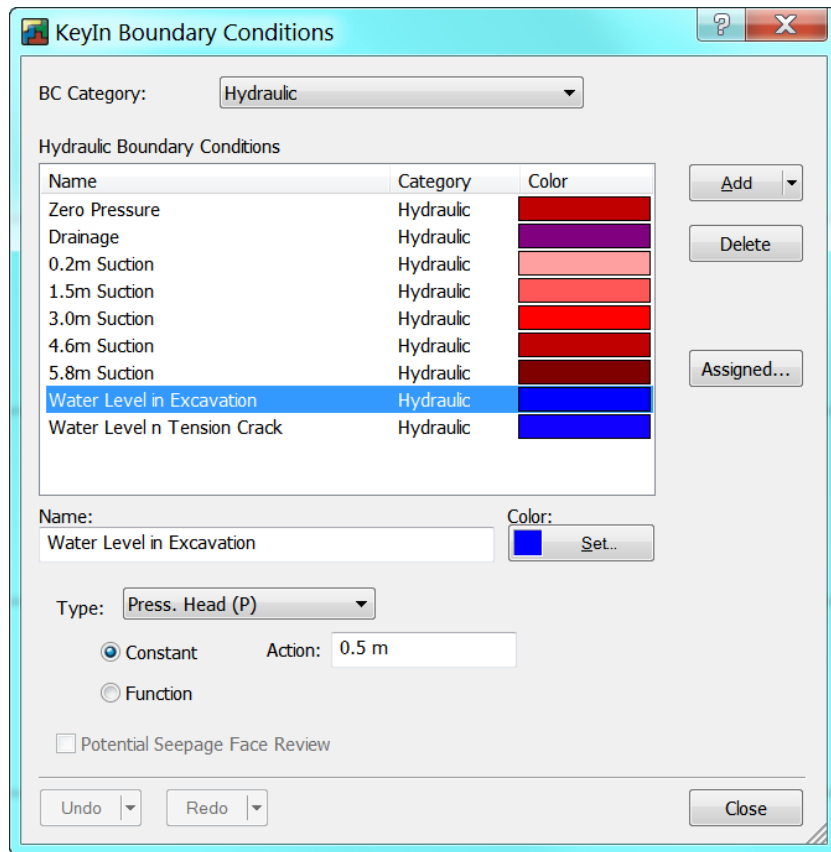
Figure 78 - Permeability function.

## 11.2 Seep/W Analysis

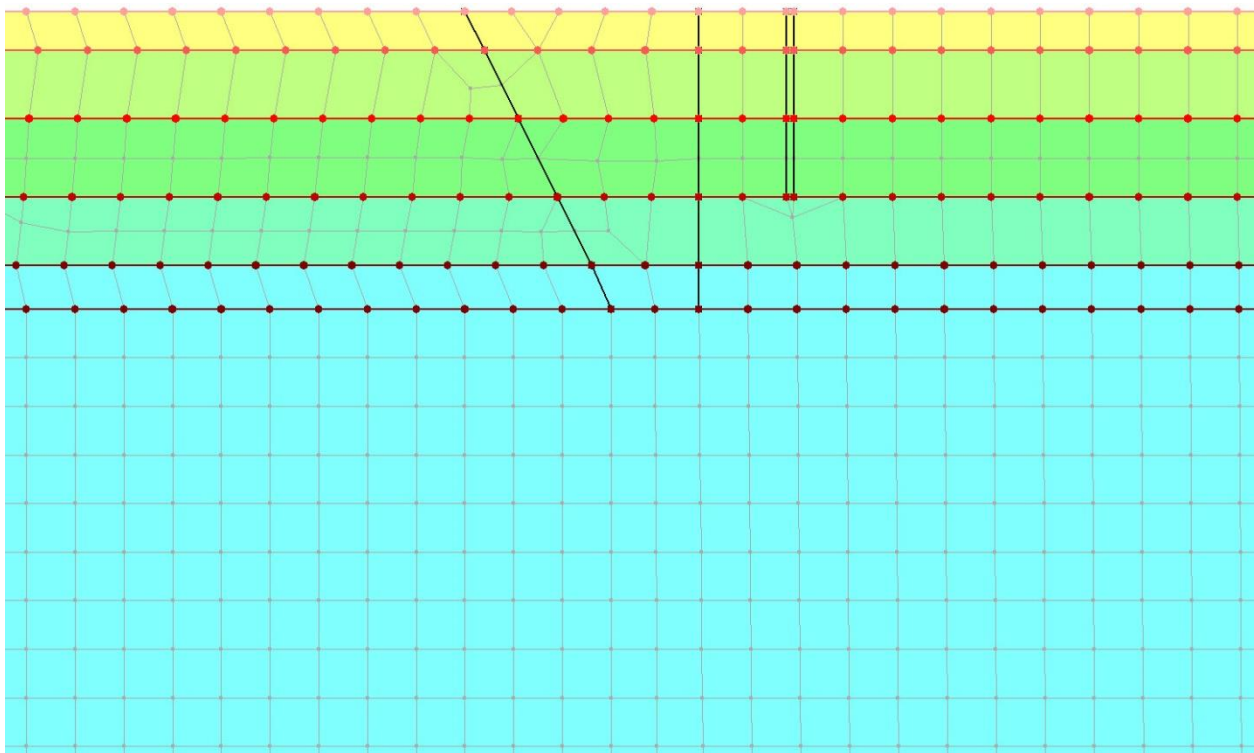
Table 23 shows the boundary conditions that were input as the initial conditions for the Seep/W analyses. The input dialogue, and the profile view of the initial applied pore pressures are shown in Figure 79 and Figure 80.

Table 23 – Boundary conditions for transient seepage model.

Layer ID	Pressure Head (P)
0.2m Suction	-5.0 m
1.5m Suction	-4.0 m
3.0m Suction	-2.4 m
4.6m Suction	-1.8 m
5.8m Suction	-1.5 m
Zero Pressure	0.0 m
Water in Excavation	+0.5 m
Water in Tension Crack	+2.0 m



**Figure 79 - Initial boundary conditions for Seep/w analysis.**



**Figure 80 - Seepage model initial boundary conditions profile view.**

The results of the transient seepage analysis is summarized in Figure 81. The combination of the water in the bottom of the trench combined with the water in the tension crack created a zone along the failure plane where the matric suction was eliminated. The pore pressures were plotted with depth for both the steady state, and the critical condition (Figure 82). The difference in pore pressure caused by the water in the excavation and tension crack can be seen from this plot.

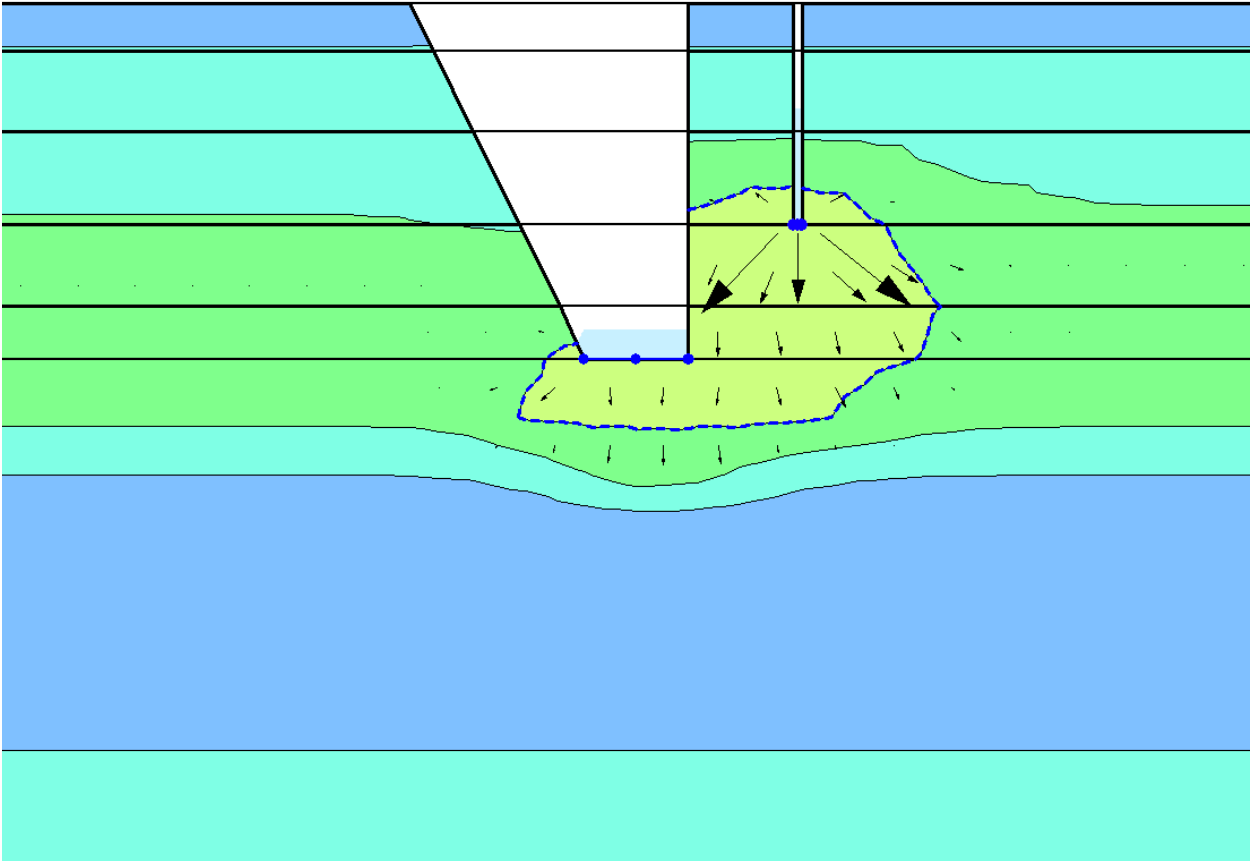


**Figure 81 - Transient seepage model results (profile view).**

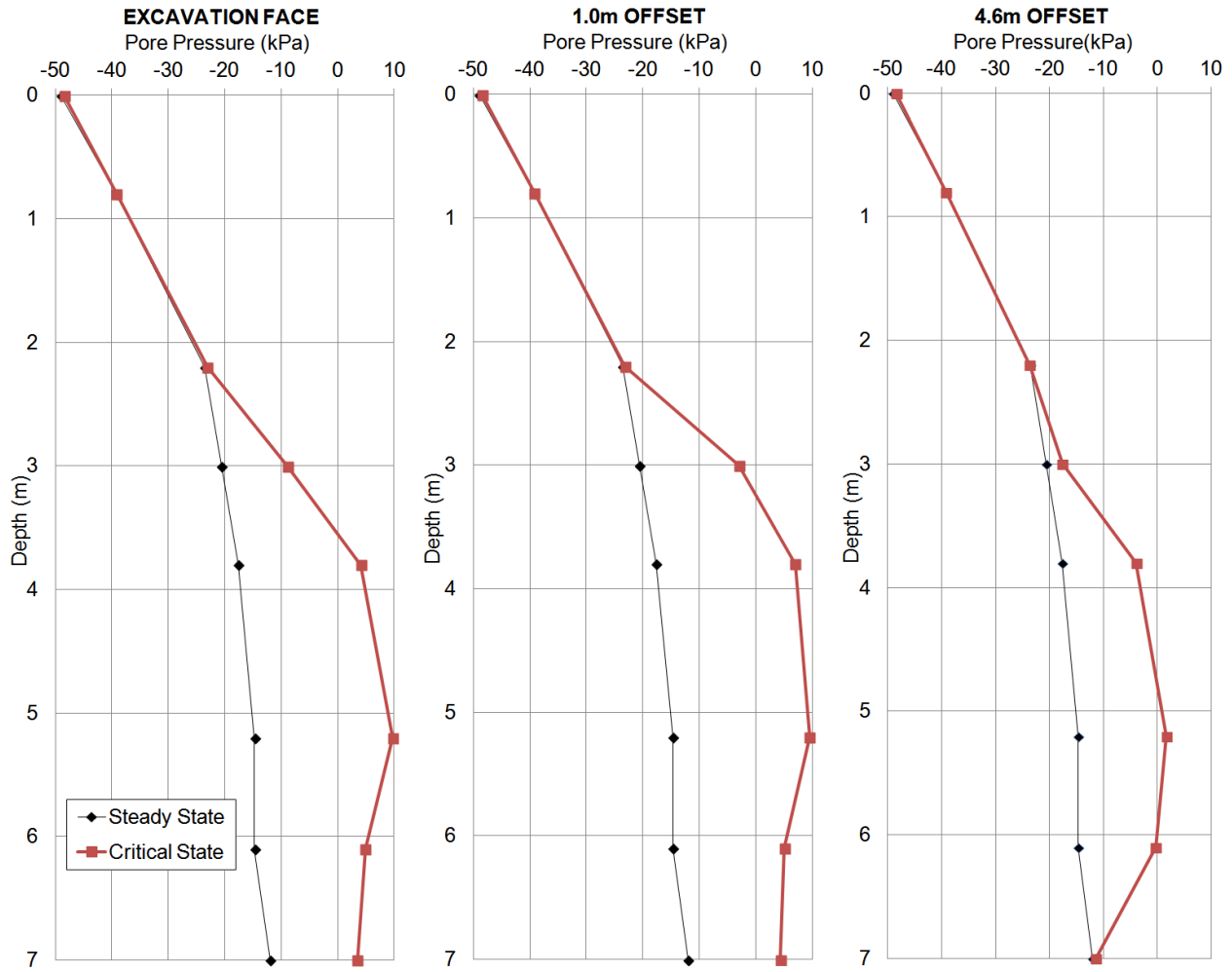
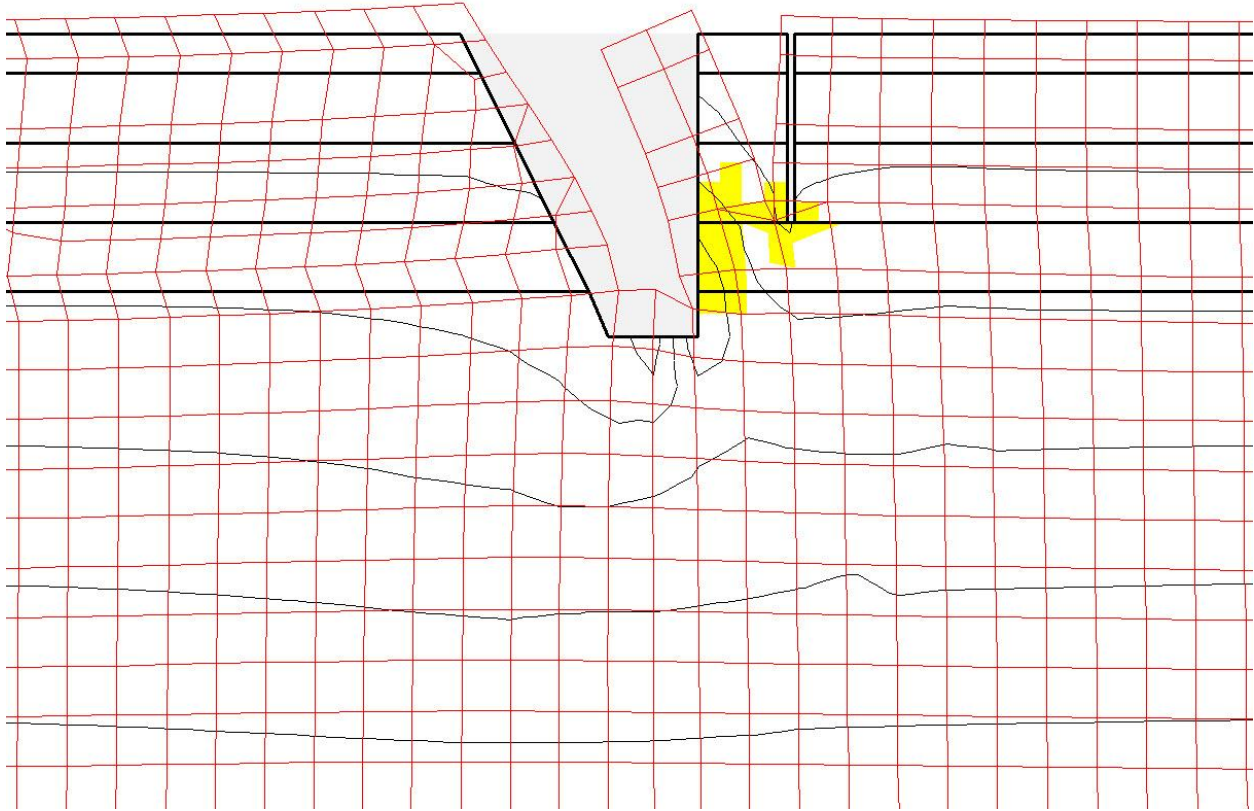


Figure 82 – Model predicted pore pressures vs. depth.

### 11.3 Sigma/W Analysis #2

After the pore water pressures were generated for the critical state, the Sigma/w analysis was conducted a second time to determine the amount of deformation / yielding that occurred between the storm event, and the time of failure. Figure 83 shows the deformed mesh at the time of failure for the excavation. In this figure, the yielded cells are highlighted, indicating that failure was probable for the plane connecting the bottom of the tension crack to the bottom of the excavation.



**Figure 83 - Results of Sigma/W analysis at critical state (15x exaggeration).**

The model predicted displacements from the time of initial excavation to the time of failure are shown in Figure 84. For comparison purposes, the maximum deflection measured by the slope inclinometers in the field are plotted on the same graph. The inclinometer results for compared reasonably well to the predicted deflections from the finite element model however, since both inclinometers from Excavation #1 became unreadable after failure had occurred, the maximum recorded values were not necessarily representative of the total deflection that would have occurred for the duration of the test.

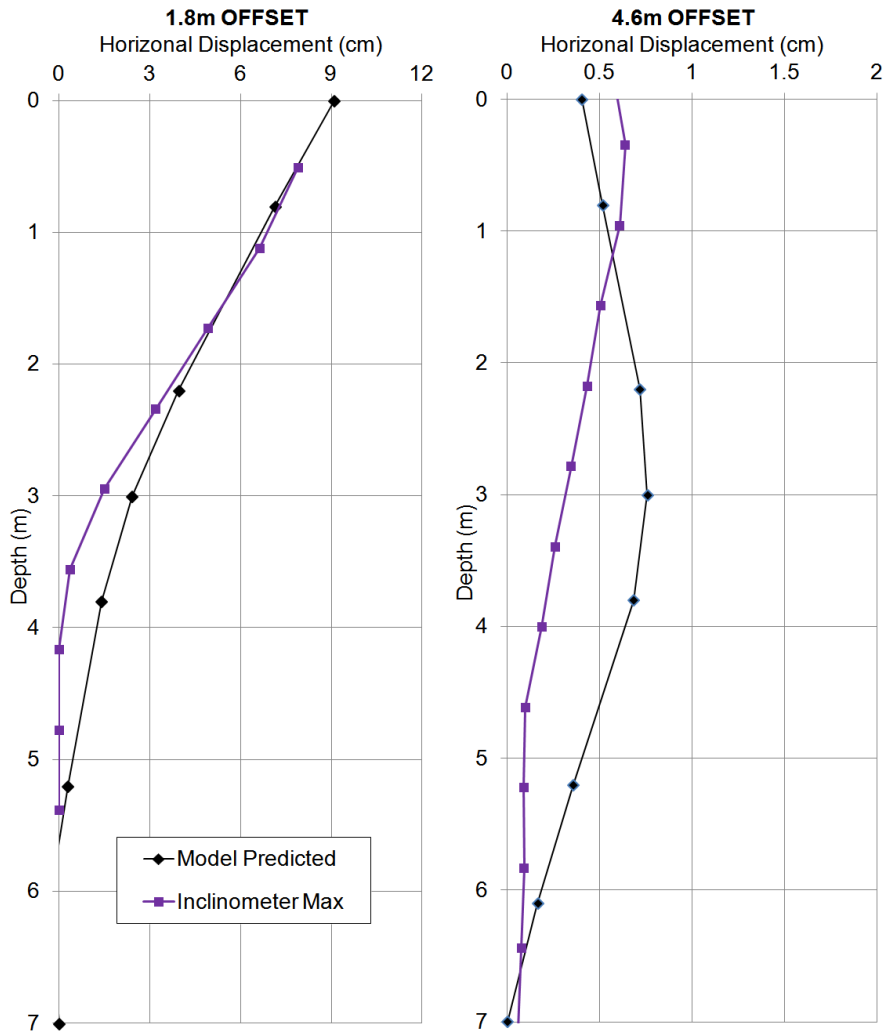


Figure 84 - Predicted lateral displacement at time of failure.

### 11.4 Slope/W Analysis

The properties from the critical state Sigma/W analysis were used to conduct slope stability analyses of the deformed mesh at the time of failure. Figure 85 shows the critical slip surface that was generated for the finite element slope stability model. The slip surface was generated from the bottom of the tension crack, and intersected the bottom of the excavation (as seen in the field). This figure also shows that the entire slip surface lies in the zone where  $u \geq 0$ .

In addition to the finite element slope stability analysis, traditional limit equilibrium analyses were also conducted on the deformed mesh for the sake of comparison. The results of

these analyses are shown in Table 24. The fact that the results of the slope stability analysis were all close to one indicate that the boundary conditions used in the model are relatively close to the field conditions at the time of failure.

**Table 24 - Slope stability analysis results for various methods.**

Slope Stability Analysis Method	Minimum Factor of Safety
Finite Element	0.954
Ordinary	0.931
Bishop	0.948
Janbu	0.943
Morgenstern-Price	0.939

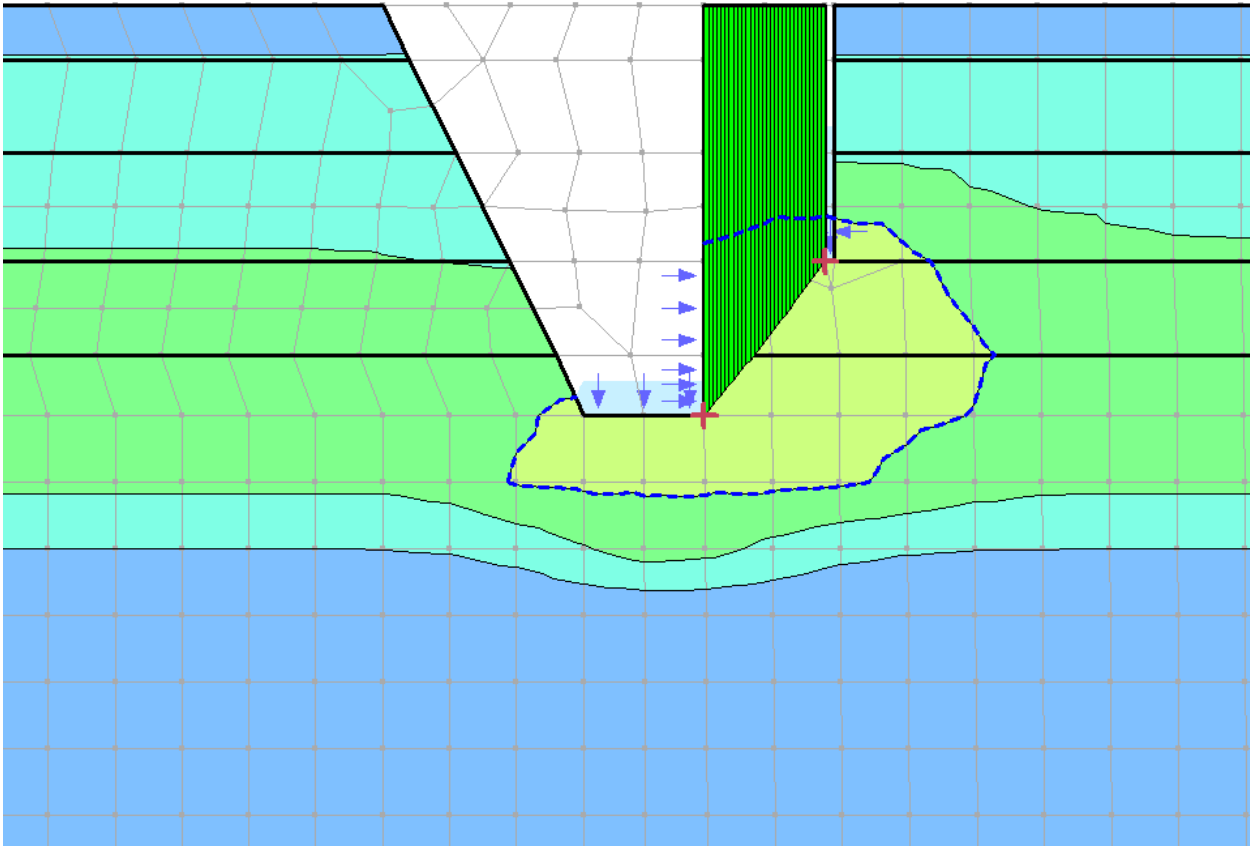


**Figure 85 - Slope stability analysis critical slip surface.**

A sensitivity analysis was performed to determine the impact that the water level in the tension crack had on the factor of safety of the excavation. The sensor measurements showed

evidence of water entering the tension crack with higher intensity storm events, however, since the sensors were only able to measure matric suction, the level of water in the tension crack at failure was uncertain. The depth was assumed to be 2.0m the previous analysis, which would be approximately half full. Table 25 shows the factors of safety for water levels ranging from 0m to 4m (empty to full).

**Table 25 - Calculated factors of safety for various water levels in tension crack.**

Water Level in Tension Crack	Finite Element	Ordinary	Bishop	Janbu	Morgenstern Price
4.0m	0.831	0.913	0.956	0.949	0.944
2.0m	0.954	0.931	0.948	0.943	0.939
0.2m	1.137	0.985	0.987	0.987	1.230
0.0m	1.161	1.006	1.007	1.006	1.239

A similar analysis was performed to determine how the matric suction impacts the factor of safety of the excavation. Table 26 shows calculated factors of safety for the matric suction measured by the sensors during dry conditions, and after heavy rainfall (at the critical state just before failure).

**Table 26 - Calculated factors of safety for various pore pressure conditions.**

Matric Suction	Finite Element	Ordinary	Bishop	Janbu	Morgenstern Price
Dry Conditions	1.283	1.096	1.097	1.096	1.097
After Heavy Rainfall	0.954	0.931	0.948	0.943	0.939

Table 27 shows a comparison between the finite element factor of safety, and the Mohr-Coulomb strength parameters for the soil. For this comparison, critical-state conditions were simulated and the tension crack was assumed to be half full. This table identifies the conservative nature of assuming  $c'=0$  for residual soils, as well as the danger of overestimating the cohesion by including the apparent cohesion in the  $c'$  calculation.

**Table 27 - Mohr-Coulomb strength parameters vs. finite element factor of safety (critical state).**

c' (kPa)	$\varphi=0^\circ$	$\varphi=20^\circ$	$\varphi=25^\circ$	$\varphi=30^\circ$	$\varphi=35^\circ$
0 kPa	FS	FS	FS	0.53	0.62
10 kPa	0.42	0.67	0.67	0.76	0.80
20 kPa	0.79	0.81	0.84	0.93	1.03
30 kPa	1.04	1.02	1.09	1.19	1.32
40 kPa	1.13	1.28	1.37	1.46	1.56

## CHAPTER 12: CONCLUSIONS

The main goal of this project was to learn more about the behavior of unsaturated residual soils, and to be able to apply this knowledge to classical engineering design methods to both promote efficiency, and safety in design. Based on the results of this experiment, the following conclusions were drawn:

### 12.1 Validity of Experiment

The fact that the finite element model predicted failure at approximately the same boundary conditions as those measured in the field gives validity to the material properties and boundary conditions that were calculated from the instrumentation and characterization methods. Additionally, the deformation predicted by the finite element model was reasonably accurate when compared to the deflections measured by the slope inclinometer indicating that the material properties were within a tolerable margin of error. Also, the fact that the two excavations both behaved in a similar manor, and failure was observed in similar conditions, gives validity to the experiment.

### 12.2 Residual Soil Properties

The modeling results support the theory that residual soil behaves as a  $c-\phi$  soil having both frictional and cohesive properties. However, thin layers of materials with little cohesion were also identified, which could cause localized slope stability failures, especially when oriented along a potential slip surface.

The results of the finite element analysis concluded that the  $c'$  and  $\phi'$  values determined by consolidated-drained triaxial testing were accurate for modeling the behavior of residual soil. However, because of the heterogeneous nature of residual soil, high quantities of tests may be necessary to accurately define the layers and identify any weak layers, which could make this type of testing unfeasible for many projects.

While reducing triaxial data, it was realized that care must be taken when determining the triaxial  $\phi'$  and  $c'$  as to not overestimate the cohesive component. Forcing a linear trendline to a  $p'$ - $q$  diagram may have a tendency to overestimate the value for cohesion because the mohr-coulomb failure envelope is non-linear (Lambe and Whitman, 1969). This is especially true when forcing a linear trendline using only tests at higher effective confining pressures. The finite element model resulted in overestimates in the factors of safety by magnitudes as great as 0.3 when fitting a linear trendline to tests with confining pressures greater than or equal to 70kPa. The impact that cohesion has on the factor of safety is better illustrated by Table 27.

### **12.3 Unsaturated Behavior**

The strength properties of unsaturated soils can be much higher than the strength when  $u \geq 0$ . The model results showed that the factor of safety for the excavation was approximately 0.3 higher in dry conditions than after a significant rain event, indicating a significant influence of matric suction. Also, the collected data proved that the excavations both failed as a result of increased pore pressures due to rainfall.

The instrumentation showed that the pore pressures remain fairly constant below a depth of approximately 1m (even with heavy rainfall), however, the tension cracks provided a path for water to enter the soil, and reduce the suction along the critical failure surface enough to initiate failure.

The collected field data and modeling results did not show a significant change in suction as a result of creating the excavation. It was suspected that the initial deflection of the soil toward the excavation may result in a change in the pore pressure, but from the data, it appeared that the only changes in negative pore pressure were due to the change in moisture content of the soil with rain events, and seasonal weather patterns.

#### **12.4 Mode of Failure**

For this experiment, it was determined that the infiltration of rain water was the primary catalyst for failure. Since both excavations developed a tension crack almost immediately after excavation, and both eventually failed along that same tension crack, it was also concluded that the tension crack was an important factor impacting the stability of the excavations, because it gave a path for water to easily saturate the critical failure plane, and it allowed hydrostatic pressure to buildup behind the soil mass.

A finite element model was used to conduct a slope stability analysis on the conditions before and after the simulated rainfall, and it was estimated that the factor of safety was reduced by approximately 0.3 after the water was able to enter the tension crack and saturate the soil along the failure plane. Observational results also showed that the presence of water at the base of the excavation caused small failures near the bottom of the excavation which enlarged over time, undermining soil mass, and therefore reducing the factor of safety even more.

## CHAPTER 13: RECOMMENDATIONS

### 13.1 Residual Soil Characterization

When determining the  $c'$  and  $\phi'$  for use in geotechnical design, care must be taken not to include the apparent cohesion created by matric suction in design calculations. Many widely used insitu test methods such as the SPT, CPT, DMT, BST, and PMT are not capable of determining the portion of the strength that is attributed to negative pore pressure. The results of these tests can vary significantly depending on seasonal changes in the moisture content of the soil. Insitu permeability measurement can also be significantly altered by high levels of matric suction. In designs where these soil parameters are critical, it is recommended that they be obtained by testing saturated samples in the laboratory.

If extensive laboratory testing is not practical, an alternative method would be to use moisture content correlations to estimate the saturated properties of soil based on the results of a commonly used insitu test. The two test methods presented in this paper for determining  $\phi^b$  and measuring the SWCC, would allow the apparent cohesion to be estimated by simply knowing the insitu moisture content of the soil for each layer at the time of testing. This would work well if combined with a test like the SPT, where samples are retrieved during testing, and moisture contents could easily be obtained. The process for this type of correction would be as simple as converting the moisture content to matric suction using the SWCC, and then multiplying by  $\tan(\phi^b)$  to determine the apparent cohesion.

### **13.2 Retaining Structures and Slope Stability**

Although measured values for matric suction may seem to be relatively stable with depth, the results of these two test excavations proved that the presence of tension cracks can provide a means for water to penetrate, and saturate the soil along the critical failure plane. Because of this, it is recommended to use saturated testing methods to determine  $c'$  and  $\phi'$ , therefore excluding all apparent cohesion (caused by matric suction) from design calculations. It is also recommended that the testing program be suitable for identifying any weak layers, to ensure that the strength parameters obtained from testing truly reflect the critical state.

### **13.3 Unsaturated Soil Strength in Design**

Sufficient evidence exists in published literature to indicate that negative pore pressures may remain relatively constant depending on the permeability of the soil, and the rate at which water can infiltrate. The data collected in these tests support this theory, and showed relatively stable pore pressures (even with heavy rainfall) at greater depths, where tension cracks were not present. Because of this, certain geotechnical designs may be modified to benefit from the apparent cohesion caused by matric suction. Zhang et al. (2004) performed a numerical study on an unsaturated slope, and proved that under certain conditions, matric suction could be maintained. They also proposed that ground cover could be utilized to further stabilize the levels of suction, and emphasized the need for engineers to address more appropriate design assumptions related to the permanence of matric suction. The results of this experiment also support this recommendation and proved that as long as pore pressures can be maintained, significant strength can be provided by matric suction.

## REFERENCES

- Aas, G. (1976). Stability of a slurry trench excavation in soft clay. *Institut Fuer Grundbau und Bodenmechanik, Tu Wien*, Vol. 1.1, pp. 103-110.
- Abramson, L. W., Lee, T. S., Sharma, S., Boyce, G.M. (2002). *Slope Stability and Stabilization Methods*. John Wiley & Sons, Inc., New York, New York.
- Agus, S.S., Leong, E.C., Rahardjo, H. (2001). Soil-water characteristic curves of Singapore residual soils. *Geotechnical and Geological Engineering*, Vol. 19(3-4), pp. 285-309.
- Albrecht, B. A., Benson, C.H., & Beuermann, S. (2003). Polymer capacitance sensors for measuring soil gas humidity in drier soils. *Geotechnical Testing Journal*, Vol. 26(1), pp. 3-11.
- Allaby, A. and Allaby, M. (1999). Limit-equilibrium Analysis. *A Dictionary of Earth Sciences*, Encyclopedia.com, 6 May, 2011, <http://www.encyclopedia.com>.
- American National Standards Institute. (2010). *Safety Requirements for Excavation*, ANSI/ASSE A10.12-1998 (R2010).
- Anderson, J.B., & Ogunro, V.O. (2004). *Development of an earth pressure model for design of retaining structures in Piedmont soils*. Research Proposal to the North Carolina Department of Transportation, submitted April 12, 2004.
- Anderson, J.B., Ogunro, V.O., Detwiler, J.M., Starnes, J.R., and Burrage, R.E. (2004). *Development of an earth pressure model for design of retaining structures in Piedmont soils*. Engineering Report to the North Carolina Department of Transportation, submitted August 15, 2007.
- ASTM Standard D 2937-10: Standard Test Method for Density of Soil in Place by the Drive Cylinder Method, Annual Book of ASTM Standards, ASTM International, West Conshohocken, PA, 2010.
- ASTM Standard D 4767-04: Standard Test Method for Consolidated Undrained Triaxial Compression Test for Cohesive Soils, Annual Book of ASTM Standards, ASTM International, West Conshohocken, PA, 2004.
- ASTM Standard D 5084-00: Standard Test Methods for Measurement of Hydraulic Conductivity of Saturated Porous Materials Using a Flexible Wall Permeameter, Annual Book of ASTM Standards, ASTM International, West Conshohocken, PA, 2000.
- ASTM Standard D 5298-10: Standard Test Method for Measurement of Soil Potential (Suction) Using Filter Paper, Annual Book of ASTM Standards, ASTM International, West Conshohocken, PA, 2010.

- ASTM Standard D 6836-02: Standard Test Methods for Determination of the Soil Water Characteristic Curve for Desorption Using Hanging Column, Pressure Extractor, Chilled Mirror Hygrometer, or Centrifuge, Annual Book of ASTM Standards, ASTM International, West Conshohocken, PA, 2002.
- ASTM Standard D 7181-11: Standard Test Method for Consolidated Drained Triaxial Compression Test for Soils, Annual Book of ASTM Standards, ASTM International, West Conshohocken, PA, 2011.
- Atkinson, J.H., and Mair, R.J. (1981). Soil mechanics aspects of soft ground tunneling. *Ground Engineering*, Vol. 14(5), p. 20.
- Aung, K.K., Rahardjo, H., Leong E.C., and Toll, D.G. (2001). Relationship between porosimetry and soil-water characteristic curve for an unsaturated residual soil. *Geotechnical and Geological Engineering*, Vol. 19 (3-4), pp. 401-416.
- Barksdale, R.D., Bachus, R.C., and Calnan, M.B. (1982). Settlements of a Tower on Residual Soil. *Engineering and Construction in Tropical and Residual Soils*, ASCE Conference, Honolulu, pp. 647-664
- Barksdale, R.D., Ferry, C.T. and Lawrence, J.D. (1986). Residual soil settlement from pressuremeter moduli, *Use of In situ Tests in Geotechnical Engineering*, GSP No 6, ASCE, New York, pp. 447-461.
- Benson, C.H., Wang, X. (2006). Temperature-Compensating Calibration Procedure for Water Content Reflectometers, *Proc. TDR 2006*, West Lafayette, IN, 16 p.
- Birle, E., Heyer, D., & Vogt, N. (2008). Influence of the initial water content and dry density on the soil-water retention curve and the shrinkage behavior of a compacted clay. *Acta Geotechnica*, Vol. 3(3), pp. 191-200.
- Bishop, A.W. (1959). The principle of effective stress. *Teknisk Ukeblad I Samarbeide Med Teknikk*. Oslo, Norway. Vol. 106(39), pp. 859-863
- Bishop, A.W. and Blight, G.E. (1963). Some aspects of effective stress in saturated and unsaturated soils. *Géotechnique*, Vol. 13(3), pp. 177-197.
- Bishop, A.W., Alpan, I., Blight, G.E., and Donald, I.B. (1960). Factors controlling the shear strength of partially saturated cohesive soils. *ASCE Research Conference on the Shear Strength of Cohesive Soils*, University of Colorado, Boulder, pp. 503-532.
- Bishop, A.W., and Donald, I.B. (1961). The Experimental Study of Partially Saturated Soil in Triaxial Apparatus. *Proceedings of Fifth International Conference on Soil Mechanics and Foundation Engineering*, Vol. 1/3, pp. 13-21
- Blight, G.E. (1985). Residual soils in South Africa. In E.W. Brand and H.B. Phillipson (eds), *Sampling and Testing of Residual Soils, a Review of International Practice. Technical Committee on Sampling and Testing of Residual Soils*. Int. Soc. For Soil Mechanics and Foundation Engineering, Scorpion Press, Hong Kong: pp. 159-168.
- Blight, G.E. (1997). *Mechanics of Residual Soils: A guide to the formation, classification, and geotechnical properties of residual soils, with advice for geotechnical design*. Balkema Publishers, Rotterdam, Netherlands.

- Blight, G.E. (1997b). Origin and formation of residual soils. *Mechanics of Residual Soils: A guide to the formation, classification and geotechnical properties of residual soils, with advice for geotechnical design*, Blight, G.E. pp. 1-16.
- Blight, G. E., & Leong, E. C. (2012). *Mechanics of Residual Soils, Second Edition*. CRC Press, Taylor and Francis Group, London, UK. 392p.
- Borden, R.H., Shao, L., and Gupta, A. (1996). Dynamic properties of piedmont residual soils. *Journal of Geotechnical Engineering*, ASCE, Vol. 122(10), pp.813-821.
- Box, J.E. and Taylor, S.A. (1962), Influence of soil bulk density on matric potential. *Soil Science Society of America Journal*, Vol. 26(2), pp. 119-122.
- Brand, E.W. and Phillipson, H.B. (1985). *Sampling and testing of residual soils: a review of international practice*. Southeast Asian Geotechnical Society, Scorpion Press, Hong Kong.
- Brenner, R.P., Garga, V.K. and Blight, G.E. (1997). Shear strength behavior and measurement of shear strength in residual soil. *Mechanics of Residual Soils: A guide to the formation, classification and geotechnical properties of residual soils, with advice for geotechnical design*, Blight, G.E. (ed), pp. 155-220.
- Brown, D.A. and Vinson, J. (1998). Comparison of strength and stiffness parameters for a Piedmont residual soil, *Geotechnical Site Characterization, Vol. 2, (Proc. ISC'98, Atlanta)*, Balkema, Rotterdam, pp. 1229-1234.
- Burland, J.B., Longworth, T.I., Moore, J.F.A. (1977). A study of ground movement and progressive failure caused by a deep excavation in Oxford Clay. *Géotechnique*, Vol. 27(4), pp. 557-591.
- Burrage, R.E. (2007). *The Development of a Lateral Earth Pressure Model for the Design of Retaining Walls in Piedmont Residual Soil* (Master's thesis). Department of Civil and Environmental Engineering, The University of North Carolina at Charlotte. Charlotte, NC, 239 p.
- Burrage, R.E., Anderson, J.B., Pando, M.A., Ogunro, V.O., Cottingham, M.A. (2011). A Cost Effective Triaxial Test Method for Unsaturated Soils. *Geotechnical Testing Journal*, Vol. 35(1), pp. 50-59.
- Cabarkapa, Z., and Cuccovillo, T. (2006). Automated Triaxial Apparatus for Testing Unsaturated Soils. *Geotechnical Testing Journal*, Vol. 29, No. 1, pp. 21-29
- Campbell Scientific, Inc. (2006). *CS616 and CS625 Water Content Reflectometers*. Retrieved 8/2010, <http://www.campbellsci.com/documents/manuals/cs616.pdf>
- Campbell Scientific, Inc. (2009). *Models 253-L and 257-L (Watermark 200) Soil Matrix Potential Sensors*, Retrieved 8/2010, <http://www.campbellsci.com/documents/manuals/253-257.pdf>
- Campbell, G.S., and Gardner, W.H. (1971). Psychrometer Measurement of Soil Water Potential: Temperature and Bulk Density Effects, *Soil Science Society of America Journal*, Vol. 35, pp. 8-12.

- Carter, B.T., and Steltenpohl, M.G. (2002). Geologic map of the 1:24,000 Parkers Crossroads, Alabama. U.S.G.S. Topographic Quadrangle: Alabama Geological Survey Open-File Special Map.
- Cassel, D. K., & Klute, A. (1986). Water potential: tensiometry. *Methods of Soil Analysis: Part 1—Physical and Mineralogical Methods*, pp. 563-596.
- Chard, J. (2002). *Watermark Soil Moisture Sensors: Characteristics and Operating Instructions*. Utah State University, 8 p.
- Chen, S.X., and Chen, S.Y. (2001). *Analysis of stability of unsaturated soil slope due to permeation of rainwater*. LRSM Laboratory, Institute of Rock and Soil Mechanics, The Chinese Academy of Sciences, Wuhan 430071, China.
- Cheng, M.Y., Ko, C.H., Chang, C.H. (2002). Computer-aided DSS for safety monitoring of geotechnical construction. *Automation in Construction*, Vol. 11(4), pp.375-390.
- Cho, S.E., and Lee, S.R. (2001). Instability of unsaturated soil slopes due to infiltration. *Computers and Geotechnics*, Vol. 28 (3), pp.185-208
- Clough, G.W., and O'Rourke, T.D. (1990). Construction induced movements of insitu walls. *Design and Performance of Earth Retaining Structures*, GSP No. 25, ASCE, New York, NY, pp. 439-470.
- Coleman, J.D. (1962). Stress/ strain relations for partly saturated soils. *Géotechnique*, Vol. 12(4), pp. 348-350
- Coulomb, C.A. (1776). *Essai sur une application des règles de maximis & minimis à quelques problèmes de statique, relatifs à l'architecture*. De l'Imprimerie Royale.
- Cruz, N., Viana da Fonseca, A., and Neves, E. (2004). Evaluation of effective cohesive intercept on residual soils by DMT and CPT. *Proceedings ISC-2 on Geotechnical and Geophysical Site Characterization*, Viana da Fonseca and Maine (eds.), pp. 1275-1278.
- Cui, Y.J., Tang, A.M., Marcial, D., Terpereau, J.M., Marchadier, G., and Boulay, X. (2007). Use of a Differential Pressure Transducer for the Monitoring of Soil Volume Change in Cyclic Triaxial Test on Unsaturated Soils. *Geotechnical Testing Journal*, Vol. 30(3), pp. 227-233.
- Daintith, J. (2004). Finite-Difference Method. *A Dictionary of Computing*, Encyclopedia.com, 6 May, 2011, <http://www.encyclopedia.com>.
- Dane, J.H., and Hruska, S. (1983). In-Situ Determination of Soil Hydraulic Properties during Drainage. *Soil Science Society of America Journal*, Vol. 47(4), pp. 619-624.
- DiBiagio, E., and Myrvoll, F. (1972). Full scale field tests with a slurry trench excavation in soft clay. *Norwegian Geotechnical Institute Publ., No.91*, pp. 39-49
- Duncan, J.M., and Wright, S.G. (2005). *Soil Strength and Slope Stability*, John Wiley and Sons, Inc., Hoboken, New Jersey.
- Dunlop, P. and Duncan, J.M. (1970). Development of Failure around Excavated Slopes. *Journal of the Soil Mechanics and Foundations Division*, ASCE, Vol. 96(2), pp. 471-493.
- Eisenstein, Z., and Samarasekera, L. (1992). Stability of unsupported tunnels in clay. *Canadian Geotechnical Journal*, Vol. 29(4), pp. 609-613.

- Eldredge, E.P., Shock, C.C., and Stieber, T.D. (1993). Calibration of Granular Matrix Sensors for Irrigation Management. *Agronomy Journal*, Vol. 85, pp. 1228-1232.
- El-Ramly, H., Morgenstern, N.R., & Cruden, D.M. (2005). Probabilistic assessment of stability of a cut slope in residual soil. *Geotechnique*, Vol. 55(1), pp. 77-84.
- Escario, V. (1980). Suction-controlled penetration and shear tests. *Proceedings of the 4th International Conference on Expansive Soils*, Denver, CO, pp. 781-787.
- Failmezger, R.A., Rom, D., and Ziegler, S.B. (1999). SPT? – A better approach to site characterization of residual soils using other in-situ tests. *Behavioral Characteristics of Residual Soils (GSP No. 92)*, Edelen, B. (ed), ASCE, Reston, pp. 158-169.
- Fang, Y., Chen, J., and Chen, C. (1997). Earth pressures with sloping backfill. *Journal of Geotechnical Engineering*, Vol. 123(3), pp. 250-259.
- Fang, Y., Chen, T., and Wu, B. (1994). Passive earth pressures with various wall movements. *Journal of Geotechnical Engineering*, Vol. 120(8), pp. 1307-1323.
- Fawcett, R.G., & Collis-George, N. (1967). A filter-paper method for determining the moisture characteristics of soil. *Animal Production Science*, Vol. 7(25), pp. 162-167.
- Fellenius, W. (1922). *Vattenbyggnadslaboratoriets vid Kungl. Tekniska Hogskolan ut.*
- Fellenius, W. (1927). *Erdstatische Berechnungen, Revised Edition*. W. W Ernst u. Sons, Berlin.
- Finke, K.A. (1998). *Piezocone penetration testing in Piedmont residual soils* (Master's Thesis). School of Civil and Environmental Engineering, Georgia Institute of Technology, Atlanta, 265 p.
- Finke, K.A. and Mayne, P.W. (1999). Piezocone tests in U.S. Atlantic Piedmont residual soils. *Proceeding, XI Pan American Conference on Soil Mechanics & Geotechnical Engineering*, Vol. 1, Foz do Iguassu, Brazil, pp. 329-334.
- Finke, K.A., Mayne, P.W., and Klopp, R.A. (1999). Characteristic piezocone response in Piedmont residual soils. *Behavioral Characteristics of Residual Soils (GSP No. 92)*. Edelen, B. (ed), ASCE, Reston, 1-11.
- Flint, A.L., Campbell, G.S., Ellett, K.M., & Calissendorff, C. (2002). Calibration and temperature correction of heat dissipation matric potential sensors. *Soil Science Society of America Journal*, Vol. 66(5), pp. 1439-1445.
- Foss, I. (1973). Red Soil From Kenya as a Foundation Material. *Proceedings, Eighth International Conference on Soil Mechanics and Foundation Engineering*, Moscow, U.S.S.R. Vol. 2.2.
- Fourie, A.B. (1997). Classification and index tests. *Mechanics of Residual Soils: A guide to the formation, classification and geotechnical properties of residual soils, with advice for geotechnical design*. Blight, G.E. (ed), pp. 57-64.
- Frank, A.R. (1990). *Development of an automated data acquisition system for an electric cone used for the correlation of the SPT, DMT, and CPT in Piedmont residual soils* (Master's Thesis). School of Civil and Environmental Engineering, Georgia Institute of Technology, Atlanta, Georgia, 210 p.

- Fredlund, D.G. (1980). Remarks on the validity of stability analyses: Discussion. *Canadian Geotechnical Journal*, Vol. 17(4), pp. 641-642.
- Fredlund, D.G., & Wong, D.K. (1989). Calibration of thermal conductivity sensors for measuring soil suction. *Geotechnical Testing Journal*, Vol. 12(3), pp. 188-194.
- Fredlund, D.G., and Morgenstern, N.R. (1977). Stress State Variables for Unsaturated Soils. *Journal of Geotechnical Engineering Division*, Vol. 103, pp. 447-466.
- Fredlund, D.G., Shuai, F., Feng, M., Rahardjo, H., Toll, D.G., & Leong, E.C. (2000). Use of a new thermal conductivity sensor for laboratory suction measurement. *Unsaturated soils for Asia. Proceedings of the Asian Conference on Unsaturated Soils, UNSAT-Asia 2000*, Singapore, 18-19 May, 2000, AA Balkema, pp. 275-280.
- Fredlund, D.G. (1973). *Volume Change Behavior of Unsaturated Soils* (Ph.D. Dissertation). University of Alberta, Edmonton, Canada.
- Fredlund, D.G. (2006). Unsaturated Soil Mechanics in Engineering Practice. *Journal of Geotechnical and Geoenvironmental Engineering*, Vol. 132(3), pp. 286-321.
- Fredlund, D.G., and Rahardjo, H. (1993). *Soil Mechanics for Unsaturated Soils*. John Wiley and Sons, Inc., New York.
- Fredlund, D.G., Morgenstern, N.R., and Widger, R.A. (1978). Shear Strength of Unsaturated Soils. *Canadian Geotechnical Journal*, Vol. 15(3), pp. 313-321.
- Fredlund, D.G., Xing, A., Huang, S. (1994). Predicting the permeability function for unsaturated soils using the soil-water characteristic curve. *Canadian Geotechnical Journal*, Vol. 31(4), pp. 533-546.
- Gachet, P., Geiser, F.X., Laloui, L., & Vulliet, L. (2007). Automated digital image processing for volume change measurement in triaxial cells. *Geotechnical Testing Journal*, Vol. 30(2), pp. 16-38.
- Gallipoli, D., Wheeler, J. and Karstunen, M. (2003). Modeling the variation of degree of saturation in a deformable unsaturated soil. *Géotechnique*, Vol. 53(2), pp. 273-277.
- Gasmo, J.M., Rahardjo, H., & Leong, E.C. (2000). Infiltration effects on stability of a residual soil slope. *Computers and Geotechnics*, Vol. 26(2), pp. 145-165.
- Gasmo, J., Hritzuk, K.J., Rahardjo, H., and Leong, E.C. (1999). Instrumentation of an Unsaturated Residual Soil Slope. *Geotechnical Testing Journal*, Vol. 22, No. 2, pp. 128-137.
- Gee, G.W., Campbell, M.D., Campbell, G.S., & Campbell, J.H. (1992). Rapid measurement of low soil water potentials using a water activity meter. *Soil Science Society of America Journal*, Vol. 56(4), pp. 1068-1070.
- Georgiadis, M. and Anagnostopoulos, C. (1998). Lateral pressure on sheet pile walls due to strip load. *Journal of Geotechnical & Geoenvironmental Engineering*, Vol. 124(1), pp. 95-98.
- Geo-Slope International Ltd. (2012). *GeoStudio 2012* [Computer Software]. Calgary, Alberta, T2P 2Y5, Canada.
- Google Maps. (2012). *Springvilla Park*. Retrieved from <https://www.google.com/maps/place/Springvilla+Park/@32.6436269,-85.2394777,233933m/data=!3m1!1e3!4m2!3m1!1s0x0:0x72ab3727b21e4ed!6m1!1e1>

- Greninger, P.J., Sud, Y.K., and Nielsen, D.R. (1985). Spatial Variability of Field-Measured Soil-Water Characteristics. *Soil Science Society of America Journal*, Vol. 49(5), pp. 1075-1082.
- Harp, E.L., Wells II, W.G., Sarmiento, J.G. (1990). Pore pressure response during failure in soils. *Geological Society of America Bulletin*, Vol. 102(4), pp. 428-438.
- Heartz, W.T. (1986). *Properties of a Piedmont residual soil* (Ph.D. Dissertation). North Carolina State University, Raleigh, NC.
- Hilf, J.W. (1956). An investigation of pore water pressure in compacted cohesive soils. *Technical Memorandum 654*, U.S. Department of Interior, Bureau of Reclamation, Denver, CO, USA.
- Ho, D.Y.F., and Fredlund, D.G. (1982). A Multistage Triaxial Test for Unsaturated Soils. *Geotechnical Testing Journal*, Vol. 5(1/2), pp. 18-25.
- Ho, D.Y.F., and Fredlund, D.G. (1982b). Increase in shear strength due to suction for two Hong Kong soils. *Proceedings of the ASCE Geotechnical Conference Engineering and Construction in Tropical Residual Soils*, Honolulu, HI, pp. 263-295.
- Houston, S.L., Houston, W.N., & Wagner, A.M. (1994). Laboratory filter paper suction measurements. *Geotechnical Testing Journal*, Vol. 17(2), pp. 185-194.
- Houston, S.L., Houston, W.N., & Wagner, A.M. (1994). Laboratory filter paper suction measurements. *Geotechnical Testing Journal*, Vol. 17(2), pp. 185-194.
- Hoyos, L., Jr. and Macari, E.J. (1999). Influence of in-situ factors on dynamic response of Piedmont residual soils. *Journal of Geotechnical and Geoenvironmental Engineering*, Vol. 125 (4), pp. 271-279.
- Huat, B.B., Ali, F.H., & Low, T.H. (2006). Water infiltration characteristics of unsaturated soil slope and its effect on suction and stability. *Geotechnical & Geological Engineering*, Vol. 24(5), pp. 1293-1306.
- Huat, B.K., Ali, F.H., Low, T.H. (2006). Water infiltration characteristics of unsaturated soil slope and its effect on suction and stability. *Geotechnical and Geological Engineering*, Springer, Vol. 24(5), pp. 1293-1306.
- Jennings J.E., and Burland, J.B. (1962). Limitations to the use of effective stresses in partly saturated soils. *Géotechnique*, Vol. 12(2), pp. 125-144.
- Jiru, Z. (2002). Finite element simulation and stability analysis on slope excavation. *Chinese Journal of Rock Mechanics and Engineering*, 2002-06.
- Jotisankasa, A., Coop, M. and Ridley, A. (2007). The Development of a Suction Control System for a Triaxial Apparatus. *Geotechnical Testing Journal*, Vol. 30(1), pp. 69-75.
- Khalili, N., Geiser, F., Blight, G.E. (2004). Effective Stress in unsaturated soils, a review with new evidence. *International Journal of Geomechanics*, Vol. 4(2), pp. 115-126.
- Kort, D.A. (2002). *Steel sheet pile walls in soft soil*. Delft University Press, Delft, The Netherlands.
- Kovacevic, N., Hight, D.W., Potts, D.M. (2007). Predicting the stand-up time of temporary London clay slopes at Terminal 5 Heathrow Airport. *Géotechnique*, Vol. 57(1), pp. 63-74.

- Krahn, J., Fredlund, D.G., and Klassen, M.J. (1989). Effect of soil suction on slope stability at Notch Hill. *Canadian Geotechnical Journal*, Vol. 26(2), pp. 269-278.
- Lambe, T. W., and Whitman, R. V. (1969). *Soil Mechanics*. John Wiley and Sons, New York.
- Leong, E.C., Agus, S.S., and Rahardjo, H. (2004). Volume Change Measurement of Soil Specimen in Triaxial Test. *Geotechnical Testing Journal*, Vol. 27(1), pp. 47-56.
- Leroueli, S. (2001). Natural slopes and cuts: movement and failure mechanisms. *Géotechnique*, Vol. 54(3), pp.197-243.
- Likos, W.J., & Lu, N. (2003). Automated humidity system for measuring total suction characteristics of clay. *Geotechnical Testing Journal*, Vol. 26(2), pp. 179-190.
- Likos, W.J., & Lu, N. (2001). Automated measurement of total suction characteristics in high-suction range: Application to assessment of swelling potential. *Transportation Research Record: Journal of the Transportation Research Board*, (1755), pp. 119-128.
- Likos, W.J., & Lu, N. (2002). Filter paper technique for measuring total soil suction. *Transportation Research Record: Journal of the Transportation Research Board*, (1786), 120-128.
- Lim, T.T., Rahardjo, H., Chang, M.F., and Fredlund, D.G. (1996). Effect of rainfall on matric suctions in a residual soil slope. *Canadian Geotechnical Journal*, Vol. 33, pp. 618-628.
- Long, M. (2001). Database for retaining wall and ground movements due to deep excavations. *Journal of Geotechnical and Geoenvironmental Engineering*, Vol. 127(3), pp. 203-224.
- Lu, N. and Likos, W.J. (2006). Suction Stress Characteristic Curve for Unsaturated Soil. *Journal of Geotechnical and Geoenvironmental Engineering*, Vol. 132(2), pp. 131-142.
- Lu, N., and Likos, W.J. (2004). *Unsaturated Soil Mechanics*. John Wiley and Sons, Inc., Hoboken, New Jersey.
- Lunne, T., Berre, T., & Strandvik, S. (1997). Sample disturbance effects in soft low plastic Norwegian clay. *In Symposium on Recent Developments in Soil and Pavement Mechanics*. pp. 81-102
- Lutenegger, A.J., Cerato, A.B., and Harrington, N. (2003). Some Physical and Chemical Properties of Some Piedmont Residual Soils. *Proceedings of 12<sup>th</sup> Panamerican Conference on Soil Mechanics and Geotechnical Engineering*, Patricia J. Culligan, Herbert H. Einstein and Andrew J. Whittle Eds., Cambridge, MA, June. pp. 775-782.
- Macari, E.J., Parken, J.K., & Costes, N.C. (1997). Measurement of volume changes in triaxial tests using digital imaging techniques. *Geotechnical Testing Journal*, Vol. 20(1), pp. 103-109.
- Malicki, M.A., Plagge, R., Renger, M., and Walczak, R.T. (1992). Application of time-domain reflectometry (TDR) soil moisture miniprobe for the determination of unsaturated soil water characteristics from undisturbed soil cores. *Irrigation Science*, Vol. 13, pp. 65-72.
- Mariappan, S. (2010). *Characteristic of Unsaturated Residual Soil*. VDM Verlag Dr. Müller GmbH & Co KG, Saarbrücken, Germany.
- Martin, G.K., and Mayne, P.W. (1998). Seismic flat dilatometer tests in Piedmont residual soils, *Geotechnical Site Characterization*, Vol. 2, Balkema Rotterdam, 837-843.

- Mayne, P.W., Brown, D.A., Vinson, J.L., Schneider, J.A., and Finke, K.A. (2000). Site Characterization of Piedmont Residual Soils at the NGES, Opelika, Alabama. *National Geotechnical Experimentation Sites, ASCE GSP No. 93*, pp. 160-185.
- Mayne, P.W., and Brown, D.A. (2003). Site Characterization of Piedmont residuum of North America. *Characterization and Engineering Properties of Natural Soils*, Vol. 2, pp. 1323-1339.
- McCarthy, D.F. (2002). *Essentials of Soil Mechanics and Foundations Basic Geotechnics*, 6th ed., Prentice Hall, Upper Saddle River, New Jersey. 157 p.
- McQueen, I. S., & Miller, R.F. (1968). Calibration and evaluation of a wide-range gravimetric method for measuring moisture stress. *Soil Science*, Vol. 106(3), pp. 225-231.
- Miller, C.J., Yesiller, N., Yaldo, K., Merayyan, S. (2002). Impact of Soil Type and Compaction Conditions on Soil Water Characteristic. *Journal of Geotechnical and Geoenvironmental Engineering*, Vol. 128, pp. 733-742.
- Miller, G.A., Khoury, C.N., Muraleetharan, K.K., Liu, C. and Kibbey, T.C.G. (200) Effects of soil skeleton deformations on hysteretic soil water characteristic curves: Experiments and Simulations. *Water Resources Research*, Vol. 44(5), W00C06.
- Mitchell, J.K., and Sitar, N. (1982). Engineering properties of tropical residual soils. *Proc., Conference on Engineering and Construction in Tropical and Residual Soils*. Honolulu, Hawaii.
- Mohamedzein, Y., and Mohammed H.A. (2006). Compressibility and shear strength of a residual soil. *Geotechnical and Geological Engineering*, Vol. 24, pp. 1385 -1401.
- Muraleetharan, K.K., Liu, C., Wei, C., Kibbey, T.C.G., Chen, L. (2009). An elastoplastic framework for coupling hydraulic and mechanical behavior of unsaturated soils. *Int J Plast*, Vol. 25, pp.473-490.
- Myriantthis, M.L. and Leach, B. (1978). Basic geotechnical and mineralogical properties of the weathered Athenian schist. *Rock Mech Felsmech Mec Roches*, Vol. 10(3), pp. 151-164.
- Newill, D. (1961). A Laboratory Investigation of Two Red Clays from Kenya. *Geotechnique*, Vol. XI.
- Ng, C.W.W., and Pang, Y.W. (2000). Influence of Stress State on Soil-Water Characteristics and Slope Stability. *Journal of Geotechnical and Geoenvironmental Engineering*, Vol. 126 (2), 10 p.
- Ng, C.W.W., Zhan, L.T., Bao, C.G., Fredlund, D.G., & Gong, B.W. (2003). Performance of an unsaturated expansive soil slope subjected to artificial rainfall infiltration. *Geotechnique*, Vol. 53(2), pp. 143-157.
- Nielson, D.R., Biggar, J.W., Erh, K.T. (1973). Spatial Variability of Field-Measured Soil-Water Properties. *Hilgardia*, Vol. 42 (7), pp. 215-259.
- O'Neill, M.W. and Gazioglu, S.M. (1984). Evaluation of p-y relationships in cohesive soils. *Proceedings, Analysis and Design of Pile Foundations, ASCE Technical Council on Codes and Standards*, ASCE National Convention, San Francisco, California, J. Meyers Editor, pp. 192-213.

- O'Neill, M.W., and Murchison, J.M. (1983). *An evaluation of p-y relationships in sands*. Research Report No. GT-DF02-83, Department of Civil Engineering, University of Houston, Houston, May.
- Osborne, W.E., Copeland, C.W., and Neathery, T.L. (1988). *Alabama stratigraphy*. Circular 140, Geological Survey of Alabama, Stratigraphy and Paleontology Division, 101p.
- Padilla, J.M., and Perera, Y.Y. (2005). A New Soil-Water Characteristic Curve Device. *Proceedings of Advanced Experimental Unsaturated Soil Mechanics - an International Symposium*, EXPERUS 2005, Trento, Italy, pp. 15-22.
- Padilla, J.M., Houston, W.N., Lawrence, C.A., Fredlund, D.G., Houston, S.L., and Perez, N.P. (2006). An Automated Triaxial Testing Device for Unsaturated Soils. *Unsaturated Soils 2006*, ASCE GSP147, pp. 1775-1786.
- Padilla, J.M., Perera, Y.Y., Houston, W.N., Perez, N., and Fredlund, D.G. (2006b). Quantification of air diffusion through high air-entry ceramic disks, *Unsaturated Soils 2006*, ASCE, pp.1852-1863.
- Paquet, J.M., Caron, J., Banton, O. (1993). In situ determination of the water desorption characteristics of peat substrates. *Canadian Journal of Soil Science*, Vol. 73(3), pp. 329-339.
- Peck, R.B. (1969). Deep excavations and tunneling in soft ground. *Proceedings of the 7<sup>th</sup> International Conference of Soil Mechanics and Foundation Engineering*. Mexico City, pp. 225-290.
- Peterson, M., Brand, S., Roldan, R., Sommerfield, G. (1999). Residual soil characterization for a power plant. *Behavioral Characteristics of Residual Soils Geotechnical Special Publication No. 92*, Bill Edelen Ed., ASCE, Charlotte, NC, pp. 26-42.
- Pham, H.Q., Fredlund, D G., and Barbour, S. L. (2003). A practical hysteresis model for the soil-water characteristic curve for soils with negligible volume change. *Geotechnique*, Vol. 53(2), pp. 293-298.
- Phene, C.J., Hoffman, G.J., & Rawlins, S.L. (1971). Measuring soil matric potential in situ by sensing heat dissipation within a porous body: I. Theory and sensor construction. *Soil Science Society of America Journal*, Vol. 35(1), pp. 27-33.
- Phene, C.J., Rawlins, S.L., & Hoffman, G.J. (1971). Measuring soil matric potential in situ by sensing heat dissipation within a porous body: II. Experimental results. *Soil Science Society of America Journal*, Vol. 35(2), pp. 225-229.
- Pictometry International Corp. (2012). *Springvilla, AL*. Retrieved from <http://www.bing.com/mapspreview?&cp=pdz5107wrpbz&lvl=20&style=b&v=2&sV=1&form=S00027>
- Prusza, Z., Kleiner, D.E., and Sundaram, A.V. (1983). Characteristics of Guri Soils. *ASCE Special Publication, Geological Environment and Soil Properties*, Houston, TX.
- Rahardjo, H., Aung, K.K., Leong, E.C., and Rezaur, R.B. (2004). Characteristics of Residual Soils in Singapore as formed by weathering. *Engineering Geology*, Vol. 73, pp. 157-169.
- Rahardjo, H., Lee, T.T., Leong, E.C., Rezaur, R.B. (2005). Response of a residual soil slope to rainfall. *Canadian Geotechnical Journal*, Vol. 42(2), pp. 340-351.

- Rankine, W.M. (1857). On the stability of loose earth. *Philosophical Transactions of the Royal Society of London*, Vol. 147, pp. 9-27.
- Reese, L.C., Cox, W.R., and Koop, F.D. (1974). Analysis of laterally loaded piles in sand. Paper No. OTC 2080, *Proceedings, Fifth Annual Offshore Technology Conference*, Houston, Texas, (GESA Report No. D-75-9).
- Robertson, P.K., Campanella, R.G., Brown, P.T., Grof, I., and Hughes, J.M. (1985). Design of axially and laterally loaded piles using insitu tests: a case history. *Canadian Geotechnical Journal*, Vol. 22(4), pp. 518-527.
- Robertson, P.K., Davies, M.P., and Campanella, R.G. (1989). Design of laterally loaded driven piles using the flat dilatometer. *Geotechnical Testing Journal*, Vol. 12(1), pp. 30-38.
- Rouse, W.C., Reading, A.J. and Walsh, R.P.D. (1986). Volcanic soil properties in Dominica, West Indies. *Engineering Geology* Vol. 23, pp. 1-28.
- Salager, S., Nuth, M., Ferreri, A., Laloui, L. (2013). Investigation into water retention behavior of deformable soils. *Canadian Geotechnical Journal*, Vol. 50, pp.1-9.
- Schneider, J.A., Hoyos Jr., L., Mayne, P.W., Macari, E.J. and Rix, G.J. (1999). Field and laboratory measurements of dynamic shear modulus of piedmont residual soils. *Behavioral Characteristics of Residual Soils*, Geotechnical Special Publication No. 92, ASCE, pp. 158-175.
- Sheng D., Zhou A.N. (2011). Coupling hydraulic with mechanical models for unsaturated soils. *Canadian Geotechnical Journal*, Vol. 48(5), pp. 826-840.
- Shock, C., Feibert, E., and Jaderholm, S. (2001). A Comparison of Six Soil Moisture Sensors. *Malheur Experiment Station*, Oregon State University, Ontario, OR, 7 p.
- Shock, C.C., Barnum, J.M., and Seddigh, M. (1998). Calibration of Watermark Soil Moisture Sensors for Irrigation Management. *Proceedings of the International Irrigation Show*, San Diego, CA Irrigation Association, pp. 139-146.
- Sivakumar, R., Sivakumar, V., Blatz, J., and Vimalan, J. (2006). Twin-Cell Stress Path Apparatus for Testing Unsaturated Soils. *Geotechnical Testing Journal*, Vol. 29(2), pp. 175-179.
- Sowers, G.F. (1994). Residual soil settlement related to the weathering profile, *Vertical and Horizontal Deformations of Foundations and Embankments*, Geotechnical Special Publication No. 40, Vol. 2, ASCE, New York, pp. 1689-1702.
- Sowers, G.F. and Richardson, T.L. (1983). Residual soils of the Piedmont and Blue Ridge, *Transportation Research Record* 919, National Academy Press, Washington, D.C., pp. 10-16.
- Sowers, G.F. (1954). Soil Problems in the Southern Piedmont Region. *Proceedings from the ASCE*, Vol. 80, Separate 416, pp. 1-15.
- Sowers, G.F. (1963). Engineering Properties of Residual Soil Derived From Igneous and Metamorphic Rocks. *Proceedings from the 2nd Pan American Conference on Soil Mechanics and Foundation Engineering*, Rio De Janerio, Vol. 1, pp. 39-61.

- Spanner, D. C. (1951). The Peltier effect and its use in the measurement of suction pressure. *Journal of Experimental Botany*, pp. 145-168.
- Stanevich, R.L., and Middleton, D.C. (1988). An Exploratory Analysis of Excavation Cave-In Fatalities. *Professional Safety*, Vol. 33, pp. 24-28.
- Stannard, D.I. (1992). Chapter B - Bowen-Ratio Measurements at Sites C and F. *Water-resources Investigations*, Vol.91, 19p.
- Taylor, D.W. (1937). Stability of Earth Slopes. *J. Boston Soc. Civil Eng.*, Vol. 24(3), Reprinted in: *Contributions to Soil Mechanics 1925 to 1940*, Boston Society of Civil Engineers, pp. 337-386.
- Terzaghi, K. (1943). *Theoretical Soil Mechanics*. Wiley, New York.
- Terzaghi, K. (1958). Design and performance of Sasumua Dam. *Proceedings I.C.E.* 9, pp. 369-394.
- Terzaghi, K., and Peck, R. B. (1948). *Soil Mechanics in Engineering Practice*. John Wiley and Sons, New York.
- Terzaghi, V. K. (1936). The shearing resistance of saturated soils and the angle between the planes of shear. *Proceedings of the 1st international conference on soil mechanics and foundation engineering*, Harvard University Press Cambridge, MA. Vol. 1, pp. 54-56.
- The National Institute for Occupational Safety and Health. (2006). *Trench Safety Awareness*, DHHS (NIOSH) Publication Number 2006-133D. Centers for Disease Control and Prevention, Atlanta, GA.
- Thom, R., Sivakumar, V., Brown, J., and Hughes, D. (2008). A Simple Triaxial System for Evaluating the Performance of Unsaturated Soils Under Repeated Loading. *Geotechnical Testing Journal*, Vol. 31(2), pp. 107-114.
- Thompson, S.J., and Armstrong, C.F. (1987). Calibration of the Watermark Model 200 Soil Moisture Sensor. *Applied Engineering in Agriculture*, Vol. 3(2), pp. 186-189.
- Townsend, F.C. (1985). Geotechnical characteristics of residual soils. *Journal of Geotechnical Engineering*, Vol. 111(1), pp. 77-94.
- Townsend, F.C., Manke, P.G., and Parcher, J.V. (1969). *Effects of Remolding on the Properties of a Lateritic Soil*. Highway Research Board, Rec. 284 p.
- Toyosawa, Y., Horii, N., Tamate, S. (1993). Analysis of fatal accidents caused by trench failure. *Third International Conference on Case Histories in Geotechnical Engineering*, Paper 2.
- Tsai, J.S., and Chang, J.C. (1996). Three-dimensional stability analysis for slurry-filled trench wall in cohesionless soil. *Canadian Geotechnical Journal*, Vol. 33(5), pp. 798-808.
- Tsai, J.S., Jou, L.D., Hsieh, H.S. (2000). A Full Scale Stability Experiment on a Diaphragm Wall Trench. *Canadian Geotechnical Journal*, Vol. 37 (2), pp. 379-392.
- Tsagaras, I., Rahardjo, H., Toll, D.G., Leong, E.C. (2003). Infiltration characteristics of two instrumented residual soil slopes. *Canadian Geotechnical Journal*, Vol. 40(5), pp.1012-1032.

- United States Army (2014). *US Army Corps of Engineers Safety and Health Requirements, EM 385-1-1*, Washington, D.C.
- United States Department of Labor: Occupational Safety and Health Administration (2005). *29 CFR 1926; Construction Industry Standards*. Revised February 1, 2005. Washington, D.C.
- United States Geological Survey (2001). *Map of the Piedmont and the Blue Ridge Physiographic Provinces*. Retrieved from <http://va.water.usgs.gov/PiedWkshop/map.htm>
- University of Alabama (2012). *Alabama Soils*. Retrieved from [http://alabamamaps.ua.edu/contemporarymaps/alabama/physical/soils\\_map.jpg](http://alabamamaps.ua.edu/contemporarymaps/alabama/physical/soils_map.jpg)
- Vanapalli, S.K., Fredlund, D.G., Pufahl, D.E. (1999). The influence of soil structure and stress history on the soil–water characteristics of a compacted till. *Géotechnique*, Vol. 44, pp. 892-898.
- Vargas, M. (1973). Structurally Unstable Soils in Southern Brazil. *Eighth International Conference on Soil Mechanics and Foundation Engineering*. Moscow, U.S.S.R., Vol. 22.
- Vaughan, P.R. (1988). Keynote paper: Characterising the mechanical properties of in situ residual soil. *Proc. 2<sup>nd</sup> Int. Congr. IAEG, Sao Paulo I*: 5.1-5.26.
- Vaunat, J., Amador, C., Romero, E., & Dejeran-Maigre, I. (2006). Residual Strength of a Low Plasticity Clay at High Suctions. *Unsaturated Soils*, ASCE, pp. 1279-1289.
- Viana de Fonseca, A., Matos Fernandes, M., Cardoso, A.S., and Martinis, J. (1994). Portuguese experience on geotechnical characterization of residual soils from granite. *Proceedings, 13<sup>th</sup> International Conference on Soil Mechanics and Foundation Engineering*, New Delhi, India, Vol. 1, pp. 277-380.
- Vinson, J.L and Brown, D.A. (1997). *Site characterization of the Spring Villa geotechnical test site and a comparison of strength and stiffness parameters for a Piedmont residual soil*. Report No. IR-97-04, Highway Research Center, Harbert Engineering Center, Auburn University, AL, 385 p.
- Waisnor, B.M., Ducote-Price, A., Jarosz, B., Duncan, J.M., & Smith, C.J. (2001). *Geotechnical engineering within the Piedmont physiographic province*. Center for Geotechnical Practice and Research. 27 p.
- Wang, E.W., and Borden, R.H. (1996). Deformation Characteristics of Piedmont Residual Soils. *Journal of Geotechnical Engineering*, Vol. 122(10), pp. 822-830.
- Wang, S., and Reese, L.C. (1993). Com624P - laterally loaded pile analysis program for the microcomputer version 2.0 [Computer Software]. USDOT Publication No. FHWA-SA-91-048.
- Wesley, L.D. (1994). The use of consolidometer tests to estimate settlement in residual soil. *Proceedings, XIII Intl. Conf. on Soil Mechanics & Foundation Engr.*, Vol. 2, New Delhi, pp. 929-934.
- Wheeler, S.J., Sharma, R.S. and Buisson, M.S.R (2003). Coupling of hydraulic hysteresis and stress-strain behaviour in unsaturated soils. *Géotechnique*, Vol. 53(1), pp. 41-54.
- Wiederhold, P.R. (1997). *Water vapor measurement: methods and instrumentation (Vol. 1)*. CRC Press.

- Willmer, J.L., Futrell, G.E. and Langfelder, J. (1982). Settlement predictions in Piedmont Residual Soil. *Engineering and Construction in Tropical and Residual Soils*, ASCE Conference, Honolulu, pp. 629-646.
- Winterkorn, H.F. and Chandrasekharan, E.C. (1951). *Lateritic Soils and Their Stabilization*. Highway Research Board, Rec. 44.
- Wong, I.H., Low, B.K., Pang, P.Y., & Raju, V.R. (1997). Field Performance of Nailed Soil Wall in Residual Soil. *Journal of Performance of Constructed Facilities*, Vol. 11, pp. 105-112.
- Wulfsohn, D., Adams, B.A., and Fredlund, D.G. (1998). Triaxial Testing of Unsaturated Agricultural Soils. *J. Agric. Engng Res.*, Vol. 69, pp. 317-330.
- Young, J. F. (1967). Humidity control in the laboratory using salt solutions—a review. *Journal of Applied Chemistry*, Vol. 17(9), pp. 241-245.
- Zhan, T.L.T., Ng, C.W.W. and Fredlund, D.G. (2006). Instrumentation of an Unsaturated Expansive Soil Slope. *Geotechnical Testing Journal*, Vol. 30(2), pp. 128-137.
- Zhang, L.L., Fredlund, D.G., Zhang, L.M., Tang, W.H. (2004) Numerical study of soil conditions under which matric suction can be maintained. *Canadian Geotechnical Journal*, Vol. 41 pp. 569-582.
- Zhou, J. and Yu, J. (2005). Influences affecting the soil-water characteristic curve. *Journal of Zhejiang University SCIENCE*, Vol. 6A(8), pp. 797-804.

## APPENDIX A - DATALOGGER WIRING DIAGRAMS

### Excavation #1 Wiring Diagram

#### Multiplexer #1 to Datalogger

AM16/32 Multiplexer #1 (2x32 mode)	CR1000
COM ODD H	1H
COM ODD L	$\frac{1}{\equiv}$
GND	G
COM Ground	G
12V	12V
RES	C3
CLK	C4
	1H
1 kOhm 0.1% Resistor	EX1

#### Watermark / Temp. Sensors to Multiplexer #1

Watermark / Temp. Sensor (1)	AM16/32 Multiplexer #1
Black	1H
White	1L
Clear	$\frac{1}{\equiv}$

Watermark / Temp. Sensor (2)	AM16/32 Multiplexer #1
Black	2H
White	2L
Clear	$\frac{1}{\equiv}$

\*Typical for Sensors (3-22)

#### CS616 WCR to Datalogger

CS616 WCR (1)	CR1000
Green	2H
Clear	G
Black	G
Red	12V
Orange	C5

CS616 WCR (2)	CR1000
Green	2L
Clear	G
Black	G
Red	12V
Orange	C6

## Excavation #2 Wiring Diagram

### Multiplexer #1 to Datalogger

AM16/32 Multiplexer #1 (2x32 mode)	CR1000
COM ODD H	1H
COM ODD L	$\frac{1}{2}$
GND	G
COM Ground	G
12V	12V
RES	C3
CLK	C4
	1H
1 kOhm 0.1% Resistor	EX1

### Vibrating Wire Interface to Datalogger

AVW 200 (RS232 9 Pin)	CR1000
White	C2
Brown	C1
Yellow	G
Clear	$\frac{1}{2}$

### Multiplexer #2 to Vibrating Wire Interface

AM16/32 Multiplexer #2 (4x16 mode)	AVW 200
RES	C3
CLK	C2
GND	G
12V	12V (POWER)
ODD H	1V+
ODD L	1V-
EVEN H	1T+
EVEN L	1T-
AG	G

### CS616 WCR to Datalogger

CS616 WCR (1)	CR1000
Green	2H
Clear	G
Black	G
Red	12V
Orange	C5

CS616 WCR (2)	CR1000
Green	2L
Clear	G
Black	G
Red	12V
Orange	C6

### Irrrometer Tensiometer to Datalogger

Irrrometer Tensiometer (1)	CR1000
Red	5V
Black	G
White	3H

Irrrometer Tensiometer (2)	CR1000
Red	5V
Black	G
White	3L

### Watermark / Temp. Sensors to Multiplexer #1

Watermark / Temp. Sensor (1)	AM16/32 Multiplexer #1
Black	1H
White	1L
Clear	$\frac{1}{2}$

Watermark / Temp. Sensor (2)	AM16/32 Multiplexer #1
Black	2H
White	2L
Clear	$\frac{1}{2}$

\*Typical for Watermark / Temp Sensors (3-32)

### Geokon 4500 Sensors to Multiplexer #2

Geokon 4500 (1)	AM16/32 Multiplexer #2
COIL H (Red)	2H
COIL L (Black)	G
THERM H (Green)	G
THERM L (White)	12V

Geokon 4500 (2)	AM16/32 Multiplexer #2
COIL H (Red)	2H
COIL L (Black)	G
THERM H (Green)	G
THERM L (White)	12V

\*Typical for Geokon Sensors (3-8)

## APPENDIX B - DATALOGGER PROGRAMS

### Excavation #1 Datalogger Program

'CR1000

'Auburn Excavation August 2010

'Declare Variables and Units

Public I

Public Batt\_Volt

Public PTemp\_C

Public kOhms(22)

Public WP\_kPa(22)

Public VW

Public PA\_uS

Public VW\_2

Public PA\_uS\_2

Units Batt\_Volt=Volts

Units PTemp\_C=Deg C

Units kOhms=kOhms

Units WP\_kPa=kPa

Units PA\_uS=uSec

Units PA\_uS\_2=uSec

'Define Data Tables

DataTable(Table1,True,-1)

    DataInterval(0,0,0,10)

    CardOut(0,-1)

    Sample(1,kOhms(1),FP2)

    Sample(1,kOhms(2),FP2)

    Sample(1,kOhms(3),FP2)

    Sample(1,kOhms(4),FP2)

    Sample(1,kOhms(5),FP2)

    Sample(1,kOhms(6),FP2)

    Sample(1,kOhms(7),FP2)

    Sample(1,kOhms(8),FP2)

    Sample(1,kOhms(9),FP2)

    Sample(1,kOhms(10),FP2)

    Sample(1,kOhms(11),FP2)

    Sample(1,kOhms(12),FP2)

    Sample(1,kOhms(13),FP2)

    Sample(1,kOhms(14),FP2)

    Sample(1,kOhms(15),FP2)

    Sample(1,kOhms(16),FP2)

    Sample(1,kOhms(17),FP2)

    Sample(1,kOhms(18),FP2)

    Sample(1,kOhms(19),FP2)

```

    Sample(1,kOhms(20),FP2)
    Sample(1,kOhms(21),FP2)
    Sample(1,kOhms(22),FP2)
EndTable

DataTable(Table2,True,-1)
    DataInterval(0,0,0,10)
    CardOut(0,-1)
    Minimum(1,Batt_Volt,FP2,False,False)
    Sample(1,PTemp_C,FP2)
    Sample(1,VW,FP2)
    Sample(1,VW_2,FP2)
    Sample(1,PA_uS,FP2)
    Sample(1,PA_uS_2,FP2)
EndTable

'Main Program
BeginProg
    SerialOpen(Com1,38400,0,0,10000)
    Scan(30,Min,1,0)
        'Default Datalogger Battery Voltage measurement Batt_Volt:
        Battery(Batt_Volt)
        PanelTemp(PTemp_C,250)
        'Turn AM16/32 Multiplexer On
        PortSet(4,1)
        Delay(0,150,mSec)
        I=1
        SubScan(0,uSec,22)
            'Switch to next AM16/32 Multiplexer channel
            PulsePort(3,10000)
            '253 Soil Moisture Sensor measurements kOhms and WP_kPa on the AM16/32
Multiplexer:
            BrHalf(kOhms(I),1,mV250,1,1,1,250,True,20000,1000,1,0)
            'Convert resistance ratios to kOhms
            kOhms(I)=kOhms(I)/(1-kOhms(I))
            'Convert kOhms to water potential
            WP_kPa(I)=(0.07407*(kOhms(I)/1-(0.018*(PTemp_C-21)))-0.03704)*100
            I = I +1
            NextSubScan
            'Turn AM16/32 Multiplexer Off
            PortSet(4,0)
            'CS616 Water Content Reflectometer measurements VW and PA_uS:
            CS616(PA_uS,1,3,5,1,1,0)
            VW=-0.0663+(-0.0063*PA_uS)+(0.0007*PA_uS^2)
            'CS616 Water Content Reflectometer measurements VW_2 and PA_uS_2:
            CS616(PA_uS_2,1,4,6,1,1,0)
            VW_2=-0.0663+(-0.0063*PA_uS_2)+(0.0007*PA_uS_2^2)

            'Call Data Tables and Store Data
            CallTable(Table1)
            CallTable(Table2)

        NextScan
EndProg

```

## Excavation #2 Datalogger Program

'CR1000

'Auburn Excavation August 2011

'Declare Variables and Units

Public I

Public Batt\_Volt

Public PTemp\_C

Public SEVolt(2)

Public AVWCommResponse ' Response code for AVW200 communications

'Declare Variables for for the Watermark Sensors and Pluckers

Public kOhms(32)

'Declare Variables for the Campbell VWC Sensors

Public VWC

Public PA\_uS

Public VWC\_2

Public PA\_uS\_2

'Declare Variables for the Geokon 4500 Piezometers

Public GeokonFreqRaw(8)

Public GeokonThermRaw(8)

Public GeokonAmp(8)

Public GeokonSNRat(8)

Public GeokonNFreq(8)

Public GeokonDRat(8)

Dim VW(8,6)

'Temperature Constants

Const A = 1.4051e-3

Const B = 2.369E-4

Const C = 1.019E-7

Units Batt\_Volt=Volts

Units PTemp\_C=Deg C

Units SEVolt=mV

Units kOhms=kOhms

Units PA\_uS=uSec

Units PA\_uS\_2=uSec

Units GeokonFreqRaw=Hz

Units GeokonThermRaw=Ohms

Units GeokonAmp=mV RMS

Units GeokonSNRat=Ratio

Units GeokonNFreq=Hz

Units GeokonDRat=Ratio

'Define Data Tables

```

DataTable(SucTemp,True,-1)
  DataInterval(0,30,min,10)
  CardOut(0,-1)
  Sample(1,kOhms(1),FP2)
  Sample(1,kOhms(2),FP2)
  Sample(1,kOhms(3),FP2)
  Sample(1,kOhms(4),FP2)
  Sample(1,kOhms(5),FP2)
  Sample(1,kOhms(6),FP2)
  Sample(1,kOhms(7),FP2)
  Sample(1,kOhms(8),FP2)
  Sample(1,kOhms(9),FP2)
  Sample(1,kOhms(10),FP2)
  Sample(1,kOhms(11),FP2)
  Sample(1,kOhms(12),FP2)
  Sample(1,kOhms(13),FP2)
  Sample(1,kOhms(14),FP2)
  Sample(1,kOhms(15),FP2)
  Sample(1,kOhms(16),FP2)
  Sample(1,kOhms(17),FP2)
  Sample(1,kOhms(18),FP2)
  Sample(1,kOhms(19),FP2)
  Sample(1,kOhms(20),FP2)
  Sample(1,kOhms(21),FP2)
  Sample(1,kOhms(22),FP2)
  Sample(1,kOhms(23),FP2)
  Sample(1,kOhms(24),FP2)
  Sample(1,kOhms(25),FP2)
  Sample(1,kOhms(26),FP2)
  Sample(1,kOhms(27),FP2)
  Sample(1,kOhms(28),FP2)
  Sample(1,kOhms(29),FP2)
  Sample(1,kOhms(30),FP2)
  Sample(1,kOhms(31),FP2)
  Sample(1,kOhms(32),FP2)
EndTable

```

```

DataTable(SWCC,True,-1)
  DataInterval(0,30,min,10)
  CardOut(0,-1)
  Minimum(1,Batt_Volt,FP2,False,False)
  Sample(1,PTemp_C,FP2)
  Sample(1,VWC,FP2)
  Sample(1,VWC_2,FP2)
  Sample(1,PA_uS,FP2)
  Sample(1,PA_uS_2,FP2)
  Sample(1,SEVolt(1),FP2)
  Sample(1,SEVolt(2),FP2)
EndTable

```

```

DataTable (VWFreq,True,-1)
  DataInterval (0,30,min,10)
  CardOut (0,-1)
  Sample (8,GeokonFreqRaw(),IEEE4)
EndTable

```

```

DataTable (VWTempRaw,True,-1)
  DataInterval (0,30,min,10)
  CardOut (0,-1)
  Sample (8,GeokonThermRaw(),FP2)
EndTable

Main Program
BeginProg
  SerialOpen(Com1,38400,0,0,10000)
  Scan(30,Min,1,0)
  'Default Datalogger Battery Voltage measurement Batt_Volt:
  Battery(Batt_Volt)
  PanelTemp(PTemp_C,250)

' ***** Geokon VW Measurement *****
AVW200(AVWCommResponse,Com1,0,200,VW(1,1),1,1,8,400,6000,1,_60Hz,1,0)
For I=1 To 8
  GeokonFreqRaw(I)=VW(I,1)
  GeokonAmp(I)=VW(I,2)
  GeokonSNRat(I)=VW(I,3)
  GeokonNFreq(I)=VW(I,4)
  GeokonDRat(I)=VW(I,5)
  GeokonThermRaw(I)=VW(I,6)
Next

' ***** Watermark 253 Soil and Plucker Measurements *****
  'Turn AM16/32 Multiplexer On
  PortSet(4,1)
  Delay(0,150,mSec)
  I=1
  SubScan(0,uSec,32)
  'Switch to next AM16/32 Multiplexer channel
  PulsePort(3,10000)
  '253 Soil Moisture Sensor measurements kOhms and WP_kPa on the AM16/32
Multiplexer:
  BrHalf(kOhms(I),1,mV250,1,1,1,250,True,20000,1000,1,0)
  'Convert resistance ratios to kOhms
  kOhms(I)=kOhms(I)/(1-kOhms(I))
  I = I +1
  NextSubScan
  'Turn AM16/32 Multiplexer Off
  PortSet(4,0)

'***** Campbell VWC Sensor Measurements *****
  'CS616 Water Content Reflectometer measurements VWC and PA_uS:
  CS616(PA_uS,1,3,5,1,1,0)
  VWC=-0.0663+(-0.0063*PA_uS)+(0.0007*PA_uS^2)
  'CS616 Water Content Reflectometer measurements VWC_2 and PA_uS_2:
  CS616(PA_uS_2,1,4,6,1,1,0)
  VWC_2=-0.0663+(-0.0063*PA_uS_2)+(0.0007*PA_uS_2^2)

' ***** Generic Single-Ended Voltage measurements SEVolt() *****
  VoltSe(SEVolt(),2,mV5000,5,True,0,_60Hz,1,0)

'***** Call Data Tables and Store Data *****
  CallTable(SucTemp)

```

```
CallTable(SWCC)  
CallTable(VWFreq)  
CallTable(VWTempRaw)
```

```
NextScan  
EndProg
```

**APPENDIX C - INSITU SOIL TEST DATA**



**Auburn University**  
 Civil Engineering Department  
 238 Harbert Center  
 Auburn University, AL 36849-5337

LOG OF BORING: **B-1**

SHEET 1 OF 1

DATE DRILLED: 8/2/2011

PROJECT NO: 2011-001

PROJECT: Auburn NGES Excavation #2

LOCATION: Opelika, AL

TOTAL DEPTH: 21.2 ft.

REFUSAL: NA ft.

DRILL METHOD: Hollow Stem Auger RIG TYPE: CME550X

BORING DIAMETER: 6" HAMMER: Automatic

SURFACE ELE: NA ft. CAVE-IN DEPTH: NA ft.

INITIAL GWL: NA ft. DELAYED GWL: NA ft.

SAMPLE TYPE:  DISTURBED  SPT SAMPLE  SHELBY TUBE  NO REVOCERY  CORE

E L E V (ft)	D E P T H (ft)	MATERIAL CLASSIFICATION AND REMARKS	L I T H	G W L	SAMPLES		● SPT N (bpf)    □ LL (%) △ PL (%)        ○ NMC (%) × FINES (%)							
					T Y P E	B L O W S P E R 6 I N.	10	20	30	40				
	0	RESIDUUM: Stiff, dry red SILT w/ sand (ML)												
	5	RESIDUUM: Stiff, moist, tan and red SILT (ML)				5	6	6		● 12				
	10	RESIDUUM: Stiff, moist, tan to brown SILT w/ sand, schist and veins of weathered rock (ML)				3	6	7		● 13	○ 13	△	□	×
	15	RESIDUUM: Stiff, moist, tan to brown SILT w/ sand, schist and veins of weathered rock (ML)				3	5	7		● 12				
	20	RESIDUUM: Very stiff, moist, tan, SILT, w/ veins of weathered schist and gneiss rock (ML)				7	8	10		● 18				

**ABBREVIATIONS:**

GWL - Groundwater Level    PL - Plastic Limit    NMC - Natural Moisture Content    LITH - Lithologic Symbol    LL - Liquid Limit



**Auburn University**  
 Civil Engineering Department  
 238 Harbert Center  
 Auburn University, AL 36849-5337

LOG OF BORING: **B-2**

SHEET 1 OF 1

DATE DRILLED: 8/2/2011

PROJECT NO: 2011-001

PROJECT: Auburn NGES Excavation #2

LOCATION: Opelika, AL

TOTAL DEPTH: 21.0 ft.

REFUSAL: NA ft.

DRILL METHOD: Hollow Stem Auger RIG TYPE: CME550X

BORING DIAMETER: 6" HAMMER: Automatic

SURFACE ELE: NA ft. CAVE-IN DEPTH: NA ft.

INITIAL GWL: NWTE ft. DELAYED GWL: NA ft.

SAMPLE TYPE:  DISTURBED  SPT SAMPLE  SHELBY TUBE  NO REVOCERY  CORE

E L E V (ft)	D E P T H (ft)	MATERIAL CLASSIFICATION AND REMARKS	L I T H	G W L	SAMPLES		● SPT N (bpf)    □ LL (%) △ PL (%)        ○ NMC (%) × FINES (%)							
					T Y P E	B L O W S P E R 6 I N.	10	20	30	40				
	0	RESIDUUM: Stiff, moist, tan and red SILT w/ mica, and veins of weathered schist and gneiss (ML)												
	5				3 5 4		9		×					
	10				4 4 5		9		○	△	□			
	15				3 3 5		8							
	20	RESIDUUM: Medium, moist, tan and white SILT with veins of weathered gneiss (ML)			2 3 4		7							
	25													
	30													
	35													

**ABBREVIATIONS:**

GWL - Groundwater Level    PL - Plastic Limit    NMC - Natural Moisture Content    LITH - Lithologic Symbol    LL - Liquid Limit



**Auburn University**  
 Civil Engineering Department  
 238 Harbert Center  
 Auburn University, AL 36849-5337

LOG OF BORING: **B-3**

SHEET 1 OF 1

DATE DRILLED: 8/2/2011

PROJECT NO: 2011-001

PROJECT: Auburn NGES Excavation #2

LOCATION: Opelika, AL

TOTAL DEPTH: 21.5 ft.

REFUSAL: NA ft.

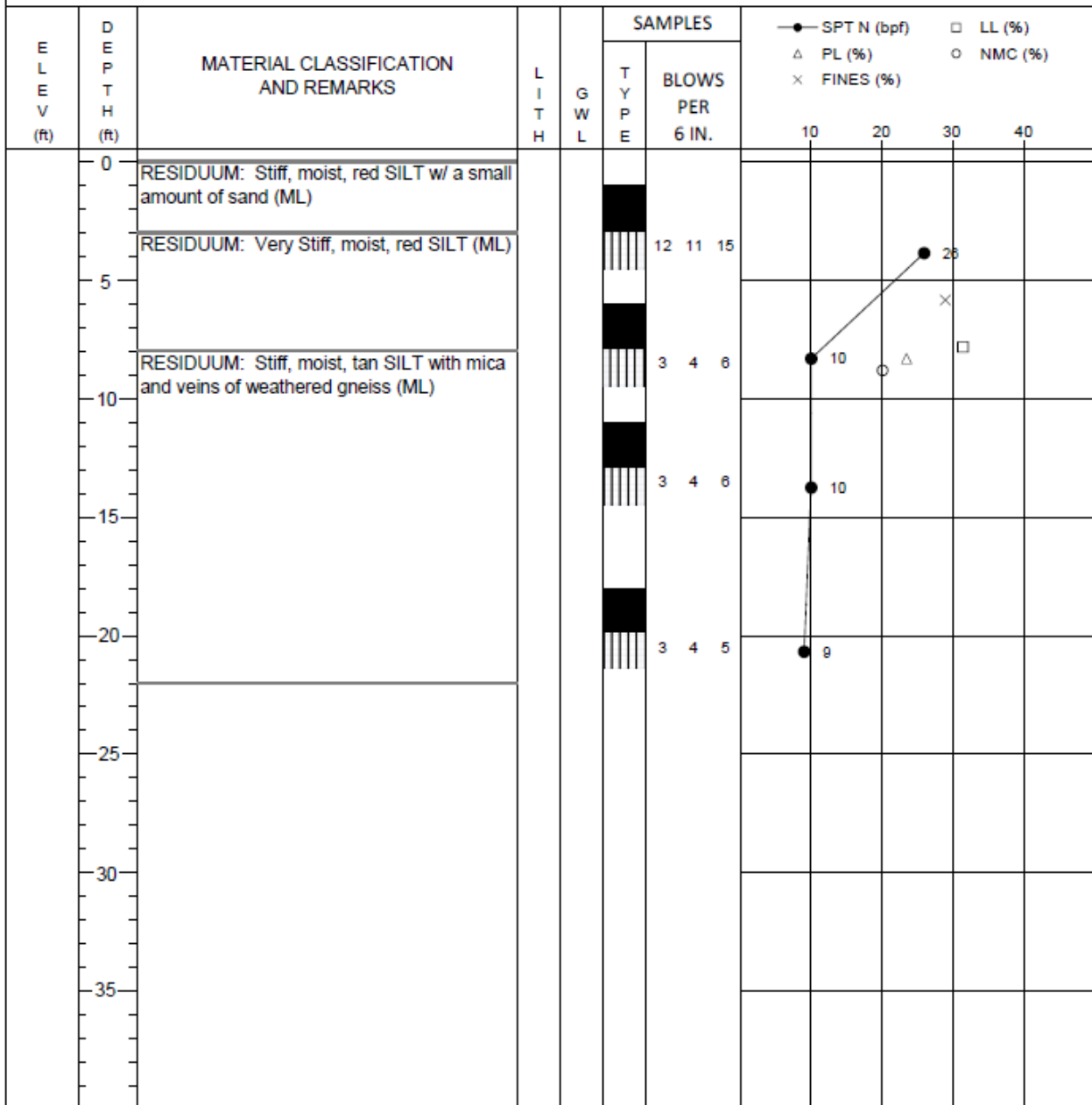
DRILL METHOD: Hollow Stem Auger RIG TYPE: CME550X

BORING DIAMETER: 6" HAMMER: Automatic

SURFACE ELE: NA ft. CAVE-IN DEPTH: NA ft.

INITIAL GWL: NWTE ft. DELAYED GWL: NA ft.

SAMPLE TYPE:  DISTURBED  SPT SAMPLE  SHELBY TUBE  NO REVOCERY  CORE



**ABBREVIATIONS:**

GWL - Groundwater Level PL - Plastic Limit NMC - Natural Moisture Content LITH - Lithologic Symbol LL - Liquid Limit

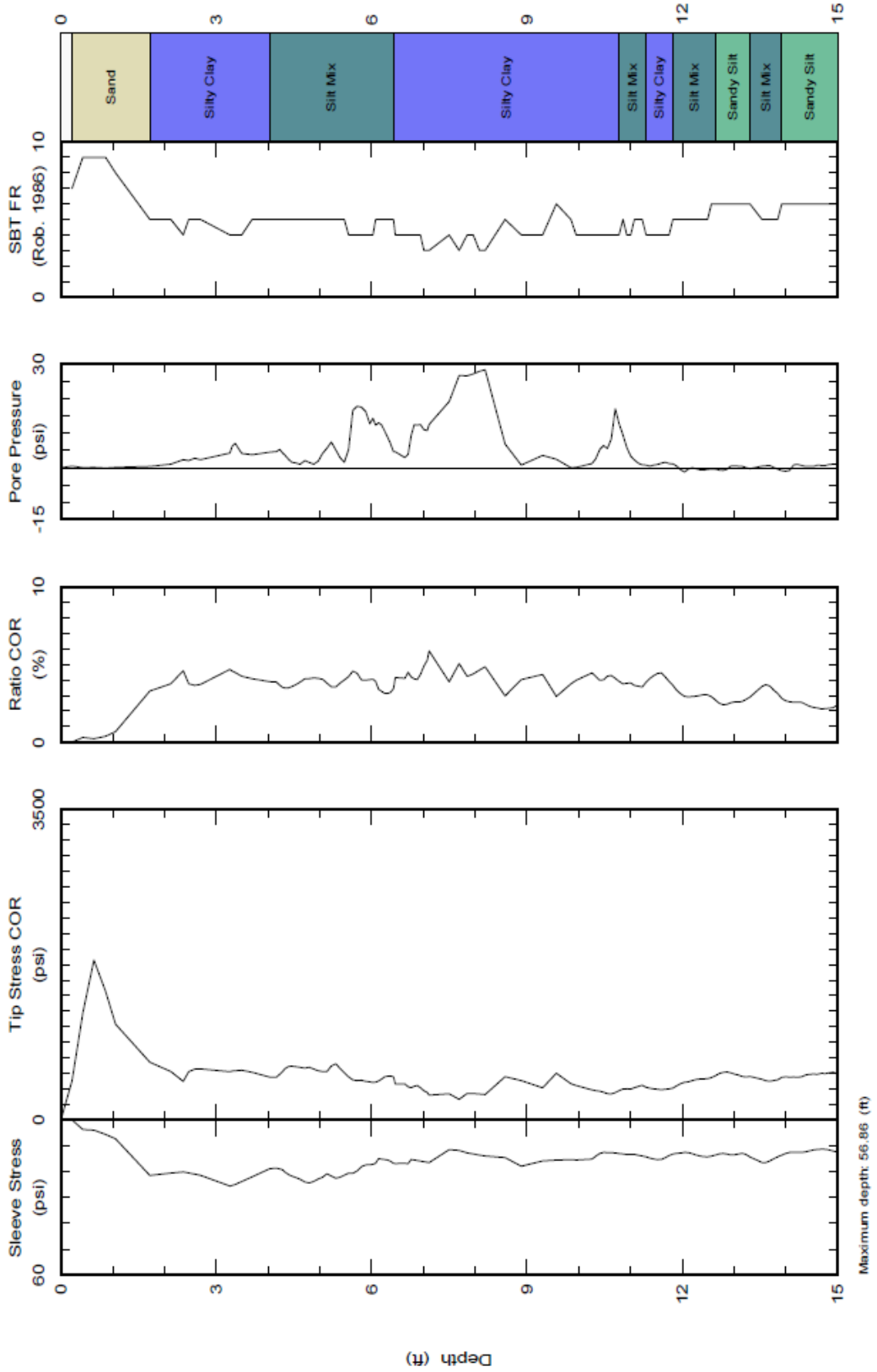


Lankelma, Inc.  
 1500 Bingle Rd. Houston, TX 77055  
 415-265-1614  
 virgilbaker@Lankelma.com  
 www.Lankelma.com

Northing:  
 Easting:  
 Elevation:

Customer: Auburn U  
 Job Site: Opelika

Date: 27/Jul/2010  
 Test ID: T1-EXC  
 Project: Auburn R&D

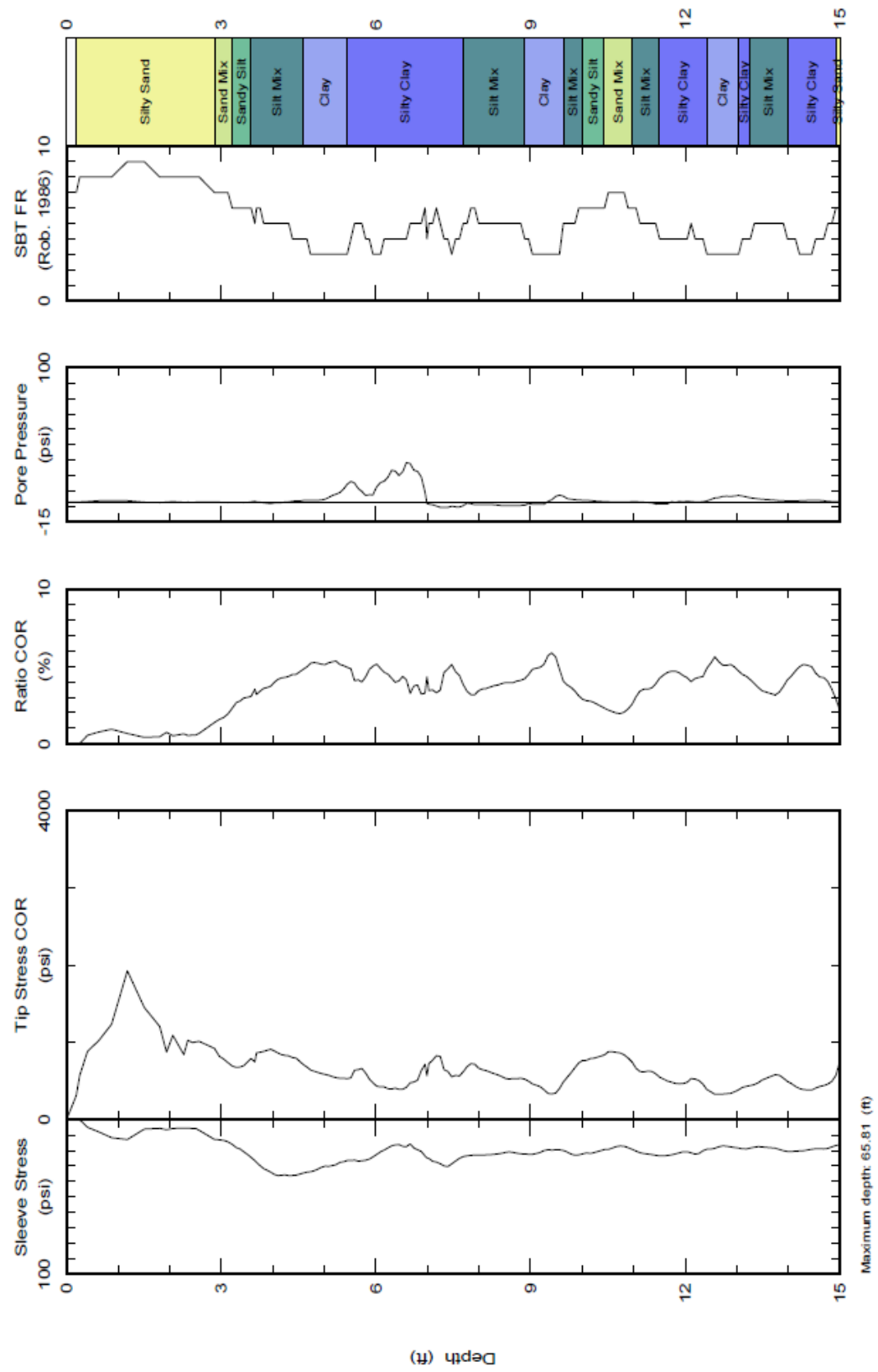




Lankelma, Inc.  
 1500 Bingle Rd. Houston, TX 77055  
 415-265-1614  
 virgilbaker@Lankelma.com  
 www.Lankelma.com

Northing:  
 Easting:  
 Elevation:  
 Customer: Auburn U  
 Job Site: Opelika

Date: 27/Jul/2010  
 Test ID: T2-EXC  
 Project: Auburn R&D

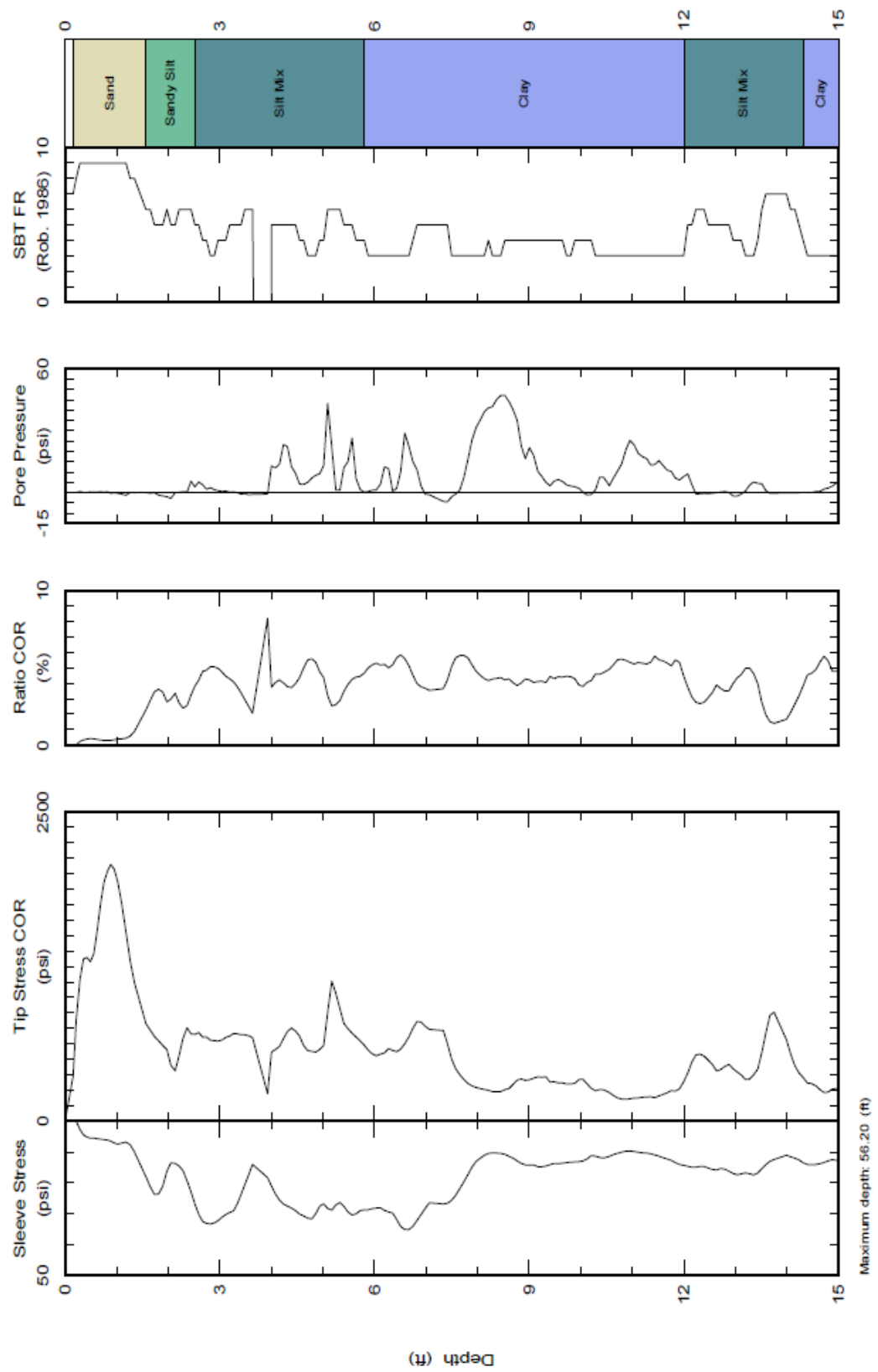




Lankelma, Inc.  
 1500 Bingle Rd. Houston, TX 77055  
 415-265-1614  
 virgilbaker@Lankelma.com  
 www.Lankelma.com

Northing:  
 Easting:  
 Elevation:  
 Customer: Auburn U  
 Job Site: Opelika

Date: 27/Jul/2010  
 Test ID: T3-EXC  
 Project: Auburn R&D





Lankelma, Inc.  
1500 Bingle Rd. Houston, TX 77055  
415-265-1614  
virgilbaker@Lankelma.com  
www.Lankelma.com

Northing:  
Easting:  
Elevation:  
Customer: Auburn U  
Job Site: Opelika

Date: 28/Jul/2010  
Test ID: T4-GTO  
Project: Auburn R&D

